

## ABSTRACT

Title of Dissertation:                   HIPPOCAMPAL GLUCOSE TRANSPORT  
AND OXIDATION IN RESPONSE TO  
DISRUPTED BLOOD FLOW IN AN AGING  
RAT MODEL OF HEART FAILURE

Gabriel S. Pena, Doctor of Philosophy, 2023

Dissertation directed by:           Professor J. Carson Smith, Ph.D. Department of  
Kinesiology

The primary objective of this dissertation was to investigate, in a rodent model of cardiovascular disease promoted by transverse aortic constriction (TAC), whether cerebral hypoperfusion stemming from chronic high pulsatile blood flow, and cerebral hypoperfusion stemming from low cerebral blood flow differentially affected hippocampal glucose transport and hippocampal mitochondrial function. We first, characterized the changes in right and left carotid hemodynamics and diameter in response to TAC and in a SHAM control group at three different time points (20-, 30-, and 40 weeks) post-surgery. Then, right, and left hippocampal mitochondrial content and substrate oxidation were investigated, and protein expression of glucose transporters and mitochondrial quality control markers were quantified. In this study, both the SHAM and TAC conditions included male and female rats to address possible sex differences. We report that all time points within TAC, right carotid blood flow velocities and pulsatility were greater than the left, but did not worsen over time. No differences in mitochondrial content were found within TAC nor between TAC and SHAM, but within TAC animals there were impairments in right hippocampal coupled and uncoupled respiration when compared to the left. When compared to the SHAM controls, right and left hippocampi of TAC animals had higher protein expression of mitochondrial quality control markers, but no differences in glucose transporter expression were found. Thus, while both high blood flow and/or pulsatility as well as low cerebral blood flow may lead to brain hypoperfusion, the metabolic consequences of the two may not be the same. The results from this dissertation contribute to the expanding literature characterizing the intersection between cardiovascular disease and neurodegeneration.

HIPPOCAMPAL GLUCOSE TRANSPORT AND OXIDATION IN RESPONSE  
TO DISRUPTED BLOOD FLOW IN AN AGING RAT MODEL OF HEART  
FAILURE.

by

Gabriel Santiago Pena

Dissertation submitted to the Faculty of the Graduate School of the  
University of Maryland, College Park, in partial fulfillment  
of the requirements for the degree of  
Doctor of Philosophy  
2023

Advisory Committee:

Professor J. Carson Smith, Ph.D., Chair

Assistant Professor Sarah Kuzmiak-Glancy, Ph.D., Co-Chair

Associate Professor Steven J. Prior, Ph.D.

Associate Professor Sushant Ranadive, Ph.D.

Assistant Research Professor James P. Barrett, Ph.D.

Professor, Robin Puett, Ph.D.

© Copyright by  
Gabriel Santiago Pena  
2023

## Dedication

This dissertation is dedicated to my wife, Annaleah Morse. You have shared with me every high and low of this academic endeavor, and this achievement is as much yours as it is mine. Your unwavering love and support got me through some of the most challenging periods of my life thus far. I am fortunate to have you in my life, and your existence is the best part of my own.

I also dedicate this work to my parents, Rafael Peña and Elsa Sanchez, and my siblings, Rafael, and Maria Jose Peña. As a family, we have overcome circumstances that built the perseverance and work ethic I needed to reach this point. This work is a direct consequence of the roles you continue to play in my life.

## Acknowledgements

This dissertation is a product of the mentoring, support, and opportunities I have been granted by the devoted and generous scientists that shaped my graduate career.

First, I would like to thank the American Heart Association for funding this work under the pre-doctoral fellowship titled: *Hippocampal Glucose Transport and Oxidation in Response to Disrupted Perfusion in an Aging Rat Model of Heart Failure* (Award: 23PRE1020728). My sincere gratitude to the Department of Kinesiology at the University of Maryland-College Park for providing additional funding to the Kuzmiak-Glancy Lab and the Exercise for Brain Health Lab that made this work possible.

I would also like to thank my colleagues and lab mates: Jun Won, Maria Canellas Da Silva, Yuan Liu, Bill Evans, Harry Li, Lauren Eagan, Kyle Pietro, Alex Shaver, Emily Blake, Catherine Springer-Sapp, and Jim Heilman. I was lucky to have shared this time with you, and was at many times, inspired by your resilience when facing adversity. Each one of you has given me much needed support throughout my time in the program, and in the process, become a dear friend. I will always look back fondly at the many happy hours we pursued, the dark humor we learned to perfect, and sharing Kyle's home-made brews.

To my previous mentor, Dr. Michael Whitehurst, many of the lessons you instilled in me throughout my time at FAU allowed me to find a footing after leaving the safety of your lab. I will forever be grateful to you for your mentorship and the role you played in getting me to this point.

I am also grateful to my dissertation committee, Drs. Prior, Ranadive, Barrett, and Puett. Although I may have abused the open-door policy with my endless questions, you were always kind and provided the clarifying guidance I desperately needed. I cannot thank you enough for generously giving your time and expertise to make me a better scientist, academic, and person.

Lastly, no dissertation can be achieved without the wisdom, support, and guidance of a chair. In my case, I was lucky enough to have two chairs that shaped every step of my graduate degree. Dr. J. Carson Smith, I want to thank you for extending an olive branch and bringing me to UMD-CP; This act of generosity was crucial in helping me rekindle my passion for science after a series of disappointments. Your patience and calm demeanor over the years gave me much needed perspective and I thank you for the many years of guidance you gave me. To Dr. Sarah-Kuzmiak Glancy, words will never properly convey my gratitude towards you. I am a proud Glancy Lab adopted child not only because of the quality of work you encourage, but also because you provided an environment where my scientific ambitions could be pursued. Your dedication to student success is something I will always admire and be grateful for. This department is fortunate to have a scientist of your caliber as a faculty member, and I cannot wait to see the inevitable growth the Glancy Lab will experience. I sincerely thank you for allowing me to be part of your group and for taking me on as one of your own.

# Table of Contents

Dedication .....	ii
Acknowledgements .....	iii
Table of Contents .....	v
List of Tables .....	vii
List of Figures .....	viii
List of Abbreviations .....	ix
Chapter 1: Review of The Literature .....	1
Project Overview .....	1
Significance.....	3
Vascular Contributions to Cognitive Impairment and Dementia .....	4
Behavioral Manifestations of VCI and VaD.....	11
Cerebral Blood Flow and Neural Glucose Transport .....	13
Glucose Oxidation by Neural Mitochondria.....	14
Mitochondrial Energetics and Quality Control.....	16
Transverse Aortic Constriction as a Model to Study Vascular Dementia .....	19
Chapter 2: The Longitudinal Diametric Bilateral Carotid Artery Hemodynamic Response to Transverse Aortic Constriction.....	23
Chapter Overview .....	23
Methods.....	24
Study Design.....	24
Transverse Aortic Constriction .....	24
Statistical Analysis.....	28
Results.....	29
Animal Characteristics.....	29
Alterations in Carotid Artery Hemodynamic and Diameter in TAC and SHAM31 Within Condition Sex Differences in Carotid Artery Hemodynamics .....	45
Discussion .....	51
Longitudinal characterization of carotid artery hemodynamics in response to TAC.....	52
Sex differences in carotid artery hemodynamics and artery diameter .....	55
Study Limitations.....	57
Conclusion .....	58
Chapter 3: Glucose Transport, Oxidation, and Mitochondrial Quality Control in Transverse Aortic Constriction. ....	60
Chapter Overview .....	60
Methods.....	62
Study Design.....	62
Transverse Aortic Constriction Surgery .....	62
Euthanasia and Tissue Isolation .....	63
Hippocampal Respiration.....	64
Hippocampal Mitochondrial Content .....	65
Protein Quantification and Western Blot.....	65
Statistical Analysis.....	66

Results.....	67
Animal Characteristics.....	67
Hippocampal Respiration and Mitochondrial Content in TAC and SHAM Animals.....	69
Expression of Glucose Transporter Proteins in TAC and SHAM Animals.....	74
Expression of Mitochondrial Quality Control Proteins in TAC and SHAM Animals.....	75
Sex Differences in TAC and SHAM Animals.....	78
Discussion.....	82
Animal Characteristics.....	83
Mitochondrial Respiration and Content.....	84
Glucose Transport and Mitochondrial Quality Control.....	87
Sex Differences.....	90
Limitations.....	93
Conclusion.....	94
Chapter 4: Summary of Findings.....	96
Future Directions.....	99
Bibliography.....	103

## List of Tables

Table 1: Animal Characteristics.....	31
Table 2: Effects of Condition and Hemisphere on systolic artery diameter. ....	41
Table 3: Effects of Condition and Hemisphere on diastolic artery diameter.....	41
Table 4: Effects of Time on carotid artery hemodynamics.....	42
Table 5: Effects of Time on carotid artery diameter.....	42
Table 6: Animal Characteristics.....	68

## List of Figures

Figure 1: Aortic banding in rat model of transverse aortic constriction. ....	24
Figure 2: Sample Analysis of Carotid Artery Hemodynamics and Diameter. ....	27
Figure 3: Severe TAC Carotid Blood Flow Phenotype. ....	29
Figure 4: TAC Lowers Blood Flow Velocities in the Left Carotid and Increases Blood Flow Pulsatility in the Right Carotid 20 Weeks Post-Surgery. ....	34
Figure 5: TAC-Related Changes 30 Weeks Post-Surgery Parallel Those Seen 20 Weeks Post-Surgery. ....	37
Figure 6: TAC-Related Changes in Carotid Artery Velocities and Pulsatility Remain Steady 40 Weeks Post-Surgery. ....	40
Figure 7: Carotid Artery Hemodynamics in TAC do not Worsen with Time. ....	43
Figure 8: Carotid Artery Diameters in TAC do Not Change with Time. ....	44
Figure 9: Sex Dimorphisms in Carotid Artery Velocities in TAC are Constrained to the Right Hemisphere and Present as Early as 30-Weeks Post-Surgery. ....	47
Figure 10: Sex Dimorphisms in Carotid Artery Velocities in SHAM are Present in the Right and Left Hemisphere but Appear Later in Time Than TAC. ....	48
Figure 11: Impaired Mitochondrial Respiration in the Right, but not Left Hippocampus of TAC. ....	71
Figure 12: Transverse Aortic Constriction Does Not Lower Mitochondrial Content. ....	72
Figure 13: High Carotid Artery Velocity and Pulsatility is Negatively Associated with Hippocampal Mitochondrial Respiration. ....	73
Figure 14: Protein Expression of Glucose Transporters is not Altered by Transverse Aortic Constriction. ....	74
Figure 15: Greater Protein Expression of Mitochondrial Fusion Markers in Right and Left Hippocampus of TAC. ....	77
Figure 16: Lower Mitochondrial Content in Female TAC is Coupled to the Upregulation of Mitochondrial Fusion. ....	79
Figure 17: Right and Left Hippocampal Respiration is Impaired in Female SHAM. ....	81

## List of Abbreviations

AD – Alzheimer’s disease

ATP – Adenosine triphosphate

UPR<sup>MT</sup> – Mitochondria unfolded protein response

TAC – Transverse aortic constriction

PD – Parkinson’s disease

ALS – Amyotrophic lateral sclerosis

HD – Huntington’s disease

VCID – Vascular contributions to cognitive impairment and dementia

VCI – Vascular cognitive impairment

VaD – Vascular dementia

MCI – Mild cognitive impairment

MRI – Magnetic resonance imaging

PET – Positron emission tomography

ASL – Arterial spin labeling

FDG – Fluorodeoxyglucose

BBB – Blood-brain barrier

NVU – Neurovascular unit

GLUT – Glucose transporter

O<sub>2</sub> – Molecular oxygen

CO<sub>2</sub> – Carbon dioxide

TCA – Tricarboxylic acid cycle

ETC – Electron transport chain

ANT – Adenine nucleotide translocase

ROS – Reactive oxygen species

MFN 1 – Mitofusin 1

MFN 2 – Mitofusin 2

OPA1 – Optic atrophy gene

DRP1 – Dynamin-related protein 1

FIS1 – Fission 1

MFN – Mitochondrial fission factor

HSP – Heat shock protein

LCCA – Left common carotid artery

RCCA – Right common carotid artery

PI – Pulsatility Index

# Chapter 1: Review of The Literature

## **Project Overview**

Global disease burden and mortality rates are heavily influenced by the development of age-related chronic diseases<sup>1-3</sup>. As such, biological aging is seen as a major public health concern given that, globally, the older adult population is expected to exponentially increase and be accompanied by a significant increase in the incidence of chronic diseases<sup>4</sup>. By 2030, it is projected that over 20% of the population in the United States will consist of adults 65 years and older<sup>5</sup>. This shift in demographics is expected to not only increase the incidence of chronic diseases and related costs, but also place unsustainable strains on healthcare systems<sup>6, 7</sup>. Unsurprisingly, “healthy aging” has become a global research and public health initiative<sup>8-11</sup>.

Neurodegenerative diseases represent a spectrum of, mostly age-related, brain conditions where progressive losses in neuronal populations are coupled to losses in cognitive function, that overtime, can result in the development of dementia<sup>12</sup>. Multiple lines of evidence show pathologies of the peripheral body systems can contribute to the development and progression of neurodegenerative diseases<sup>13-16</sup>. Among these, diseases of the cardiovascular system have been consistently tied to cognitive decline and the development and progression of neurodegenerative diseases such as Alzheimer’s Disease (AD)<sup>5, 17-19</sup>. Yet, the mechanisms by which neurodegeneration can be initiated, influenced, or exacerbated by cardiovascular

disease remain poorly understood<sup>20, 21</sup>. In this context, alterations to brain hemodynamics has long been posited to be a key etiological event by which cardiovascular disease can contribute to neurodegeneration and dementia<sup>22</sup> because it can lead to decreases in tissue perfusion and substrate availability<sup>23-25</sup>.

Circulating blood glucose is the primary metabolic substrate for neurons<sup>26</sup>, and low tissue perfusion may impair glucose transport and lead to energetic deficits that compromise neurophysiological processes and neuronal health<sup>26</sup>. In neurons, mitochondria play an integral role in oxidizing glucose to generate adenosine triphosphate (ATP); the energetic currency that powers various neurophysiological processes such as, neurotransmission, synaptic plasticity, and cytoskeletal remodeling<sup>27-29</sup>. To do this, neural mitochondria can form and regulate functional energetic networks throughout neuronal compartments (e.g., soma, axon, synapse)<sup>30, 31</sup>. These mitochondrial energetic networks are governed by complex and interrelated quality control mechanisms that include fusion and fission events, mitophagy, and the mitochondrial unfolded protein response (UPR<sup>mt</sup>)<sup>32, 33</sup>. Although not fully understood, all these quality control mechanisms are reported to be dysregulated during neurodegenerative diseases<sup>29, 34-38</sup>.

While animal models of cardiovascular disease suggest glucose transport and oxidation are compromised when neuronal tissue is poorly perfused (e.g., hypoperfused)<sup>39-41</sup>, these observations stem from disparate models, time scales, and center around physically lowering cerebral blood flow to limit brain perfusion<sup>25, 42, 43</sup> despite human studies suggesting hypoperfusion may stem from low arterial compliance and high blood flow pulsatility<sup>24, 44</sup>. As such, we aim to take advantage of

the rodent model of transverse aortic constriction (TAC) where the ligation of the transverse aorta leads to divergent bilateral blood flow responses where the right common carotid displays sustained but pulsatile blood flow and the left common carotid displays decreased blood flow<sup>45</sup>. Recent work shows this blood flow response is maintained at the cerebral hemispheres, and both lead to tissue hypoperfusion<sup>46</sup>. Therefore, the TAC model of cardiovascular disease can be used to address a major gap in the literature. That is, the divergent bilateral carotid and hemispheric blood flow responses can be used to address whether hypoperfusion stemming from sustained but pulsatile blood flow and hypoperfusion from lower brain blood flow differentially affect many of the mechanisms by which cardiovascular disease could induce neurodegeneration. Specifically, this project aims to address the consequences of these hemodynamic responses on glucose transport, neuronal mitochondrial energetics, and mitochondrial quality control. Addressing these gaps in the literature will provide context to better understand the role brain hemodynamics play on neurodegenerative processes from an integrative point of view and thus, help better understand the intersection between cardiovascular disease and neurodegeneration.

### **Significance**

Cardiovascular and neurodegenerative diseases are two of the most common age-related chronic diseases among older adults today<sup>1-3</sup>, and it is estimated that 36% of the current global disease burden in older adults is made up by cardiovascular and neurodegenerative diseases alone<sup>47</sup>. Moreover, the overall global cost of cardiovascular disease and dementia are estimated to exceed \$503.2 and \$604 billion USD, respectively<sup>17, 48</sup>. Extensive research into cardiovascular and neurodegenerative

disease pathology show a close association between cardiovascular health and brain health<sup>18</sup> and the development of cardiovascular pathologies can increase the risk of developing neurodegenerative diseases and dementia later in life<sup>16</sup>. This is underscored by emerging longitudinal data from separate large-scale studies where poor baseline indices of vascular health<sup>49</sup> (e.g., high arterial stiffness as measured via pulse pressure and pulse wave velocity), high multivariate cardiovascular risk scores (as measured by The Framingham General Cardiovascular Risk Score)<sup>50</sup>, or accelerated cumulative cardiovascular disease burden trajectory<sup>19</sup>, have been identified as prominent components in the likelihood of developing dementia. Although it is not fully understood, these observations highlight that common age-related pathologies may be more intricately related than previously thought<sup>20, 21, 51</sup>. As such, there is a growing need for work that involves an integrative approach to common chronic diseases and that can provide additional context to existing isolated disease studies<sup>10, 13, 14, 52</sup>.

### **Vascular Contributions to Cognitive Impairment and Dementia**

Clinically, dementia represents a myriad of diverse and, oftentimes, age-related neurodegenerative conditions that lead to deficits in cognitive function of such severity that activities of daily living and independence are compromised<sup>53</sup>. Alzheimer's Disease (AD) is the most common neurodegenerative disease among older adults today<sup>5</sup>, and over 40% of individuals with dementia are clinically classified as having AD<sup>54</sup>. However, most clinical cases of AD in older adults are characterized by the dual presence of AD-related pathology and advanced vascular pathology<sup>53</sup>. While it is challenging to delineate in such cases whether cognitive

deterioration is primarily caused by AD pathology or vascular pathology<sup>55</sup>, it is widely accepted that vascular disease speeds up the rate of progression in dementia<sup>51</sup>. Vascular disease has not been exclusively linked to AD, and multiple studies have found cardiovascular disease can be involved in the development of other age-related neurodegenerative diseases such as Parkinson's Disease (PD), as well as other neurodegenerative conditions found throughout the lifespan such as Amyotrophic Lateral Sclerosis (ALS) and Huntington's Disease (HD)<sup>56</sup>. Given this, the vascular contributions to cognitive impairment and dementia (VCID) represents a growing field of study that attempts to better characterize the specific roles vascular risk factors and cardiovascular diagnoses play in the development of cognitive dysfunction throughout the lifespan<sup>51</sup>. Critically, it is important to note here that work on VCID has led to the identification and classification of other types of dementia including vascular cognitive impairment (VCI) and vascular dementia (VaD)<sup>55</sup>. VCI and VaD represent a spectrum of deficits in brain function and structure stemming from chronic primary vascular pathologies<sup>16, 57</sup>, where subclinical or clinical vascular insults result in brain injury and cognitive impairment affecting one or more cognitive domains<sup>55</sup>. Just as mild cognitive impairment (MCI) is traditionally seen as a prodromal form of AD, VCI can be seen as a prodromal form of VaD<sup>55</sup>. Epidemiological data suggests VaD is the second most common type of dementia among older adults, accounting for ~20% of dementia cases today, and this is expected to triple by 2050<sup>16, 20</sup>. Despite this, compared to AD, VaD remains a pathology with limited representation in clinical trials, limited animal models, and possibly heavily underreported in the clinic<sup>44</sup>. Therefore, considering that the

incidence of dementia is expected to surpass 13 million older adults by 2050<sup>5</sup>, VaD is a large component of a growing public health concern that is in dire need of comprehensive study<sup>5, 20</sup>.

The etiology of VCI and VaD has been difficult to characterize in humans given disease progression and the cognitive deficits it elicits are dependent on the primary vascular pathology (e.g., small vessel disease v. microinfarction), the neural substrates affected (e.g., frontal v. temporal cortex), and the vessels involved (e.g., middle cerebral artery v. posterior cerebral artery)<sup>16, 21, 58</sup>. Nevertheless, a growing interest in VCI and VaD as stand-alone pathologies (e.g., independent from related pathologies such as AD) has led to the identification of possible physiological mechanisms that promote the development of VCI and VaD<sup>16, 17, 58</sup>. Among these, pulsatile blood flow and cerebral hypoperfusion are firmly grounded as a key etiological mechanism of brain dysfunction in VCI and VaD<sup>16, 44, 58</sup>. Indeed, because chronic blood flow pulsatility is associated with sustained mechanical stress, it can result in sustained end-organ damage that compromises the ability to couple neuronal activity to blood flow, and therefore<sup>24</sup>, lead to tissue hypoperfusion and reduced oxygen and substrate availability<sup>44</sup>.

Human studies employing clinical imaging techniques such as Doppler ultrasound imaging, magnetic resonance imaging (MRI), and positron emission tomography (PET) all suggest changes in large artery structure and function and the maladaptive hemodynamic responses that ensue are an etiological hallmark in VCI and VaD<sup>24</sup>. For example, Doppler ultrasound studies have shown that increased aortic stiffness, as measured via pulse wave velocity, is positively associated with cognitive

decline, as well as gray and white matter damage<sup>24</sup>. Increased stiffness in large conduit arteries (e.g., aortic and carotid) are harmful to cognitive and brain health because arterial compliance dissipates blood flow pulsatility, protecting cerebral microvessels and brain tissue from end-organ damage<sup>24</sup>. Pulsatile blood flow represents the oscillatory waveforms that are generated by the pressure difference between systolic and diastolic blood pressure each cardiac cycle<sup>24, 46</sup>. When this pressure difference increases (as seen in hypertension or increased vessel stiffness), the amplitude of the oscillatory waveforms is greater, and thus, the pulsatility of blood flow also increases<sup>24, 59</sup>. Since cerebral microvessels lack an external elastic lamina, pulsatile flow is dampened into steady capillary flow by large arteries, which then prevents the propagation of harmful pulsatile wave forms into brain microvessels and tissue; a phenomena known as the Windkessel effect<sup>18, 24</sup>. Thus, increased arterial stiffness and an impaired Windkessel effect may facilitate the accretion of mechanical stress and structural damage to cerebral microvessels and neurons, that overtime, may manifest as cognitive impairment and dementia<sup>23, 24</sup>.

Beyond acting as a buffer to mechanical stress, the Windkessel effect also plays an important role in cerebral blood flow autoregulation<sup>24</sup> because the maintenance of microvessel and neuronal integrity are important for the myogenic response and regulation of neurovascular coupling<sup>26, 59, 60</sup>. The myogenic response represents the ability of small arteries and arterioles to constrict when blood pressure increases (normalizes wall tension) and dilate when mean arterial pressure falls (reduces vessel resistance)<sup>59, 61</sup>. On the other hand, neurovascular coupling is the process by which increases in neuronal activity are accompanied by the increases in

blood flow and the delivery of oxygen, glucose, and nutrient-rich blood necessary to sustain neuronal communication<sup>26, 60</sup>. In this context, autoregulation of brain blood flow allows for the precise distribution of blood flow to sites of high neuronal activity (neurovascular coupling) while sustaining cerebral blood flow and perfusion pressures constant across a range of blood flow velocities and pressures (myogenic response)<sup>61</sup>. As such, when the Windkessel effect is impaired such that large arteries stiffen and pulsatile flow increases, the mechanical stress associated with this can induce physical damage to brain small arteries and arterioles that eventually propagates into neurons<sup>18, 24, 26, 59</sup>. Over time, as this damage accrues, the microvascular wall in cerebral vessels may begin to lose its myogenic response leading to sustained damage to neurons and an inability to properly induce neurovascular coupling<sup>24, 44</sup>. This series of chronic events may ultimately present in clinic as altered pathological cerebral blood flow (e.g., low cerebral blood flow and tissue perfusion), lower brain glucose uptake, and cognitive decline<sup>18, 24, 26, 59</sup>. Indeed, ultrasound Doppler studies<sup>62</sup> show cerebral blood flow is impaired during VCI and VaD, and MRI-Arterial Spin Labeling (ASL) studies have reported decreases in cerebral blood flow are matched by losses in brain perfusion signal<sup>63, 64</sup>. Unsurprisingly, structural MRI studies show changes in blood flow and perfusion are coupled to increased white matter lesions, microbleeds, and other ischemic lesions that are indicative of a loss in cerebral microvessel integrity<sup>16, 21</sup>. Lastly, fluorodeoxyglucose (FDG)-PET studies of VaD report decreases in cerebral blood flow are accompanied by decreases in neuronal glucose uptake that further suggest deficits in neurovascular coupling<sup>65</sup>. Therefore, a secondary effect of low arterial

compliance may be a disruption to the mechanisms that regulate cerebral blood flow, perfusion, and transport of substrates into active neurons. Despite the insights gained from human studies, these studies are limited because the clinical symptoms of dementia occur late in disease progression<sup>66</sup> when older adults will often present additional comorbidities such as mental health conditions (e.g., depression)<sup>67</sup>, and concurrent cardiovascular/cerebrovascular pathologies (e.g., hypertension with cerebral small vessel disease<sup>16, 21</sup>) that make it extremely challenging to isolate the etiological roles any given primary vascular pathology may play towards cognitive decline<sup>16, 25, 68</sup>.

In theory, because most animal studies can mimic specific cardiovascular pathologies, these models aid in isolating the independent contributions divergent vascular pathologies have towards cognitive decline from a mechanistic point of view<sup>69</sup>. Animal studies have revealed various potential molecular mechanisms for VCI and VaD including, dysregulation of blood-brain barrier (BBB) integrity, cerebral hypoperfusion, trophic uncoupling, and the inability of the neurovascular unit (NVU) to cope with chronic biological insults<sup>17, 53</sup>. Acute hypertension can lower the expression of BBB tight junction proteins such as claudin-3,-5, and -12, and also increase the penetration of blood-brain barrier impermeable agents such as the Evans blue dye in rats<sup>70</sup>. Because losses in BBB integrity are commonly found in animal models of cardiovascular disease<sup>71, 72</sup>, this suggests there is structural damage at the NVU<sup>69, 73</sup>; a possibility already substantiated by data from human studies<sup>60, 65, 74</sup>. The NVU is a cellular complex made up by a consortium of cells that include neurons, astrocytes, pericytes, microglia, brain capillary endothelial cells, and

oligodendrocytes, and where neurovascular coupling takes place<sup>26</sup>. Though not entirely understood, altered blood flow and losses in arterial compliance in cardiovascular disease can lead to a mismatch in the provision of oxygen and glucose to active neurons<sup>25, 73</sup>. In murine FDG-PET studies, low brain blood flow from bilateral carotid artery stenosis leads to impaired glucose metabolism within the cortex and hippocampus<sup>75</sup>. Further, mouse models of spontaneous hypertension show increased aortic stiffness is related to reduced cerebral blood flow, lower expression of mainly endothelial glucose transporter 1 (GLUT1) mRNA, mitochondrial dysfunction, and deficits in memory and learning<sup>39, 76, 77</sup>. Thus, animal models provide compelling evidence to show increased arterial stiffness and altered hemodynamics in cardiovascular disease may lead to mechanical damage of the NVU and impair the transport of glucose into neurons and their ability to oxidize it; leaving neurons unable to sustain neural communication, and thus, cognitive function<sup>20</sup>.

However, it must be noted here that the disparate and somewhat limited number in animal models used to study VCID, as well as the experimental time periods involved make it challenging to fully determine the etiological hallmarks of pure VCI and VaD<sup>25</sup>. Indeed, as stated above disrupted cerebral blood flow and hypoperfusion stemming from a loss in arterial compliance and increased brain blood flow pulsatility are widely regarded as etiological hallmarks of human VCI and VaD<sup>53</sup>. Yet, much of the animal research used to study the neurobiological consequences of hypoperfusion involves the use of large-artery occlusion (e.g., bilateral common carotid stenosis, asymmetric common carotid constriction) or genetic knockout models (e.g., *ApoE* *-/-*, *LDLr* *-/-*) that either do not entirely reflect

the hemodynamic roots of hypoperfusion seen in humans, or include multiple components of cardiovascular disease (e.g., systemic inflammation) that also contribute to VaD<sup>25, 53</sup>. The widely used bilateral common carotid constriction models achieves cerebral hypoperfusion by employing small diameter coils, and ameroid constrictors (in asymmetric constriction), that occlude the right and left common carotid arteries, and therefore, physically limit the amount of blood that reaches the cerebral vasculature<sup>78</sup>. However, such models place overt focus on limiting blood volume supply and fail to reflect evidence showing chronic mechanical stress and damage may be key to hypoperfusion<sup>39, 46</sup>, BBB breakdown and cognitive decline<sup>79</sup>, and thus, human VaD<sup>44</sup>. Moreover, genetic knockout models such as the *ApoE* *-/-* model of hypercholesterolemia, have been widely used to study VCID and VaD, and observed to increase breakdown of the BBB<sup>80</sup> and lead to cognitive impairments<sup>81</sup>. Yet, the hemodynamic response of this model is yet to be comprehensively characterized<sup>25</sup>, and the knockout of *ApoE* can negatively impact the distribution of specific cell populations in the rodent adult brain<sup>82</sup>. Thus, while insightful the animal models currently used fail to represent key etiological components of VCI and VaD. Specifically, these models do not address whether pulsatile blood flow and mechanical damage and the possible tissue hypoperfusion that ensues directly impair neuronal processes that contribute to neurodegeneration<sup>53</sup>

### **Behavioral Manifestations of VCI and VaD**

Because most older adults clinically diagnosed with AD will often present evidence of mixed dementia (e.g., AD/VCI)<sup>16, 53</sup>, it is not surprising that several studies have found much overlap in the neuropsychological features of patients

diagnosed with AD and VaD<sup>44, 83</sup>. However, human neuroimaging studies have found that unlike MCI and AD, indices of structural damage within the brain of patients with major neurocognitive disorders following cerebrovascular events are largely heterogenous<sup>16, 74</sup>. That is, while MCI and AD is often associated with early damage to specific brain structures such as the hippocampus<sup>84</sup>, pure VaD may not be centralized to specific structures but to broad brain areas that negatively affect a wide array of cognitive domains<sup>16, 21</sup>. Intriguingly, some neuropsychological studies have found that although the degree and severity can vary, patients with VCI and VaD, more often than not, will display deficits in cognitive processes associated with the frontal lobes and frontostriatal circuits such as executive function, information processing, and motor behavior<sup>21, 58, 83, 85</sup>. When compared to AD, individuals with pure VaD have more difficulty with higher order processes associated with the prefrontal cortex such as emotional regulation<sup>86, 87</sup> as well as those associated with the basal ganglia such as psychomotor speed<sup>21</sup>. Thus, while not exclusive, VaD may most commonly present with behavioral changes that are regulated by frontostriatal circuits<sup>16, 21, 58, 85</sup>. This is supported by clinical neuroimaging studies that have found abnormal alterations in brain function and structure involve mainly the frontal lobe and structures of the subcortical basal ganglia such as the striatum<sup>63-65, 74, 88</sup>. Therefore, developing neuropsychological and clinical assessments that testing frontostriatal circuits may be beneficial when attempting to distinguish between MCI/AD and VCI/VaD in VCID research<sup>83, 89</sup>.

## **Cerebral Blood Flow and Neural Glucose Transport**

Adenosine triphosphate (ATP) is the main energy currency that neurons utilize to sustain homeostatic processes and communicate<sup>26, 90</sup>. While neurons can harvest ATP from multiple fuel sources such as ketone bodies and lactate, neurons preferentially metabolize glucose to synthesize ATP<sup>90</sup>, and glucose metabolism is thought to account for 95% of ATP production within these cells<sup>26</sup>. Because the brain has limited glucose stores<sup>91</sup>, circulating blood and the glucose it carries is essential for proper neuronal function and communication<sup>26, 90</sup>. As such, altered cerebral blood flow that compromises glucose availability or transport, may lead to energetic deficits within neurons that negatively impact their function and health<sup>26, 90</sup>. Glucose uptake by neurons requires an intricate collaboration within the NVU that allows glucose to be shuttled from the bloodstream into neurons via glucose transporters (GLUT) found at the cell surface of endothelial cells, astrocytes, and neurons, among others<sup>91</sup>. Specifically, glucose transport is facilitated by the expression and interaction of capillary endothelium glucose transporters (GLUT1), astrocyte membrane bound glucose transporters (GLUT1, GLUT2, and GLUT7), oligodendrocyte glucose transporters (GLUT1), and neuron bound glucose transporters (GLUT3, and GLUT4)<sup>26</sup>. Glucose in the bloodstream can passively diffuse into the NVU extracellular space or can be picked up for facilitated transport across the BBB by GLUT1 found in the capillary endothelium<sup>91</sup>. Once across the BBB, astrocytic end-feet that express GLUT1 and that surround the cerebrovascular capillaries, collect the glucose in the extracellular space of the NVU and transport it into the peri-synaptic processes that are in close vicinity to neurons<sup>26</sup>. Astrocytic GLUT1 transporters then

release glucose into the peri-synaptic space where neuronal GLUT3 and -4 intake the glucose to fuel neuronal processes<sup>26, 90</sup>. It must be noted that this process is not passive and astrocytes must breakdown some glucose via glycolysis, producing ATP, to support the movement of glucose into the peri-synaptic space<sup>26</sup>. Moreover, although to what extent is still under debate, the lactate that results from astrocytic breakdown of glucose can act as an alternative fuel source or as a neurotransmitter<sup>26</sup>.

### **Glucose Oxidation by Neural Mitochondria**

Once in neurons, the process by which ATP is harvested from glucose requires multiple steps that take place in the cytosol and the mitochondria in what is known as oxidative catabolism<sup>92</sup>. Glucose is first broken down into two pyruvate molecules through glycolysis in the cellular cytosol and in the absence of molecular oxygen (O<sub>2</sub>) (anaerobically), and producing 2 ATP during this process<sup>92</sup>. The pyruvate obtained from glycolysis is then transported into the mitochondria where the three enzyme complex of pyruvate dehydrogenase decarboxylates pyruvate resulting in one Acetyl-CoA, releasing CO<sub>2</sub>, and reducing NAD<sup>+</sup> to NADH<sup>92</sup>. Acetyl-CoA carbon then enters the tricarboxylic acid cycle (TCA)<sup>92</sup> via citrate synthase, which catalyzes the integration of the two-carbons within the acetyl group of Acetyl-CoA with the four carbon oxaloacetate resulting in the six-carbon citrate<sup>93</sup>. This is an integral step, as citrate is then oxidized in the TCA cycle, where electrons harvested during the oxidation steps are transferred onto carrier molecules NAD<sup>+</sup> and FAD that are reduced to NADH and FADH<sub>2</sub><sup>92</sup>. It is important to note here that 1) although CO<sub>2</sub> is a by-product of the TCA cycle it is not location of O<sub>2</sub> consumption and, 2) O<sub>2</sub> is essential for the TCA cycle<sup>92</sup> because it acts as the final electron acceptor at the end

of the electron transport chain (ETC)<sup>92</sup>. Therefore, the only way to regenerate the NAD<sup>+</sup> from NADH is to have it oxidized by the ETC, and limitations in O<sub>2</sub> delivery may be accompanied by low TCA cycle flux<sup>92</sup>.

The ETC is made up by four enzyme complexes (Complexes I-IV) and two electron carriers (co-enzyme Q and cytochrome c)<sup>94</sup> and is where the flow of the electrons obtained in the TCA and carried by NADH and FADH<sub>2</sub> is coupled to the synthesis of ATP<sup>92, 95</sup>. NADH and FADH<sub>2</sub> donate their electrons to the ETC at CI and CII, respectively, and the energetically favorable movement of electrons down the ETC is coupled to the movement of protons from the matrix across the inner mitochondrial membrane via proton pumps within CI, CIII, and CIV, resulting in an electrochemical gradient<sup>92, 95</sup>. Oxygen consumption occurs at CIV, when 2 electrons are transferred to the final electron acceptor ( $\frac{1}{2}$  O<sub>2</sub>), reducing it to water<sup>92</sup>. The electrochemical gradient created from the pumping of protons, known as the proton-motive force, powers ATP synthesis by facilitating the controlled movement of protons from the intermembrane space, down their electrochemical gradient, through ATP synthase, a hydrophilic pathway within the inner membrane<sup>92</sup>. As protons move down this electrochemical gradient ATP is generated via rotary catalysis<sup>92</sup> and then transported to the cytosol via carrier protein adenine nucleotide translocase (ANT) to provide energy to support neuronal processes<sup>26, 95</sup>.

An inevitable byproduct of oxidative phosphorylation is production of superoxide radical anions (O<sub>2</sub><sup>-</sup>), which is termed the electron leak<sup>95</sup>. Some electrons traveling down the ETC do not follow their path all the way to CIV: some will exit (leak out) the ETC and univalently reduce O<sub>2</sub> to O<sub>2</sub><sup>-</sup> instead of reducing  $\frac{1}{2}$ O<sub>2</sub> to H<sub>2</sub>O

at the end of CIV<sup>96</sup>. In cells, O<sub>2</sub><sup>-</sup> acts as a free radical and reactive oxygen species (ROS)<sup>95, 97</sup> that likely acts as a signaling molecule, but that in excess can damage mitochondrial components, cellular proteins, lipids, and DNA<sup>97</sup>. Although ROS can come from multiple cellular compartments, the vast majority (~90%) can be traced to the transfer of electrons through complex I and III during oxidative phosphorylation<sup>98, 99</sup>. Neurons have an inherent low antioxidant defense system and are particularly susceptible to damage from high concentrations of ROS and oxidative stress<sup>70</sup> and deficits in mitochondrial ETC complex structure may lead to not only altered energetics but also ROS production<sup>96</sup>.

In summary, proper cerebral blood flow is essential for glucose transport into neurons<sup>26</sup>, in a process that is mediated by the membrane bound glucose transporters found in the various cells of the NVU<sup>91</sup>. Once transported into neurons, glucose is oxidized in the cellular cytosol and mitochondria to generate ATP via oxidative catabolism<sup>92</sup>. Additionally, because O<sub>2</sub> facilitates the replenishment of carrier molecules that shuttle electrons from the matrix to the ETC, the diffusion of oxygen from circulating blood into neurons is also key to oxidation of glucose and the synthesis of ATP. Therefore, glucose transport and oxygen delivery are both needed to fuel key ATP-dependent neuronal processes such as the synthesis, release, and re-uptake of neurotransmitters, the maintenance of ionic gradients, and cytoskeletal remodeling<sup>90</sup>.

### **Mitochondrial Energetics and Quality Control**

Neural mitochondria are integral to the function of cells, including the maintenance of ionic gradients, neurotransmission, synaptic plasticity, and calcium

buffering, among others<sup>27-29</sup>. To support these functions, neural mitochondria form complex functional mitochondrial networks throughout the neuronal compartments<sup>30, 31, 94</sup>. Mitochondrial functional networks are maintained by quality control processes including mitochondrial dynamics (e.g., fission and fusion), mitophagy, and the unfolded protein response (UPR<sup>MT</sup>)<sup>34, 94, 100-102</sup>. Mitochondria can undergo fusion and merge or undergo fission and separate, altering the form of the mitochondrial network<sup>100</sup>. Importantly, mitochondrial quality control processes are key cellular processes by which dysfunctional mitochondria are neutralized<sup>34, 100</sup>.

Fusion is a two-step process whereby two adjacent mitochondria join to form an elongated and functional mitochondrion, whereas fission is the opposite and results in the division of a larger mitochondrion into two detached mitochondria<sup>27</sup>. It is hypothesized fusion serves to repair reversibly damaged mitochondrion by integrating them into healthy adjacent mitochondrion, while fission serves to segregate irreversibly damaged mitochondrial fragments so these can be destroyed via other quality control mechanisms (e.g., mitophagy)<sup>103</sup>. Mitochondrial fusion comprises the union of both the outer mitochondrial and the inner mitochondrial membrane, and it is mediated by outer membrane GTPases mitofusin 1 and 2 (MFN1 and MFN2) and inner membrane GTPase optic atrophy gene 1 (OPA1)<sup>101</sup>. On the other hand, fission is largely regulated by the recruitment and translocation of dynamin-related protein 1 (DRP1) and its interaction with outer membrane proteins fission 1 (FIS1), mitochondrial fission factor (MFF), and MID49<sup>27</sup>. Importantly, a balance between fission and fusion events is vital to modulate mitochondrial morphology and metabolic networks<sup>32</sup>. Mitochondrial fusion events can be influenced by the

dissipation of the mitochondrial membrane potential and low ATP levels<sup>94, 104</sup>, and fusion specific proteins (MFN2 and OPA), as well as fission specific proteins (DRP1), can all influence oxidative metabolism<sup>102</sup>. Indeed, MFN2 has been previously reported to facilitate coenzyme Q levels and ATP synthesis, while OPA1 can regulate the mitochondrial membrane potential and maximal respiration<sup>102</sup>. In addition, loss of DRP1 function can lead to an increase in proton leak and subdued mitochondrial respiration<sup>102</sup>. Thus, balanced mitochondrial dynamics are essential for proper mitochondrial function and recent studies suggest imbalances may contribute to the pathophysiology of various neurodegenerative conditions such as Alzheimer's and Parkinson's Disease<sup>94, 100, 105</sup>.

Although mitochondria hold an independent genome, the vast majority of mitochondrial proteins are nuclear encoded and must be transported into mitochondria from the nucleus in a soluble state<sup>106</sup>. Further, during fission and fusion events, mitochondria have to constantly regulate ETC stoichiometries, clear stress-denatured proteins, and ensure that the segregation or adjoining of mitochondria does not cause imbalances in the mitochondrial proteome<sup>101</sup>. These monumental tasks are largely regulated by a delicate interaction between the UPR<sup>MT</sup> and molecular protein chaperones<sup>30, 34</sup>. Another component of mitochondrial quality control, the UPR<sup>MT</sup> represents the transcriptional program that protects the mitochondria against proteotoxic stress by stabilizing protein imports and facilitating protein transport and clearance, among others<sup>34</sup>. Protein chaperones of the heat shock protein (HSP) family are a key component of the UPR<sup>MT</sup><sup>106</sup> that are involved in the transport nuclear encoded unfolded proteins into the mitochondria, facilitate the folding and assembly

of protein complexes, prevent the aggregation of stress-denatured proteins, and act as proteotoxic stress sensors for the UPR<sup>MT</sup> 106, 107. Because the nuclear encoded mitochondrial proteins are transported in an aggregate-prone and unfolded soluble form, HSPs found throughout the mitochondria are key for proper and integration of proteins<sup>30</sup>. For example, the interaction between cytosolic HSP90, HSP70 and mitochondrial translocase Tom70 allows for the initial mobilization of preproteins into the mitochondrial outer membrane<sup>30, 108</sup>. Although co-chaperones in the intermembrane space such as HtrA2 facilitate preprotein transport into the mitochondrial inner membrane, the majority of HSPs and co-chaperones can be found in the mitochondrial matrix<sup>30</sup>. This is largely because preproteins are folded into their functional state in the mitochondrial matrix before they are integrated into the mitochondria in processes that also involve HSPs<sup>30</sup>. Proper concentrations of HSPs such as HSP60, HSP10, and mtHSP70 are integral for mitochondrial proteostasis<sup>30, 107</sup>. However, it is important to keep in mind that HSPs and co-chaperone activation may be context dependent, and the mechanisms by which these become active and interact are still under heavy investigation<sup>30, 109</sup>.

### **Transverse Aortic Constriction as a Model to Study Vascular Dementia**

Although there is a growing number of animal models to study cardiovascular disease, the rodent model of transverse aortic constriction (TAC) presents unique opportunities to address some gaps in the VaD literature<sup>25</sup>. The surgical procedure used in TAC involves the partial ligation of the transverse aorta, usually between the left common carotid artery and the innominate artery, to increase left ventricular pressure overload and mimic left ventricular afterload<sup>110</sup>. This surgical approach leads

to sustained but pulsatile right carotid blood flow and decreased left carotid blood flow<sup>45, 46</sup>. Though most studies focus on short time scales (1-28 days)<sup>45, 111</sup>, these changes in cerebral blood flow have been reported 42 days post-TAC surgery<sup>46</sup>. Interestingly, the divergent hemodynamic environments in the right and left carotid can both induce hemispheric hypoperfusion, but the right hemisphere shows a larger decrease in tissue perfusion<sup>46</sup>. Moreover, losses in microvessel density and high number of cerebral microbleeds have been noted in TAC animals within the right hemisphere but not the left<sup>46</sup>. Lastly, because cognitive processes such as spatial navigation are impaired in animals with TAC<sup>46</sup>, this model is gaining popularity as an occlusion model that could be leveraged to study VaD<sup>25</sup>. Naturally, this model presents the unique advantage to study, within the same system, whether chronic pulsatile flow, as well as lower carotid and cerebral blood flow differentially affect many of the metabolic mechanisms previously implicated in VaD.

Despite the potential of the TAC model holds to study VaD, there is a paucity of data on glucose oxidation and brain mitochondrial function in this model. Namely, although increased arterial pulse pressure and BBB leakage<sup>46</sup>, brain hypoperfusion<sup>39, 46</sup>, reduced GLUT1 gene expression<sup>39</sup>, and deficits in spatial navigation<sup>46</sup> are all found in TAC, to our knowledge there are currently only two studies that suggest mitochondrial function is altered in TAC. First, one study employed TAC to induce acute hypertension and showed acute (1-7 days post-TAC procedure) TAC-related increases in right carotid artery blood pressure and higher blood flow velocity in the microcirculation of the right hemisphere, when compared to the left carotid and hemisphere<sup>111</sup>. Crucially, this study also reported that increases and decreases in

microvessel blood flow were associated with increased oxidative stress in both hemispheres; suggesting that acutely, both, increased and decreased cerebral blood flow may similarly affect brain energetics<sup>111</sup>. Abdominal aortic constriction, which would increase pulsatile blood flow in both the left and right common carotid arteries, impairs the expression of genes encoding BBB tight junction proteins, and lowers cortical antioxidant activity. Lower brain antioxidant activity may hint at higher oxidative stress, and possibly mitochondrial energetic dysfunction<sup>70</sup>. Taken together, these lines of evidence hint at possible mitochondrial dysfunction, but this possibility has not been directly studied in these (TAC and abdominal aortic) constriction models.

Brain hypoperfusion as a result of low arterial compliance and blood flow pulsatility is believed to be an etiological hallmark of VCI and VaD<sup>53</sup>, and studies utilizing TAC show both increased and decreased blood flow can result in cerebral hypoperfusion<sup>46</sup>, damage to components of the NVU<sup>79</sup>, and cognitive deficits<sup>39, 46</sup>. Yet most animal models developed to inform VaD and VCID research rely on bilateral carotid occlusion to physically lower blood flow to the brain and induce hypoperfusion. Moreover, most models have not fully explored the downstream (i.e., in neurons) consequences of damage and dysregulation of metabolic processes at the NVU. Additionally, most animal studies tend to focus on acute time scales, leaving the chronic effects of isolated cardiovascular disease models largely unaddressed<sup>25, 46, 76, 111</sup>. Lastly, while TAC can clearly be employed to study how divergent changes in carotid and hemispheric blood flow affect mechanisms implicated in VaD pathogenesis, outside of characterization of BBB integrity<sup>39, 70, 111</sup>, there are only a

handful<sup>46, 70</sup> of studies that have delved into the neurophysiological consequences of TAC. Few studies have tried to link whether the divergent hemodynamic responses in TAC translate to divergent changes in substrate transport, substrate oxidation in neural mitochondria, and overall neural mitochondrial health<sup>20, 25, 42</sup>. Thus, this dissertation aimed to address the following gaps in the literature: 1) What are the chronic TAC-related changes in carotid blood flow velocity, artery diameter, and pulsatility in TAC and SHAM rats at 20-, 30-, and 40 weeks post-surgery? 2) Does the TAC surgery lead to hemispheric (right v. left) differences in hippocampal mitochondrial glucose oxidation and mitochondrial content, and do these relate to carotid hemodynamics? 3) Are there any hemispheric (right v. left) differences in GLUT protein expression and protein expression of mitochondrial quality control markers? Addressing these gaps will build on existing human and animal work and address the possible downstream (i.e., in neuronal tissue) consequences of changes in cerebral blood flow associated with VaD.

## Chapter 2: The Longitudinal Diametric Bilateral Carotid Artery Hemodynamic Response to Transverse Aortic Constriction.

### Chapter Overview

Traditionally used to study cardiac failure and hypertension<sup>110, 112, 113</sup>, the rodent model of transverse aortic constriction (TAC) has also been noted to result in opposing carotid hemodynamics whereby the right common carotid is exposed to sustained but pulsatile blood flow and the left common carotid is exposed to decreased blood flow<sup>45, 46</sup>. Because most of the TAC literature has focused on acute time scales (<10 weeks post-surgery)<sup>113</sup>, the goal of the present study was to determine how transverse aortic constriction (TAC) altered carotid artery size and hemodynamics in the right common (upstream of the constriction) and left common (downstream of the constriction) carotid arteries, in male and female rats compared to SHAM controls from a chronic point of view. Therefore, this study characterized the bilateral (right v. left) changes in carotid artery blood flow velocity, artery diameter, and pulsatility at three different time points (20-, 30-, and 40 weeks) following the TAC and SHAM surgeries. It was hypothesized that: a) TAC would result in higher right carotid blood flow velocity and pulsatility compared to the left carotid blood velocity and pulsatility, that would be more pronounced with increasing weeks post-TAC surgery, and b) compared to SHAM, TAC would result in higher right carotid blood flow velocity and pulsatility and lower left carotid blood velocity and pulsatility.

## Methods

### Study Design

The current study was approved by the Institutional Animal Care and Use Committee (IACUC) at the University of Maryland College Park. Using a cross-sectional study design, 4-week-old male and female Sprague-Dawley rats underwent the minimally invasive procedure of transverse aortic constriction (TAC) to mimic chronic hypertension and induced heart failure with preserved ejection fraction. Control animals (SHAM) underwent a sham surgical procedure that was identical to that received by TAC animals up to the constriction of the transverse aorta. Following surgical procedures, animals were paired-housed, held on 12/12-hour light/dark cycle, fed water and food ad libitum, and left to age for 40 weeks. Carotid blood flow and artery diameter were measured 20-, 30-, and 40 weeks post-TAC surgery.

### Transverse Aortic Constriction

Male and female Sprague-Dawley rats (4 weeks old) underwent either the TAC or SHAM surgical procedures as described previously<sup>114</sup>. Briefly, each animal was weighed and anesthetized via inhalation of isoflurane [~2% isoflurane supplemented with 100% oxygen (400-500 mL/min)]. Animals were then placed in

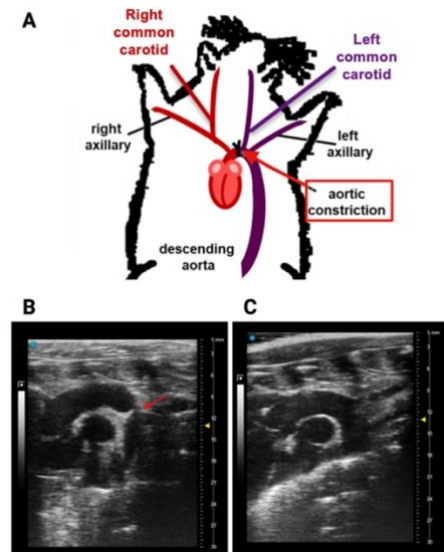


**Figure 1: Aortic banding in rat model of transverse aortic constriction.**

A) Placement of suture (red arrow) between common carotid arteries. B) Successful ligation of transverse aorta in TAC animals. C) Undisrupted aortic arch of SHAM controls.

the supine position on a heated pad, and body temperature was monitored via anal temperature probe. Once unresponsive, a single dose of buprenorphine (0.05-0.1 mg/kg) was injected via subcutaneous injection. A surgical area was clipped clean and sterilized. A horizontal skin incision was then made at the suprasternal notch region and a longitudinal ~1 cm cut was made in the sternum. In both procedures, a 4-0 silk suture attached to a blunted needle was passed around the aortic arch between the origin of the right innominate and left common carotid arteries. A bent, blunted 20-gauge needle was then placed next to the aortic arch, the suture was tightened around the needle, and the needle was then promptly removed (**Fig. 1A**). The sternum was closed with a single silk suture and the skin was sutured shut with 5-0 monofilament suture and treated with betadine. SHAM animals received the same procedure as TAC animals but did not have the suture tied around the aortic arch. Doppler ultrasound (**Fig. 1B and 1C**) and cardiac tissue specific measurements (left ventricular wall thickness and diameter) were used to confirm TAC and SHAM status of all animals used in this experiment.

#### Cardiac and Carotid Doppler Ultrasound

Carotid blood flow and artery diameter were measured with a Vevo3100 (FUJIFILM visualsonics) animal Doppler ultrasound imaging system at 20-, 30-, and 40 weeks post-surgery. Briefly, all animals were placed under anesthesia in an induction chamber with 2-5% isoflurane supplemented with 100% oxygen. Anesthesia depth was monitored with toe and tail pinches, and once animals became unresponsive, the fur around the chest was removed with clippers and ophthalmic gel was applied to both eyes. Animals were then placed on an imaging platform and paws

were taped in place over electrode gel for obtaining ECG measurements, and warmed ultrasound gel was applied to the chest. Carotid artery blood flow was determined with the use of B-mode & PW Doppler Imaging of the bilateral carotid arteries, while ultrasound imaging of the aortic arch and cardiac tissue were used to confirm aortic arch binding and obtain cardiac parameters such as cardiac output, ejection fraction, and stroke volume, respectively. Ultrasound files (PW Doppler and B-mode) were analyzed with the VevoLab software (FUJIFILM visualsonics) and carotid arterial blood flow velocity (mean and peak velocities), and artery diameter during systole and diastole were determined.

To obtain blood flow velocities, for each time point measured, at least three blood flow waveforms in each PW Doppler time series were traced manually and checked against software thresholds (**Fig. 2A**). Each wave-form trace yielded a value for mean velocity, peak velocity, pulsatility index, and velocity time integral that were then compiled and averaged to obtain an average value for each animal at each time point. A similar process was followed for arterial diameter measures where, for each time point, at least three peak systolic and peak diastolic diameters were obtained from the B-mode time series (**Fig. 2B & 2C**). These diameters were then compiled and averaged to obtain averaged peak systolic and peak diastolic arterial diameters for each animal at each time point.

The pulsatility index (PI) is a widely used measure to non-invasively address vascular resistance, and thus, indirectly address the elastic properties of blood vessels<sup>115</sup>. To calculate pulsatility index of the right and left carotid arteries, the following formula was used by the software:

$$PI = \frac{\text{Peak Systolic Velocity (PSV)} - \text{End Diastolic Velocity (EDV)}}{\text{Velocity Time Integral (VTI)}}$$

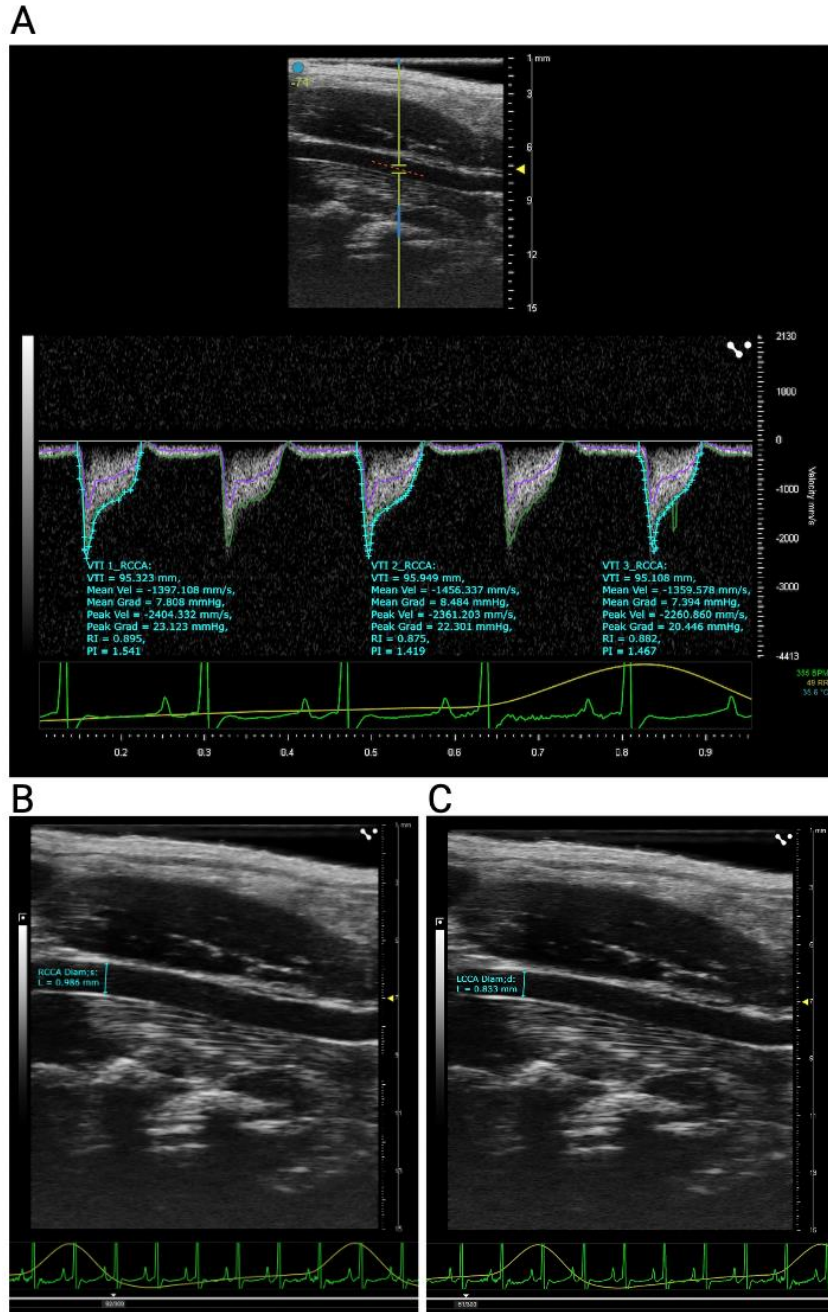


**Figure 2: Sample Analysis of Carotid Artery Hemodynamics and Diameter.**

**A)** PW Doppler time series with manual trace (blue) and software developed trace (green and purple) of blood flow waveform. **B)** Peak systolic carotid artery diameter obtained from B-Mode time series. **C)** Peak diastolic artery diameter obtained from B-Mode time series.

### Statistical Analysis

The primary purpose of this study was to characterize the time course of alterations in carotid artery blood hemodynamics and artery diameter in TAC animals and test whether these differed when compared to the SHAM controls. First, a series of 2x2 ANOVA models with Tukey's post-hoc comparisons were used to test whether there were any main effects of Condition (TAC v. SHAM), Hemisphere (right v. left), or Condition by Hemisphere interactions on carotid blood flow, pulsatility index, and artery diameter measures at each time point. Next, for each condition (TAC & SHAM) and hemisphere (right & left), a series of independently run one-way ANOVA models were used to determine whether there were any main effects of Time (20-, 30-, and 40 weeks) on carotid blood flow, pulsatility index, and artery diameter measures. Lastly, although not a primary aim in this study, separately run, independent samples t-test, or Mann-Whitney U test, were used as an exploratory analysis to address any possible sex differences on right/left carotid blood flow, pulsatility index, and artery diameter measures within either the TAC or SHAM conditions. All analyses were conducted using the statistical software JASP (version 0.17.3), and assumptions for all ANOVA models were checked. Statistical significance was set at  $p < 0.05$ .

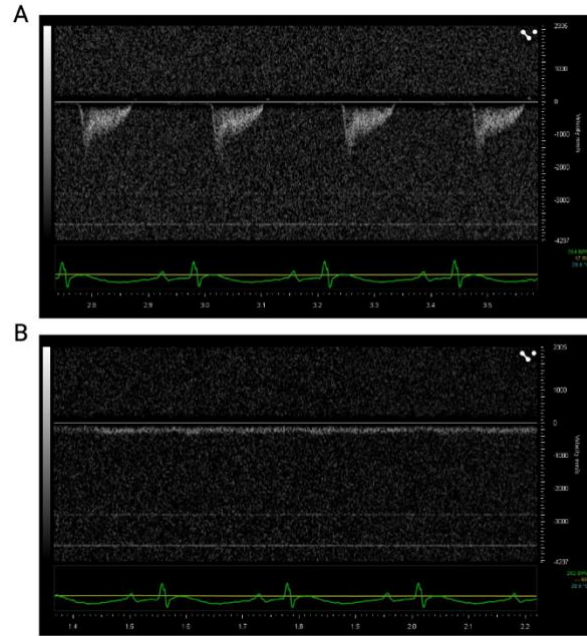


**Figure 3: Severe TAC Carotid Blood Flow Phenotype.**

**A)** Right carotid blood flow of TAC animal 20-weeks post-surgery. **B)** Left carotid blood flow in same TAC animal 20 weeks post-surgery.

## Results

### Animal Characteristics

A total of 31 animals were utilized (7 TAC male, 6 TAC female, 8 SHAM male, and 10 SHAM female) for these experiments. 1 TAC (1 female) and 8 SHAM (4 male, 4 female) animals were excluded from the analysis because of either poor ultrasound image quality or missing data. Further, Doppler ultrasound time series revealed 3 TAC animals had left carotid blood flow obstructed to such degree that blood flow wave forms could not be analyzed (e.g., flat wave forms) despite good image contrast and measurable flows on the right carotid (**Fig. 3A&B**). For these animals, the lowest measured left carotid outcomes within TAC were assigned as proxy left carotid outcome values that were then used for the present analysis. Moreover, 2 male TAC

animals with complete data at 20-, and 30- weeks but incomplete data at 40 weeks (due to poor ultrasound image resolution) were included in the analyses for which the respective data was available (e.g., 20- and 30 weeks 2x2 ANOVA) but excluded from the timepoints for which no data was available (e.g., 40 weeks 2x2 ANOVA). As such, a total of 12 TAC (7 male, 5 female) and 10 SHAM (4 male, 6 female) with a complete set of data for most time points were included for this analysis. Therefore, a total of 22 animals were used in the present analysis and all animal characteristics 40 weeks post-surgery can be found in **Table 1**. Independent samples T-test showed there were no significant differences between TAC and SHAM in any of the characteristics obtained 40 weeks post-surgery, including absolute and relative left ventricular width, heart mass, septal width, as well as cardiac parameters obtained from ultrasound imaging including cardiac output, ejection, fraction, and stroke volume (**Table 1**).

**Table 1: Animal Characteristics**

	TAC (n=12) M (SD)	SHAM (n=10) M (SD)
Sex		
Male	7	4
Female	5	6
Age (wks)	45.4 (1.32)	45.4 (1.73)
Body Mass (g)	475.8 (122.2)	463.2 (175.2)
Heart Mass (g)	1.44 (0.40)	1.27 (0.31)
Heart Mass to Body Mass (mg/g)	3.07 (0.51)	2.93 (0.70)
Left Ventricular Width (mm)	3.68 (0.50)	3.66 (0.34)
Left Ventricular Width to Body Mass (mm/mg)	8.11 (1.76)	8.85 (2.90)
Septal Width (mm)	3.27 (0.37)	2.97 (0.30)
Septal Width to Body Mass (mm/mg)	7.28 (1.83)	7.07 (2.01)
Cardiac Output (ml/min)	75.9 (13.8)	80.7 (20.4)
Stroke Volume (ul)	241.7 (37.3)	248.3 (66.4)
Ejection Fraction (%)	72.0 (13.8)	78.0 (9.07)
Tibialis Anterior Mass (g)	1.71 (0.39)	1.56 (0.51)

**Note:** TAC- transverse aortic constriction, SHAM- sham controls, wks- weeks, g- grams, mg- milligrams, mg/g- milligrams per gram, mm- millimeter, mm/mg- millimeter per milligrams, ml/min- milliliters per minute, ul- microliters, %- percent. Data presented as means (M) and standard deviation (SD).

*Alterations in Carotid Artery Hemodynamic and Diameter in TAC and SHAM*

The primary purpose of this study was to determine the time course of alterations in carotid artery hemodynamics and artery diameter in TAC and SHAM controls. To this end, we first examined whether condition (TAC v. SHAM) or hemisphere (right v. left) at each time point had any effects on mean carotid artery

velocity, peak carotid artery velocity, carotid artery pulsatility index, or systolic/diastolic carotid artery diameter.

Overall, 20 weeks post-surgery, we found that when compared to both carotids of SHAM and the left carotid of TAC, the right carotid of TAC displayed greater blood flow pulsatility, while the left carotid of TAC animals had the lowest blood flow velocities and pulsatility (**Fig. 4A**). Looking at mean carotid velocity, there was a significant main effect of Hemisphere ( $F(1,40)=19.22, p<0.001, \eta_p^2=0.32$ ), a significant Condition by Hemisphere interaction ( $F(1,40)=14.84, p<0.001, \eta_p^2=0.27$ ), but no significant effect of Condition ( $F(1,40)=1.28, p=0.26, \eta_p^2=0.03$ ). Tukey's post-hoc comparisons of the interaction term revealed that the left carotid mean velocity of TAC ( $M= 617.0 \pm 59.9$  mm/sec) animals was significantly lower than the left ( $M= 874.6 \pm 47.2$  mm/sec,  $t(40) = -3.52, p <0.01$ ) and right ( $M= 902.1 \pm 43.5$  mm/sec,  $t(40) = -3.901, p <0.01$ ) (**Fig. 4A**) of SHAM controls. Moreover, within TAC animals, the right carotid mean velocity ( $M= 1042.6 \pm 49.0$  mm/sec) was observed to be significantly higher than the left ( $M= 617.0 \pm 59.9$  mm/sec,  $t(40) = 6.10, p <0.001$ ) (**Fig. 4A**). Next, when looking at peak carotid artery velocity, similar results were seen, and there was a significant main effect of Hemisphere ( $F(1,40)=28.13, p<0.001, \eta_p^2=0.41$ ), a significant Condition by Hemisphere interaction ( $F(1,40)=19.52, p<0.001, \eta_p^2=0.32$ ), but no significant effect of Condition ( $F(1,40)=1.53, p=0.22, \eta_p^2=0.03$ ). Post-hoc comparisons showed peak carotid artery velocity was significantly lower in the left carotid of TAC ( $M= 902.1 \pm 99.4$ ) animals when compared to the left ( $M= 1376.3 \pm 73.9, t(40) = -4.00, p <0.01$ ) and right ( $M=1450.5 \pm 59.1$  mm/sec,  $t(40) = -4.62, p <0.001$ ) of SHAM animals (**Fig.**

**4B).** Further, peak artery velocity in the right carotid of TAC ( $M= 1716.8 \pm 84.9$  mm/sec) animals was found to be significantly higher when compared to the left ( $M= 902.1 \pm 99.4$  mm/sec,  $t(40) = 2.87, p < 0.05$ ) of SHAM animals, as well as the left ( $M= 902.1 \pm 99.4$  mm/sec,  $t(40) = 7.211, p < 0.001$ ) within TAC animals (**Fig.4B**). Lastly, there was also a significant main effect of Hemisphere ( $F(1,40)=43.17, p < 0.001, \eta_p^2=0.51$ ), a significant Condition by Hemisphere interaction ( $F(1,40)=20.62 p < 0.001, \eta_p^2=0.34$ ), but no significant effect of Condition ( $F(1,40)=0.45, p=0.50, \eta_p^2=0.01$ ) on carotid blood flow pulsatility. Follow up post-hoc comparisons of the interaction term showed blood flow pulsatility was significantly higher in the right carotid of TAC ( $M= 1.43 \pm 0.02$  P.I) animals when compared to the left ( $M=1.05 \pm 0.04$  P.I,  $t(40) = 8.24, p < 0.001$ ) of TAC, as well as the right ( $M= 1.30 \pm 0.03$  P.I,  $t(40) = 2.73, p < 0.05$ ) and left ( $M= 1.23 \pm 0.02$  P.I,  $t(40) = 4.16, p < 0.001$ ) of SHAM animals (**Fig. 4C**). Additionally, blood flow pulsatility was found to be lower in the left carotid of TAC when compared to the left ( $t(40) = -3.69, p < 0.01$ ) and right ( $t(40) = -5.12, p < 0.001$ ) arteries of SHAM controls (**Fig. 4C**).

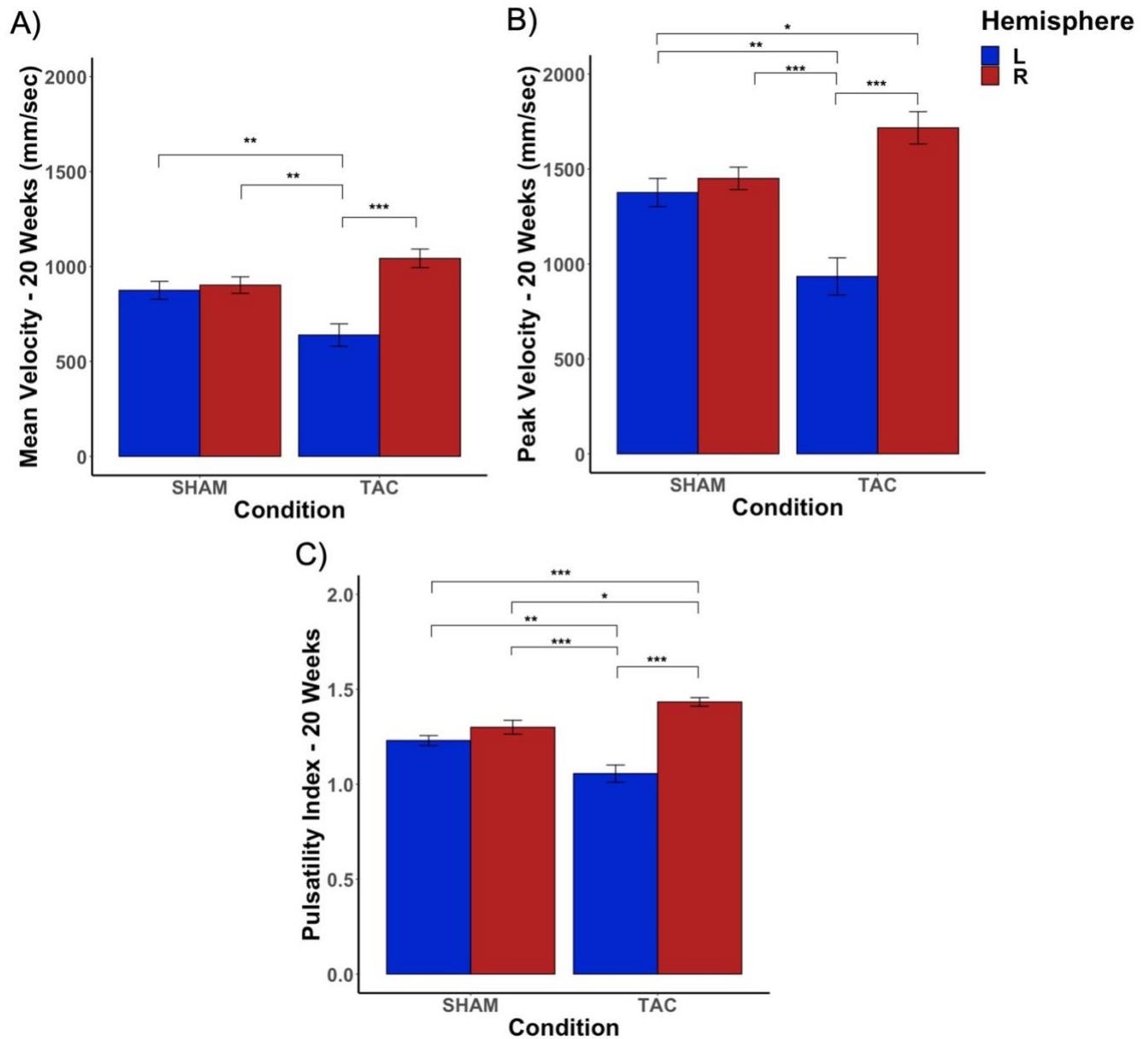


**Figure 4: TAC Lowers Blood Flow Velocities in the Left Carotid and Increases Blood Flow Pulsatility in the Right Carotid 20 Weeks Post-Surgery.**

**A)** Mean carotid artery velocity in the right and left common carotid arteries of TAC and SHAM animals. **B)** Peak blood flow velocity in the right and left common carotid arteries of TAC and SHAM animals. **C)** Blood flow pulsatility indices in the right and left common carotid arteries of TAC and SHAM animals. Data displayed as means + SEM, mm/sec- millimeters per second, R- right, L- left, TAC- Transverse aortic constriction, SHAM- sham controls, \* =  $p < 0.05$ , \*\* =  $p < 0.01$ , \*\*\* =  $p < 0.001$ .

At 30 weeks post-surgery, similar patterns as those seen 20 weeks post-surgery were observed, and the left carotid of TAC displayed lower blood flow velocities than either side of SHAM or the right side of TAC, while the right carotid of TAC displayed greater blood flow pulsatility. Specifically, there was a significant main effect of Hemisphere ( $F(1,40)=8.16, p<0.01, \eta_p^2=0.16$ ) and a Condition by Hemisphere ( $F(1,40)=12.84, p<0.001, \eta_p^2=0.24$ ) interaction, but no significant main effect of Condition ( $F(1,40)=3.35, p=0.07, \eta_p^2=0.07$ ) on mean carotid artery velocity. Tukey's post-hoc comparisons of the interaction term showed that left carotid mean velocity of TAC ( $M= 632.0 \pm 83.7$  mm/sec) was significantly lower when compared to the left ( $M= 975.2 \pm 56.8$  mm/sec,  $t(40) = -3.83, p <0.01$ ) and right ( $M= 929.1 \pm 49.1$  mm/sec,  $t(40) = -3.31, p <0.05$ ) of SHAM animals, as well as the right ( $M= 1040.1 \pm 48.9$  mm/sec,  $t(40) = -4.77, p <0.001$ ) within TAC (**Fig. 5A**). Similar results were seen on peak carotid velocities, and there was a significant main effect of Hemisphere ( $F(1,40)=14.60, p<0.001, \eta_p^2=0.26$ ), and a Condition by Hemisphere interaction ( $F(1,40)=15.69, p<0.001, \eta_p^2=0.28$ ), but no significant main effect of Condition ( $F(1,40)=3.95, p=0.054, \eta_p^2=0.09$ ). Post-hoc comparisons of the interaction term showed left carotid peak velocity ( $M= 898.5 \pm 129.2$  mm/sec) in TAC was significantly lower when compared to the left ( $M= 1505.0 \pm 92.9$  mm/sec,  $t(40) = -4.20, p <0.001$ ) and right ( $M= 1490.8 \pm 81.2$  mm/sec,  $t(40) = -4.10, p <0.01$ ) of SHAM animals, as well as the right ( $M=1692.0 \pm 85.2$  mm/sec,  $t(40) = -5.77, p <0.001$ ) within TAC (**Fig. 5B**). Lastly, there was also a significant main effect of Hemisphere ( $F(1,40)=40.25, p<0.001, \eta_p^2=0.50$ ), and a Condition by Hemisphere interaction ( $F(1,40)=22.51, p<0.001, \eta_p^2=0.36$ ), but no significant main effect of

Condition ( $F(1,40)=2.59$ ,  $p=0.115$ ,  $\eta_p^2=0.06$ ) on carotid artery pulsatility. Tukey's post-hoc comparisons of the interaction term showed left carotid artery pulsatility ( $M= 0.98 \pm 0.05$  P.I) in TAC animals was significantly lower than in the left ( $M= 1.22 \pm 0.02$  P.I,  $t(40) = -4.49$ ,  $p < 0.001$ ) and right ( $M= 1.28 \pm 0.02$  P.I,  $t(40) = -5.62$ ,  $p < 0.001$ ) carotids of SHAM animals. Moreover, right carotid pulsatility in TAC ( $M= 1.39 \pm 0.03$  P.I) animals was found to be significantly higher than the left ( $t(40) = 3.34$ ,  $p < 0.01$ ) carotid in SHAM, as well as the left ( $t(40) = 8.22$ ,  $p < 0.001$ ) carotid within TAC (**Fig. 5C**).

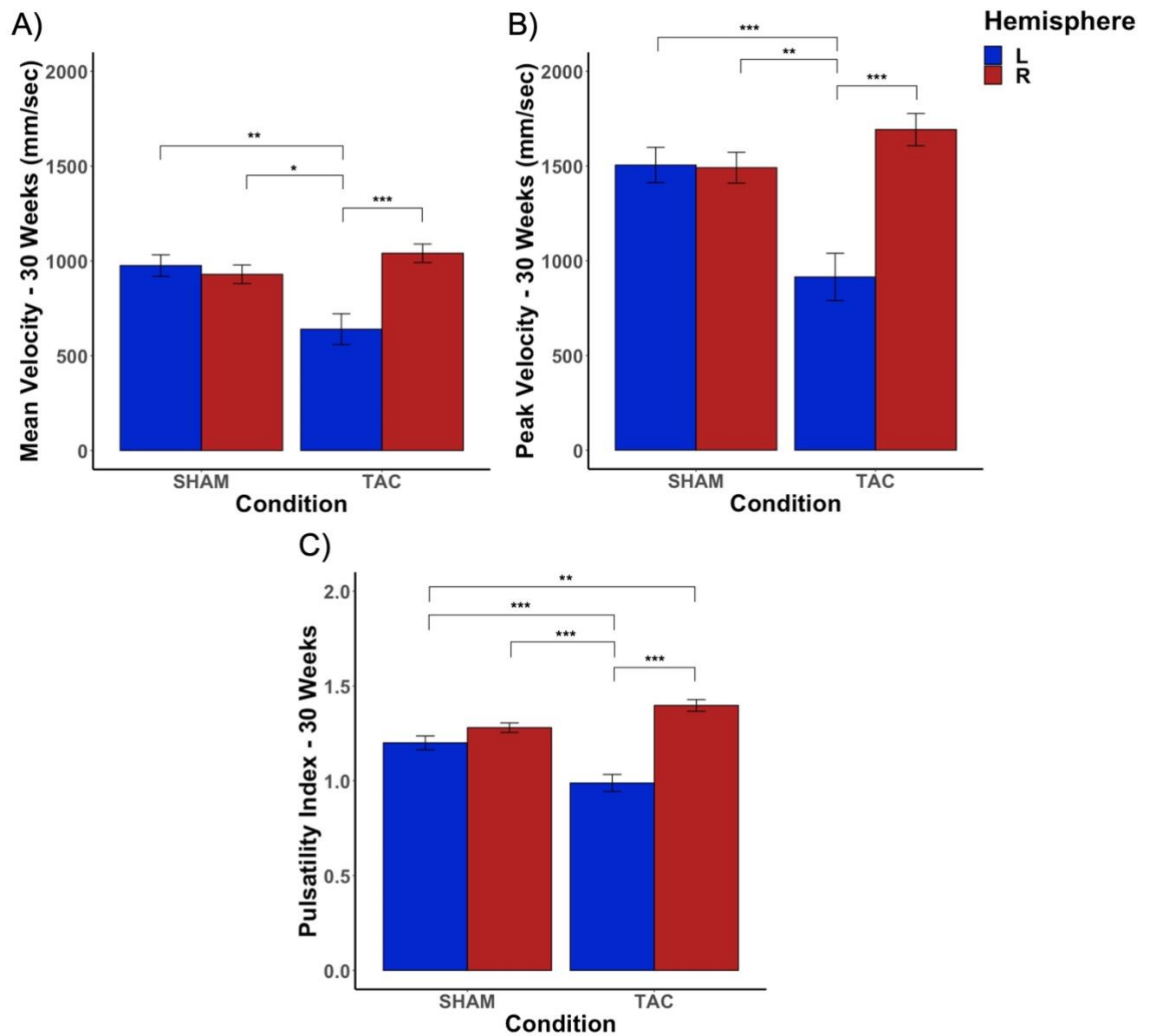


**Figure 5: TAC-Related Changes 30 Weeks Post-Surgery Parallel Those Seen 20 Weeks Post-Surgery.**

**A)** Mean carotid artery velocity in the right and left common carotid arteries of TAC and SHAM animals. **B)** Peak carotid artery velocity in the right and left common carotid arteries of TAC and SHAM animals. **C)** Blood flow pulsatility indices in the right and left common carotid arteries of TAC and SHAM animals. Data displayed as means + SEM, mm/sec- millimeters per second, R- right, L- left, TAC- Transverse aortic constriction, SHAM- sham controls, \* =  $p < 0.05$ , \*\* =  $p < 0.01$ , \*\*\* =  $p < 0.001$ .

Just as it was seen 30 weeks post-surgery, at 40 weeks the left carotid of TAC displayed lower blood flow velocities than either right or left of SHAM or the right of TAC. Meanwhile the right carotid of TAC displayed greater blood flow pulsatility 40 weeks post-surgery than the right and left of SHAM, as well as the left within TAC. As it relates to mean carotid velocity, there were significant main effects of Condition ( $F(1,37)=8.53, p<0.05, \eta_p^2=0.18$ ), Hemisphere ( $F(1,37)=13.07, p<0.001, \eta_p^2=0.26$ ), and Condition by Hemisphere interaction ( $F(1,37)=8.28, p<0.05, \eta_p^2=0.18$ ) on mean carotid artery velocity. Follow up post-hoc comparisons revealed that mean carotid artery velocity was significantly lower in the left carotid of TAC ( $M= 573.0 \pm 69.3$  mm/sec) animals when compared to the left ( $M= 915.6 \pm 47.2$  mm/sec,  $t(37) = -4.05, p <0.01$ ) and right ( $M= 959.1 \pm 71.0$  mm/sec,  $t(37) = -5.57 p <0.001$ ) of SHAM animals, as well as the right ( $M= 956.5 \pm 45.9$  mm/sec,  $t(37) = -4.64, p <0.001$ ) within TAC animals (**Fig. 6A**). Similarly, there were also significant main effects of Condition ( $F(1,37)=9.43, p<0.005, \eta_p^2=0.20$ ), Hemisphere ( $F(1,37)=19.06, p<0.001, \eta_p^2=0.34$ ), and Condition by Hemisphere interaction ( $F(1,37)=10.81, p<0.005, \eta_p^2=0.22$ ) on peak carotid artery velocity. Post-hoc comparisons of the interaction term showed peak carotid artery velocity was lower in the left of TAC ( $M= 794.9 \pm 103.6$  mm/sec) animals when compared the left ( $M= 1442.0 \pm 85.7$  mm/sec,  $t(37) = -4.44, p <0.001$ ) and right ( $M= 1551.7 \pm 131.2$  mm/sec,  $t(37) = -5.19, p <0.001$ ) of SHAM controls, as well as the right ( $M=1573.7 \pm 81.9$  mm/sec,  $t(37) = -5.47, p <0.001$ ) within TAC (**Fig. 6B**). Lastly, when addressing the effects of condition and hemisphere on carotid artery blood flow pulsatility, significant main effects of Condition ( $F(1,37)=7.88, p<0.05, \eta_p^2=0.17$ ), Hemisphere ( $F(1,37)=75.5, p<0.001,$

$\eta_p^2=0.67$ ), and Condition by Hemisphere interaction ( $F(1,37)=45.99, p<0.01, \eta_p^2=0.55$ ) were detected. Tukey's post-hoc comparisons of the interaction term showed that carotid artery pulsatility was significantly lower in the left of TAC ( $M=0.86 \pm 0.04$  P.I) animals when compared to the left ( $M= 1.22 \pm 0.02$  P.I,  $t(37) = -6.70, p <0.001$ ) and right ( $M= 1.29 \pm 0.03$  P.I,  $t(37) = -8.04, p <0.001$ ) of SHAM controls. Moreover, carotid artery pulsatility was significantly higher in the right of TAC ( $M= 1.43 \pm 0.03$  P.I) animals when compared to the left ( $t(37) = 4.21, p <0.001$ ) and right ( $t(37) = 2.84, p <0.05$ ) of SHAM controls, as well as the left ( $t(37) = 11.07, p <0.001$ ) within TAC (**Fig. 6C**). The effects of TAC and SHAM on right and left carotid artery diameter during systole and diastole were also examined at each time point. Overall, independently run 2x2 ANOVA models revealed no significant main effects of Condition, Side, or Condition by Hemisphere interaction on either systolic or diastolic carotid artery diameter at any of time points measured (**Table 2 & 3**). To ensure we addressed the variable of time, within each condition and side, a series of independently run one-way ANOVA models were used to study the effects of time on carotid blood flow, pulsatility index, and artery diameter measures in both, TAC and SHAM animals. Overall, no significant main effects of Time were observed on carotid artery mean velocity, carotid artery peak velocity, carotid artery pulsatility index, or carotid artery diameter, in either TAC or SHAM animals (**Table 4 & Table 5**) (**Fig. 7 & 8**).

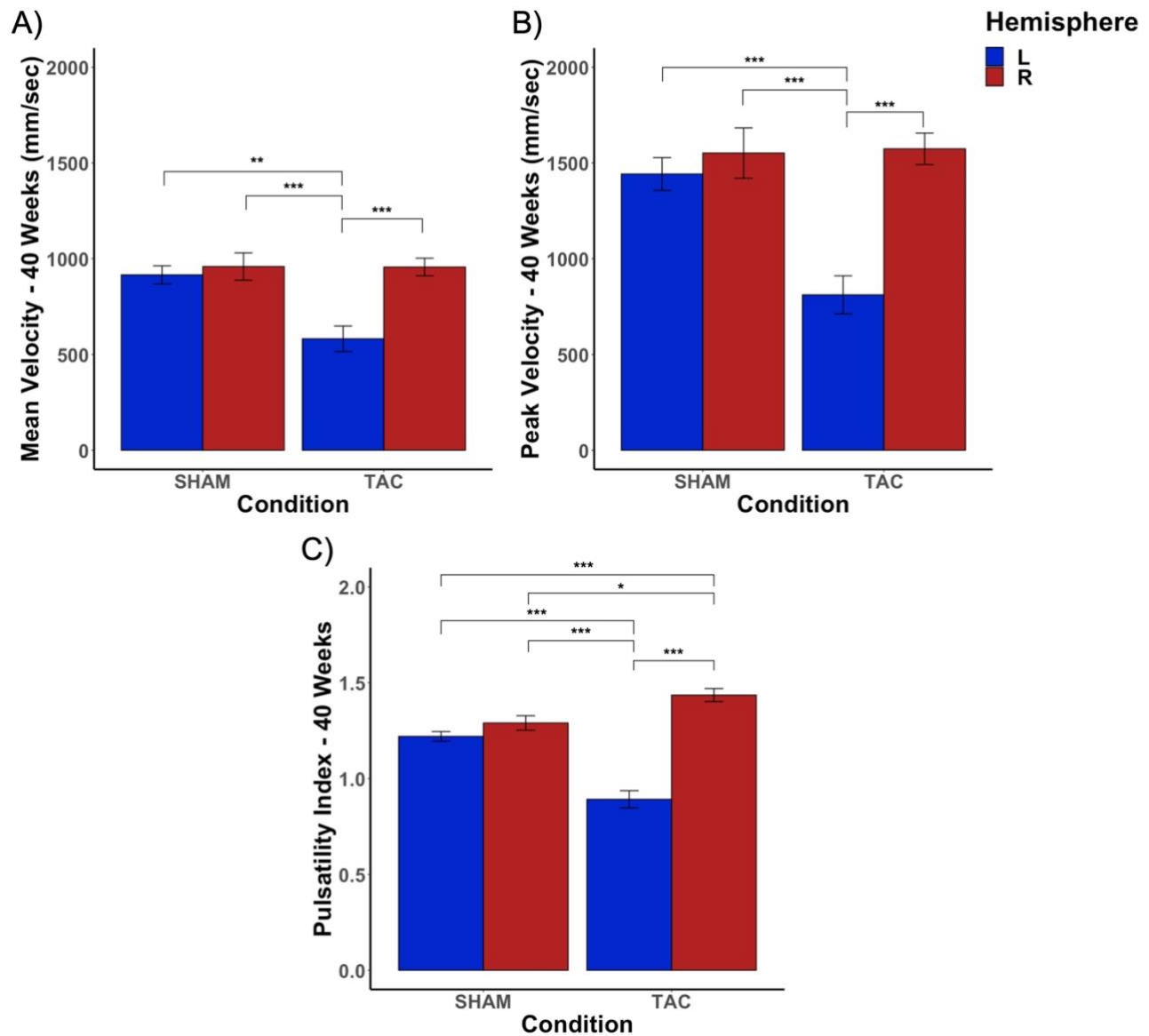


**Figure 6: TAC-Related Changes in Carotid Artery Velocities and Pulsatility Remain Steady 40 Weeks Post-Surgery.**

A) Mean blood flow velocity of the right and left common carotid arteries of TAC and SHAM. B) Peak blood flow velocity of the right and left common carotid arteries of TAC and SHAM. C) Blood flow pulsatility indices in the right and left common carotid arteries of TAC and SHAM. Data displayed as means + SEM, mm/sec-millimeters per second, R- right, L- left, TAC- Transverse aortic constriction, SHAM-sham controls, \* =  $p < 0.05$ , \*\* =  $p < 0.01$ , \*\*\* =  $p < 0.001$ .

**Table 2: Effects of Condition and Hemisphere on systolic artery diameter.**

	20 weeks			30 weeks			40 weeks		
	F ( <i>df</i> )	<i>p</i>	$\eta_p^2$	F ( <i>df</i> )	<i>p</i>	$\eta_p^2$	F ( <i>df</i> )	<i>p</i>	$\eta_p^2$
Condition	(1,40)=2.80	0.60	0.007	(1,40)=0.00003	0.99	0.00	(1,35)=0.43	0.51	0.012
Side	(1,40)=1.67	0.20	0.040	(1,40)=3.44	0.07	0.079	(1,35)=3.08	0.08	0.081
Condition*Side	(1,40)=0.51	0.47	0.013	(1,40)=0.744	0.39	0.018	(1,35)=1.66	0.20	0.045

**Table 3: Effects of Condition and Hemisphere on diastolic artery diameter.**

	20 weeks			30 weeks			40 weeks		
	F ( <i>df</i> )	<i>p</i>	$\eta_p^2$	F ( <i>df</i> )	<i>p</i>	$\eta_p^2$	F ( <i>df</i> )	<i>p</i>	$\eta_p^2$
Condition	(1,40)=0.50	0.48	0.013	(1,40)=0.0006	0.98	0.00	(1,35)=0.064	0.80	0.002
Side	(1,40)=0.36	0.55	0.009	(1,40)=0.23	0.63	0.006	(1,35)=0.59	0.44	0.017
Condition*Side	(1,40)=0.75	0.39	0.018	(1,40)=0.35	0.55	0.009	(1,35)=0.14	0.70	0.004

**Table 4: Effects of Time on carotid artery hemodynamics.**

	Mean Velocity			Peak Velocity			Pulsatility Index		
	F (df)	p	$\eta p^2$	F (df)	p	$\eta p^2$	F (df)	p	$\eta p^2$
SHAM-RCCA	(2,27)=0.26	0.77	0.019	(2,27)=0.28	0.75	0.021	(2,27)=0.08	0.91	0.007
SHAM-LCCA	(2,27)=0.99	0.38	0.069	(2,27)=0.57	0.56	0.041	(2,27)=0.26	0.76	0.019
TAC-RCCA	(2,32)=1.00	0.37	0.059	(2,32)=0.79	0.45	0.048	(2,32)=0.54	0.58	0.033
TAC-LCCA	(2,31)=0.20	0.81	0.013	(2,31)=0.33	0.71	0.021	(2,31)=3.18	0.055	0.17

**Note:** RCCA- right common carotid artery, LCCA- left common carotid artery, TAC- transverse aortic constriction, SHAM- sham controls.

**Table 5: Effects of Time on carotid artery diameter.**

	Diameter - Systole			Diameter - Diastole		
	F (df)	p	$\eta p^2$	F (df)	p	$\eta p^2$
SHAM-RCCA	(2,27)=0.40	0.67	0.029	(2,27)=0.43	0.64	0.031
SHAM-LCCA	(2,27)=0.68	0.51	0.059	(2,27)=0.35	0.70	0.026
TAC-RCCA	(2,32)=0.46	0.65	0.027	(2,32)=0.46	0.63	0.028
TAC-LCCA	(2,30)=0.02	0.98	0.001	(2,30)=0.06	0.93	0.005

**Note:** RCCA- right common carotid artery, LCCA- left common carotid artery, TAC- transverse aortic constriction, SHAM- sham controls.

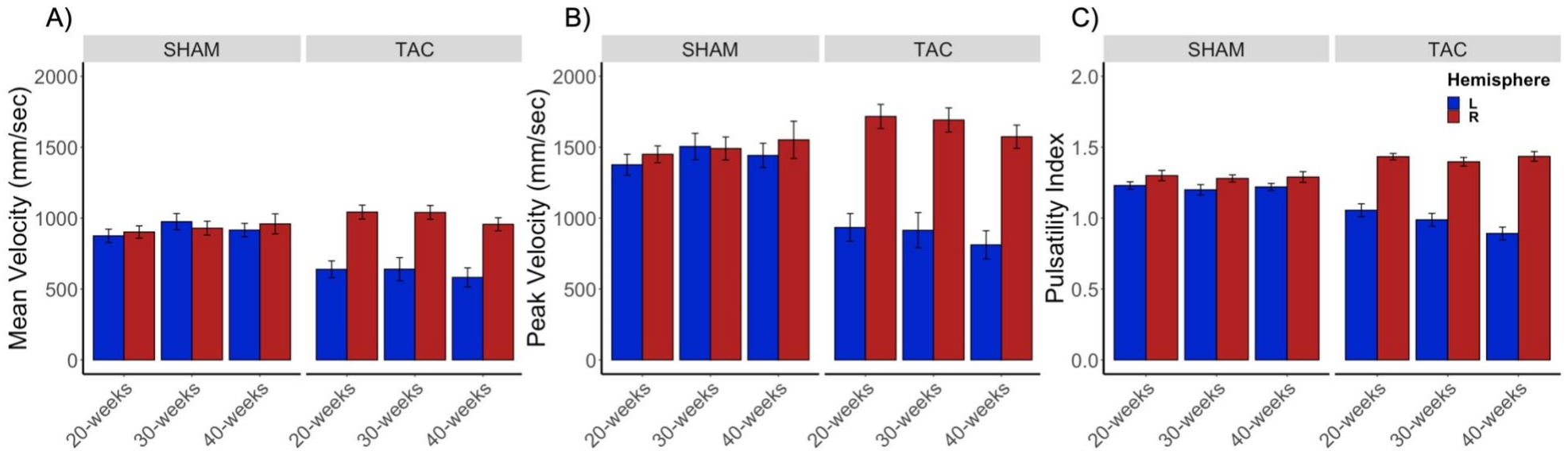


**Figure 7: Carotid Artery Hemodynamics in TAC do not Worsen with Time.**

TAC and SHAM carotid artery hemodynamics by hemisphere at 20-, 30-, and 40 weeks post-surgery. **A)** Mean carotid artery blood flow velocity. **B)** Peak carotid artery blood flow velocity. **C)** Carotid artery blood flow pulsatility. mm/sec- millimeters per second, TAC- Transverse aortic constriction, SHAM- sham controls, R- right, L- left. Data displayed as means + SEM.

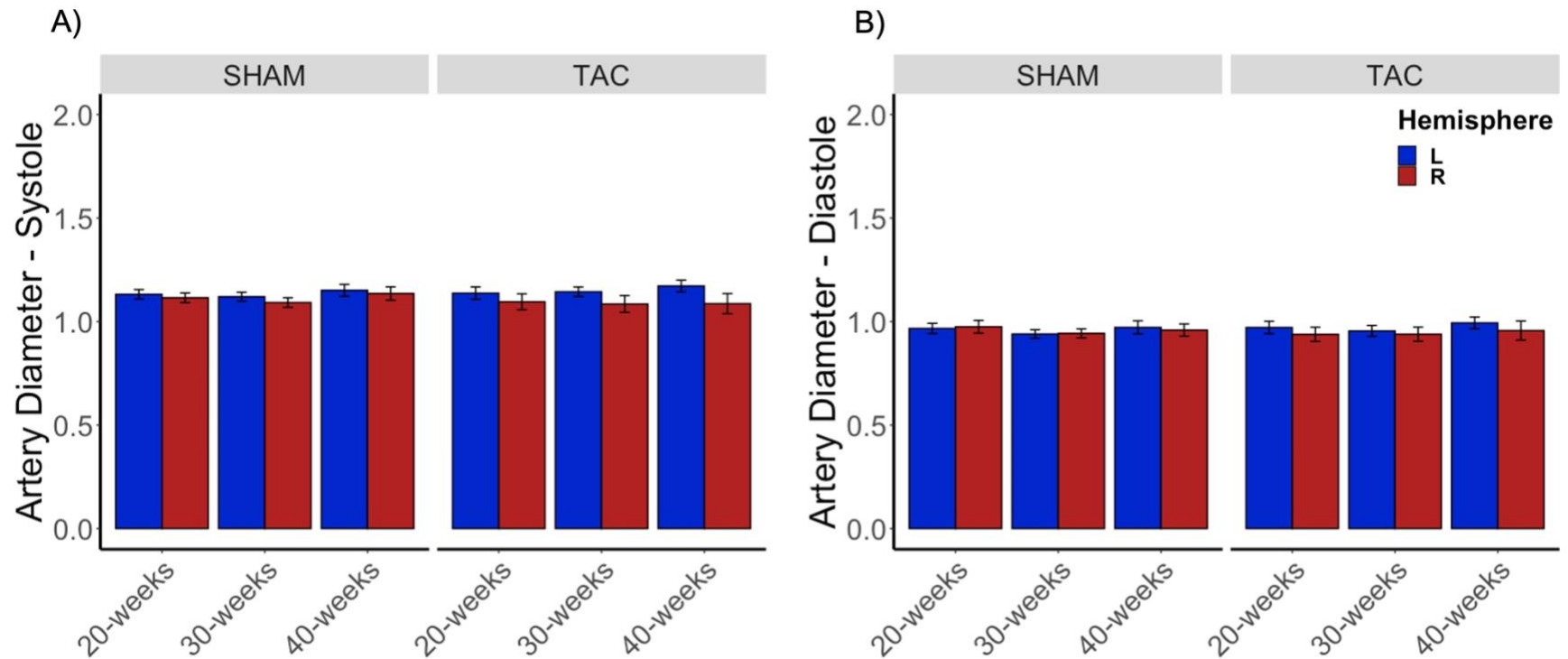


**Figure 8: Carotid Artery Diameters in TAC do Not Change with Time.**

TAC and SHAM peak systolic and diastolic artery diameters by hemisphere at 20-, 30-, and 40 weeks post-surgery. **A)** Carotid artery diameter during peak systole. **B)** Carotid artery diameter during peak diastole. TAC- Transverse aortic constriction, SHAM- sham controls, R- right, L- left. Data displayed as means + SEM.

### Within Condition Sex Differences in Carotid Artery Hemodynamics

At each time point within each condition, we performed an exploratory analysis to assess sex differences in carotid artery hemodynamics and diameter. First, because Shapiro-Wilk's test of normality revealed deviations in the assumption of normality for a specific subset of outcomes and time points in male TAC animals, potential sex differences in the left and right carotid of TAC animals were compared either with independent samples t-test when test assumptions were met, or with the non-parametric Mann-Whitney U test when assumptions were violated. First, for all time points, no significant differences in left carotid hemodynamics or artery diameter between male TAC and female TAC were observed (**Fig. 9A**). For right carotid artery velocities in TAC animals, no significant sex differences were observed at 20 weeks. However, there were sex differences in mean velocity at 30- ( $M=1155.9\pm 91.0$  v.  $M=957.4\pm 28.9$ ,  $t(10)=2.39$ ,  $p<0.05$ ,  $d=1.40$ ) and 40- ( $M=1056.9\pm 872.9$  v.  $M=872.9\pm 64.39$ ,  $t(9)=2.43$ ,  $p<0.05$ ,  $d=1.47$ ) weeks, with female TAC animals displaying higher velocities than male TAC animals (**Fig. 9A**). These sex differences were also seen in peak velocities at 30- ( $M=1896.2\pm 145.6$  v.  $M=1546.1\pm 65.0$ ,  $t(10)=2.43$ ,  $p<0.05$ ,  $d=1.42$ ), and 40- ( $M=1766.6\pm 135.3$  v.  $M=1413.0\pm 255.0$ ,  $t(9)=2.77$ ,  $p<0.05$ ,  $d=1.68$ ) weeks (**Fig. 9A**). There were also sex differences in artery diameters at 20 weeks, and TAC males were observed to have significantly higher right systolic ( $M=1.19\pm 0.073$  v.  $M=1.06\pm 0.095$ ,  $U=4.5$ ,  $p<0.05$ ,  $r=0.33$ ) and right diastolic carotid artery diameter ( $M=1.02\pm 0.074$  v.  $M=0.89\pm 0.097$ ,  $U=4.0$ ,  $p<0.05$ ,

$r=0.33$ ) when compared to TAC females (**Fig. 9B**). However, these sex differences were not present at 30- and 40 weeks post- surgery.

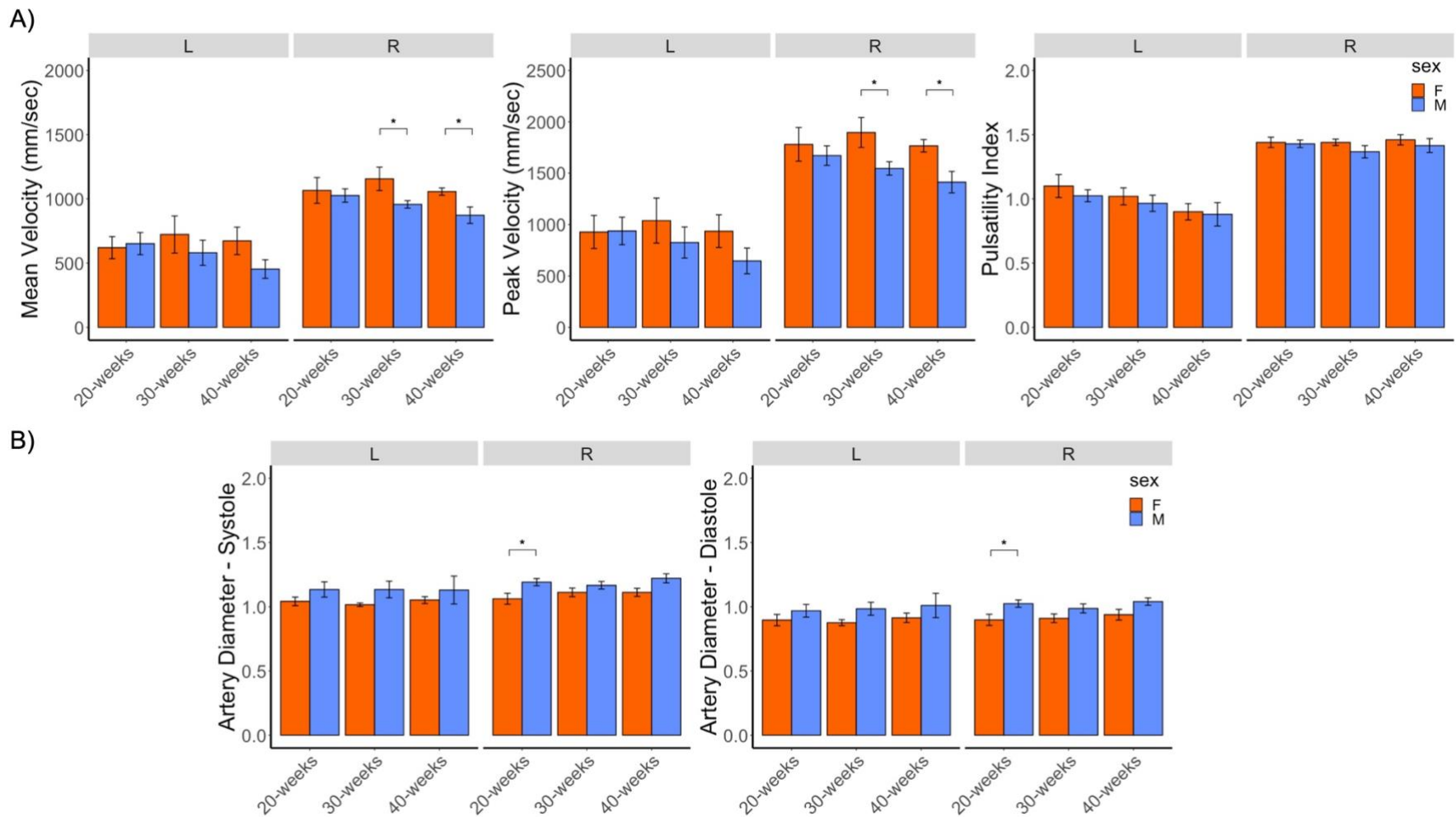


**Figure 9: Sex Dimorphisms in Carotid Artery Velocities in TAC are Constrained to the Right Hemisphere and Present as Early as 30-Weeks Post-Surgery.**

**A)** TAC hemodynamics by hemisphere and sex at 20-, 30-, and 40 weeks post-surgery. **B)** TAC peak systolic and diastolic artery diameters by hemisphere and sex at 20-, 30-, and 40 weeks post-surgery. Data displayed as means + SEM, mm/sec = millimeters per second, TAC- transverse aortic constriction, M- males, F- females, R- right, L- left, \* =  $p < 0.05$ .

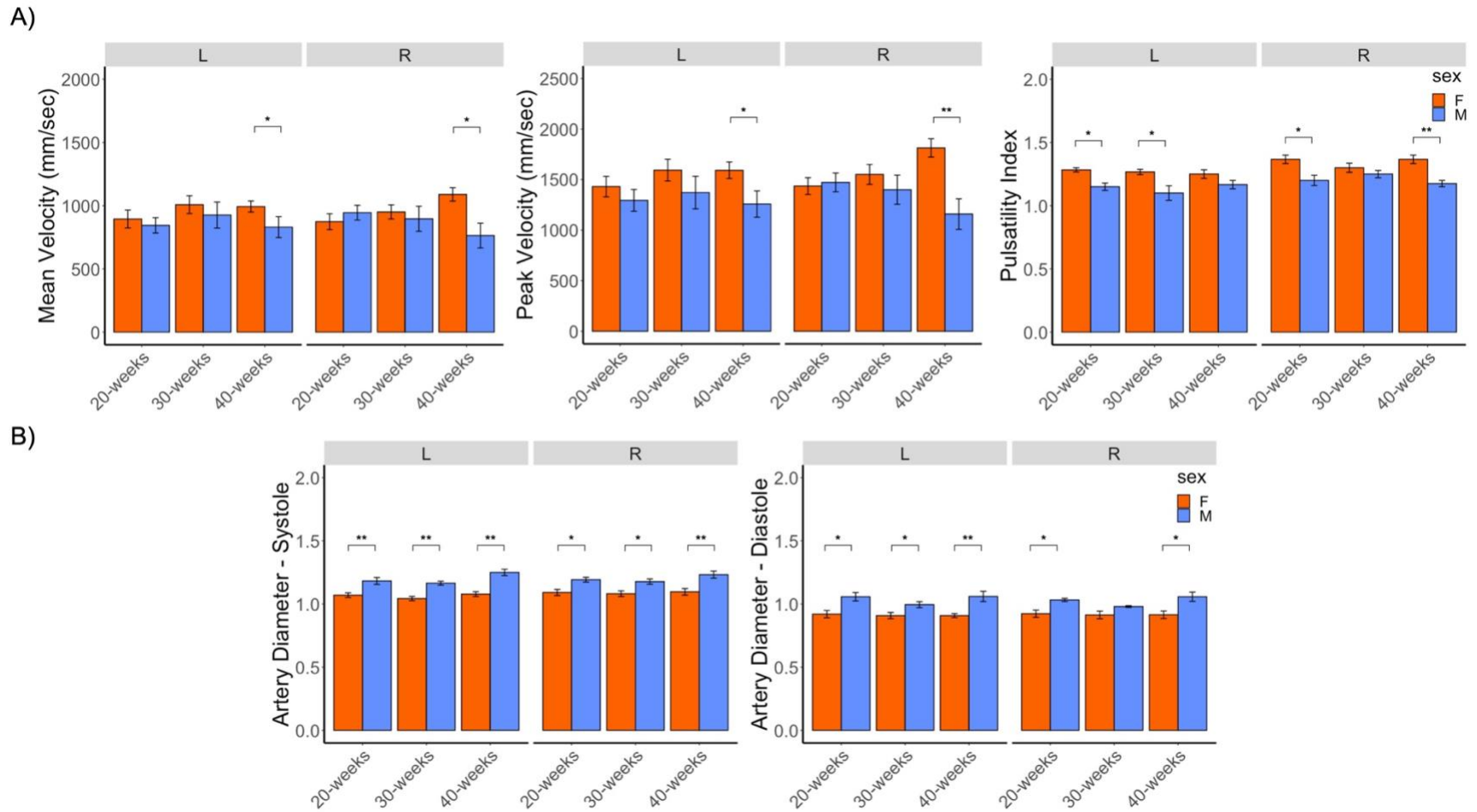


**Figure 10: Sex Dimorphisms in Carotid Artery Velocities in SHAM are Present in the Right and Left Hemisphere but Appear Later in Time Than TAC.**

**A)** SHAM hemodynamics by hemisphere and sex at 20-, 30-, and 40 weeks post-surgery. **B)** SHAM peak systolic and diastolic artery diameters by hemisphere and sex at 20-, 30-, and 40 weeks post-surgery. Data displayed as means + SEM, mm/sec = millimeters per second, SHAM- sham controls, M- males, F- females, R- right, L- left, \* =  $p < 0.05$ , \*\* =  $p < 0.01$

These analyses were also carried out separately in SHAM controls to address possible sex differences in a non-diseased state. To this end, no deviations in the assumption of normality were detected in either the right or left blood flow velocities and artery diameters of male and female SHAM animals. However, deviations in the assumption of normality were detected in both, the right and left blood flow pulsatility indices of both, male and female SHAM animals. As such, independent samples t-tests were used to address bilateral sex differences in SHAM blood flow velocity and artery diameter, while the Mann-Whitney U test was used to do the same in relation to blood flow pulsatility. In this context, sex differences in the left carotid were addressed, and independent samples t-test showed significant sex differences in left mean ( $M=993.3\pm 43.3$  v.  $M=798.9\pm 66.6$ ,  $t(8)=2.57$ ,  $p<0.05$ ,  $d=1.65$ ) and peak ( $M=1592.4\pm 81.5$  v.  $M=1216.3\pm 101.2$ ,  $t(8)=2.90$ ,  $p<0.05$ ,  $d=1.87$ ) carotid velocities at 40 weeks, but not at 20-, or 30 weeks post-surgery, with females, on average, displaying higher blood flow velocities than males (**Fig. 10A**). As it pertains to left blood flow pulsatility, there were significant sex differences at 20- ( $M=1.28\pm 0.01$  v.  $M=1.15\pm 0.02$ ,  $U=23.0$ ,  $p<0.05$ ,  $r=0.09$ ) and 30- ( $M=1.26\pm 0.02$  v.  $M=1.15\pm 0.05$ ,  $U=21.0$ ,  $p<0.05$ ,  $r=0.75$ ) weeks, with females displaying higher blood flow pulsatility than males. Sex differences in left carotid blood flow pulsatility were not detected 40 weeks post-surgery (**Fig. 10A**). Significant sex differences were also seen in left systolic artery diameter at 20- ( $M=1.07\pm 0.01$  v.  $M=1.18\pm 0.02$ ,  $t(8)=-3.58$ ,  $p<0.01$ ,  $d=-2.31$ ), 30- ( $M=1.04\pm 0.01$  v.  $1.16\pm 0.01$ ,  $t(8)=-4.94$ ,  $p<0.005$ ,  $d=-3.19$ ), and 40 ( $M=1.07\pm 0.01$  v.  $M=1.25\pm 0.02$ ,  $t(7)=-5.26$ ,  $p<0.005$ ,  $d=-3.71$ ) weeks, with females displaying lower peak systolic artery diameters than males (**Fig. 10B**). A similar

pattern was observed with peak left diastolic artery diameter at 20- ( $M=0.92\pm0.02$  v.  $M=1.05\pm0.03$ ,  $t(8)=-3.05$ ,  $p<0.05$ ,  $d=-1.97$ ), 30- ( $M=0.90\pm0.02$  v.  $M=0.99\pm0.02$ ,  $t(8)=-2.41$ ,  $p<0.05$ ,  $d=-1.55$ ), and 40- ( $M=0.90\pm0.01$  v.  $M=1.06\pm0.04$ ,  $t(7)=-4.31$ ,  $p<0.005$ ,  $d=-3.05$ ) weeks, with females displaying lower peak diastolic diameters when compared to males (**Fig. 10B**). Meanwhile, within the right carotid of SHAM animals significant sex differences in carotid artery blood flow and pulsatility were also detected. Specifically, significant differences in mean ( $M=1089.2\pm53.16$  v.  $764.0\pm97.9$ ,  $t(8)=3.18$ ,  $p<0.5$ ,  $d=2.05$ ) and peak ( $M=1813.6\pm90.6$  v.  $M=1158.9\pm151.6$ ,  $t(8)=3.96$ ,  $p<0.005$ ,  $d=2.56$ ) right carotid blood flow velocities were observed at 40 weeks, with females, on average, displaying higher blood flow velocities than males (**Fig. 10A**). No significant sex differences in blood flow velocities were detected at 20-, and 30 weeks post-surgery. When it comes to right blood flow pulsatility, there were significant sex differences at 20- ( $M=1.36\pm0.03$  v.  $M=1.20\pm0.04$ ,  $U=22.5$ ,  $p<0.05$ ,  $r=0.87$ ) and 40- ( $M=1.36\pm0.03$  v.  $M=1.17\pm0.02$ ,  $U=24.0$ ,  $p<0.05$ ,  $r=1.0$ ) weeks, with females displaying higher blood flow pulsatility than males. Sex differences in left carotid blood flow pulsatility were not detected 30-weeks post-surgery (**Fig. 10A**). Significant sex differences were also seen in peak right systolic artery diameter at 20- ( $M=1.09\pm0.03$  v.  $M=1.19\pm0.01$ ,  $t(8)=-2.95$ ,  $p<0.05$ ,  $d=-1.90$ ), 30- ( $M=1.08\pm0.02$  v.  $1.17\pm0.02$ ,  $t(8)=-2.95$ ,  $p<0.05$ ,  $d=-1.90$ ), and 40- ( $M=1.09\pm0.02$  v.  $M=1.23\pm0.02$ ,  $t(8)=-3.43$ ,  $p<0.01$ ,  $d=-2.21$ ) weeks, with females displaying lower peak systolic artery diameters than males (**Fig. 10B**). Further, sex differences in peak right diastolic artery diameter within SHAM were observed at 20- ( $M=0.92\pm0.02$  v.  $M=1.03\pm0.01$ ,  $t(8)=-2.95$ ,  $p<0.05$ ,  $d=-1.90$ ), and 40- ( $M=0.91\pm0.03$

v.  $M=1.05\pm 0.03$ ,  $t(8)=-3.02$ ,  $p<0.01$ ,  $d=-1.95$ ) weeks, with females displaying lower peak diastolic diameters when compared to males (**Fig. 10B**).

## **Discussion**

The primary purpose of this study was to expand on the acute timescales traditionally found within the TAC literature and characterize the hemodynamic phenotype of TAC animals at 20-, 30-, and 40 weeks post-surgery. We found that throughout the time-points measured, the left carotid of TAC animals displayed lower blood flow velocities than the right of TAC, and either the right or left of SHAM controls. On the other hand, blood flow pulsatility was highest in the right carotid of TAC animals when compared not only to the left within TAC, but also the left and right carotids of SHAM controls. Contrary to our initial hypotheses, these TAC-related changes in right carotid hemodynamics did not worsen with time. Yet, we did find that sex dimorphisms in carotid artery velocities occurred 10 weeks earlier in TAC animals than in SHAM controls. To our knowledge, this is the first study to focus on TAC from a chronic point of view and employ time points well beyond 15 weeks post-TAC surgery. As such, this work contributes to the general understanding of TAC as a model of chronic cardiovascular disease, and when put in the context of the existing literature, facilitate our understanding of how changes in carotid hemodynamics may influence cerebral blood flow and perfusion<sup>46</sup>

Chronic brain hypoperfusion is widely regarded as a primary mechanism by which cardiovascular disease may contribute to cognitive decline and give rise to neurodegenerative conditions such as vascular dementia (VaD)<sup>16, 44, 58</sup>. Data from human studies suggest hypoperfusion may be the result of a complex interplay

between low arterial compliance, chronic mechanical stress, and limited tissue perfusion<sup>24</sup>. Yet, most animal models of VaD ignore blood flow pulsatility and rely on arterial constriction to lower blood flow supply and induce hypoperfusion<sup>25</sup>. Although the TAC model has been traditionally employed to study heart failure and hypertension<sup>113</sup>, recent frameworks propose this model may be leveraged to better understand the consequences of brain hypoperfusion given its unique opposing bilateral hemodynamic phenotype<sup>25</sup>. Specifically, because the ligation in TAC is placed between the brachiocephalic and left common carotid arteries, this model leads to sustained but pulsatile blood flow to the right carotid artery and simultaneously lowers blood flow through the left carotid<sup>25</sup>. Recent work highlights this TAC-specific bilateral carotid blood flow phenotype can differentially affect perfusion to the cerebral hemispheres<sup>46</sup> (i.e., both hemispheres are hypoperfused, but the right is more severely hypoperfused). Thus, TAC may be of use to better understand whether the source of hypoperfusion differentially influences the mechanisms that are dysregulated in neurodegeneration<sup>116</sup>. However, because this model has not been traditionally used in the context of neurodegeneration, the longitudinal carotid hemodynamic responses of the model have not been characterized<sup>25</sup>.

#### *Longitudinal characterization of carotid artery hemodynamics in response to TAC*

Because most studies assessing brain hemodynamics following TAC have employed acute (1-day, and 7-day post-TAC)<sup>111</sup>, or pre-and post- models<sup>39, 46, 116</sup>, there is little data on hemodynamic responses to TAC from a chronic point of view. Therefore, we determined if carotid artery hemodynamics differed between conditions (TAC v. SHAM) and hemisphere (right v. left) at each time point. As

expected, mean and peak carotid velocities were lower in the left carotid of TAC animals when compared to the right carotid within TAC animals at every time point. Similarly, at every time point, mean and peak carotid velocities in the left carotid of TAC animals were lower than the right and left carotids of SHAM animals, respectively. However, an intriguing finding of this study was that, except for peak velocity at 20 weeks, mean and peak right carotid velocities of TAC did not differ when compared to the right and left carotid velocities of SHAM animals. This finding is in contrast to existing studies where at 7-days post-TAC surgery, carotid blood flow is reported to be higher than that of SHAM animals<sup>111</sup>, and lower at 3- and 8 weeks post-TAC surgery<sup>39</sup>. The temporal windows of the present study extend well beyond those reported previously and highlight the need to better characterize not only the acute and longitudinal effects, but also the intermediary (e.g., 8-20 weeks post-surgery) effects of TAC on carotid blood flow.

Importantly, while carotid velocities did not differ between the right of TAC and right/left of SHAM, we note that measures of carotid pulsatility were statistically higher in the right of TAC animals when compared to not only the left carotid within TAC, but also the right and left carotids of SHAM animals, respectively. This is in line with existing literature showing arterial pulse pressure is highest in the right carotid of TAC animals when compared to the right and left of SHAM animals<sup>46</sup> and underscores the notion that losses in arterial compliance may be greatest in the right carotid of TAC. This is particularly relevant given that losses in arterial compliance in cardiovascular disease may be a key mechanism by which cardiovascular disease may promote neurodegeneration<sup>25, 73</sup>. In fact, a recent study by De Montgolfier and

colleagues found that the divergent bilateral carotid hemodynamic response in TAC (6 weeks post-surgery) can lead to hypoperfusion in both hemispheres, but to a greater degree in the right hemisphere<sup>46</sup>. That is, while lower blood flow supply to the left hemisphere of the brain leads to hypoperfusion, the pulsatility associated with the right carotid and cerebral blood flow leads to greater levels of hypoperfusion even though the amount of blood being supplied is not limited. Moreover, when compared to the left hemisphere, the right hemisphere of TAC animals also displays greater deficits in blood brain barrier integrity, higher adverse microvascular events (e.g., microbleeds), and greater losses in microvascular density<sup>46</sup>. Therefore, the higher sustained pulsatility observed in this study may be accompanied by sustained hypoperfusion, cerebral microvascular stress, and neurovascular damage that is more pronounced in the right hemisphere than the left.

We also addressed systolic and diastolic artery diameter in TAC and SHAM animals. Overall, we did not find any difference within TAC or between TAC or SHAM in either peak systolic or peak diastolic carotid artery diameter. While there is little work done on this, because TAC can lead to high pulse pressure in the right carotid and low pulse pressure on the left carotid<sup>46</sup>, it is possible that the lack of differences are a reflection of the low arterial compliance and impaired vasodilatory responses on the right and insufficient mechanical stimulus from low blood flow in the left to induce vasodilation<sup>117</sup>. Although not fully understood, the lack of differences in artery diameters between SHAM controls and TAC may be partially explained by biological aging. Indeed, losses in arterial compliance are common even in healthy aging<sup>118</sup>, and given that the earliest time point of this study was done in

what may be considered late middle-age for the rat<sup>119</sup>, it is possible that our SHAM controls fail to display normal vasodilatory responses due to biological aging. This hypothesis should be extensively studied and was not directly addressed by the current study.

We were also interested in time as a possible factor that could influence the hemodynamic responses to TAC. As such, we set out to test whether carotid artery velocities, pulsatility, and systolic and diastolic diameter were affected by time and found that time did not influence any of our measured outcomes in either TAC or SHAM animals. While surprising at first, in acute time windows, the TAC hemodynamic phenotype has been reported to have a rapid onset with little change after being developed<sup>39, 111</sup>. In support of this, a study by Poulet and colleagues found that the divergent cerebral blood flow phenotype of TAC can develop as soon as 1 day post-surgery and remain largely unchanged 7 days post-surgery<sup>111</sup>. This same pattern has been reported in a mouse model of Alzheimer's Disease with TAC-induced brain hypoperfusion, where the bilateral hemodynamic phenotype is present 3 weeks post-TAC, and largely unchanged 8 weeks post-TAC<sup>39</sup>. Therefore, although contrary to our original hypothesis, our data are in line with acute studies, and may indicate that the TAC phenotype has a rapid onset that does not worsen with time.

#### *Sex differences in carotid artery hemodynamics and artery diameter*

Historically, cardiovascular disease has been studied within the context of male physiology and disease<sup>120</sup>, despite the fact that the prevalence of cardiovascular disease is greater in older women than older men<sup>121</sup>. Nevertheless, sex disparities in cardiovascular health is a rapidly expanding field of research<sup>122, 123</sup> and we performed

an exploratory analysis to determine whether there were sex differences in right and left carotid hemodynamics and artery diameter within TAC and SHAM. First, in TAC, we found that sex differences in carotid blood flow velocities and artery diameter were constrained to the right hemisphere and not present on the left side. Specifically, right mean and peak carotid velocities were higher in females than males at 30- and 40 weeks post-surgery, while peak systolic and diastolic artery diameters were higher in females than males at 40 weeks. Meanwhile, in SHAM animals, we also found sex differences in systolic and diastolic artery diameters 20-, 30-, and 40 weeks post-surgery, as well as in peak and mean carotid artery velocities at 40 weeks in both the right and left sides. These findings provide novel insight into possible chronic sex differences in bilateral carotid hemodynamics in both TAC and SHAM. The most intriguing finding was that sex differences in mean and peak carotid blood flow velocities in TAC were present at 30- and 40 weeks post-surgery whereas these differences were only present at 40 weeks post-surgery in SHAM controls. The sex differences in artery diameter were largely unsurprising, given that independent studies have previously shown female rat arteries have a smaller diameter than males<sup>124, 125</sup>. However, because the right side of TAC showcased the sex differences in blood flow velocities 10 weeks earlier than SHAM controls, this suggests that higher blood flow velocities and associated pulsatility may speed up the development of sex dimorphisms in vascular health. In support of this interpretation, recent work has found the cerebral vasculature of female Sprague-Dawley rats has different structural properties than male counterparts such as lower content of vascular smooth muscle cells, higher collagen deposits, and thicker internal elastic lamina<sup>126</sup>.

Moreover, these structural differences seem to impair the contractile capabilities of large cerebral arteries, lower arterial distensibility, and elevate the myogenic response, which translate into impaired functional capabilities in females when compared to males<sup>126</sup>. As such, female animals may have a reduced ability to cope with sustained higher and possibly pulsatile blood flow velocities over time, and the early manifestation of sex dimorphisms in blood flow seen in TAC could signify an early failing vasculature. Moreover, because impaired vascular function may facilitate sex differences in the development of dementia later in life<sup>127, 128</sup>, it is also possible that an early failing vasculature in female TAC could facilitate the development of cognitive impairment and, over time, dementia. However, because this study did not employ and vascular structural or functional assays, nor any behavioral assays to assess cognition (e.g., Morris Water Maze), this remains an interpretation that future work should explore further. Nevertheless, because within the TAC literature, only 66% of studies have used male animals exclusively, and only 5% included female animals for sex comparison<sup>113</sup>, our study adds valuable information to a heavily understudied topic in this animal model of cardiovascular disease.

### Study Limitations

Although this study contributes to our growing understanding of TAC and how it may influence brain blood flow, there were several limitations. Specifically, the number of animals that were lost due to poor ultrasound imaging led to a low sample size and limited our ability to address the effects of time, condition, and hemisphere in the same model. Additionally, while we were able to characterize the

hemodynamic changes in TAC and SHAM, our study did not determine if these were coupled with structural and functional changes within the carotid arteries themselves. Because of this, we are unable to fully elucidate the mechanisms within the arteries that are being influenced by TAC and the ensuing divergent bilateral blood flow phenotype. As such, more work is needed to create a comprehensive understanding of the TAC hemodynamic phenotype and the possible implications it may carry towards neurovascular integrity. Despite these limitations, this study is among few to have extended the TAC model beyond 15 weeks, and to our knowledge, the first one to characterize the bilateral carotid hemodynamic response at 20-, 30-, and 40 weeks post-surgery. Moreover, it also included males and females and allowed for the exploration of possible sex differences in at all time points between a diseased (TAC) and a healthy (SHAM) state.

### Conclusion

In summary, we report that despite being primarily used as an acute model, the TAC model can also be extended into longer timescales to study chronic cardiovascular disease and its influence on brain blood flow and perfusion. We found that the hemodynamic changes reported in acute TAC models are sustained up to 40 weeks post-surgery, and time does not worsen or dampen these TAC-related changes. These findings support the view that while the onset of hemodynamic changes may be quick after TAC surgery, the phenotype is stable over time. Of note, although we found that there were similar blood flow velocities between the right carotid of TAC animals and the right and left carotids of SHAM animals, the right carotid of TAC animals consistently displayed higher blood flow pulsatility. This sustained pulsatility

in the right carotid of TAC animals helps explain why the right cerebral hemisphere of TAC animals is more hypoperfused than the left hemisphere despite not facing a physical limitation in blood flow. Therefore, while speculative, accrued pulsatility leading to end-organ damage may cause greater disruption in neurovascular coupling than lowering cerebral blood flow. Moreover, we also found sex differences in carotid artery velocities that were detected earlier in TAC animals than SHAM animals, which suggests TAC may accelerate the presence of age-related sex dimorphisms in cardiovascular disease.

## Chapter 3: Glucose Transport, Oxidation, and Mitochondrial Quality Control in Transverse Aortic Constriction.

### Chapter Overview

Although the rodent model of transverse aortic constriction (TAC) leads to whole brain hypoperfusion, there is compelling evidence showing the severity of this hypoperfusive phenotype is highest in the right hemisphere of the TAC brain<sup>46</sup>. Because TAC is characterized by divergent bilateral carotid blood flow responses (e.g., low left carotid blood flow and higher pulsatile right carotid blood flow), hemispheric differences in cerebral hypoperfusion may suggest that the downstream consequences of hypoperfusion may differ based on the mechanisms causing the hypoperfusion (e.g., limited blood flow v. pulsatile blood flow). In this context, human studies show low glucose metabolism goes hand-in-hand with brain hypoperfusion<sup>65</sup>. In the brain, glucose metabolism is highly dependent not only on blood flow, but also on the expression of glucose transporters (GLUT) and the ability of neural mitochondria to oxidize glucose<sup>26</sup>. As such, this study aimed to determine whether 40 weeks post-surgery glucose oxidation (assessed via liquid-phase respiration), expression of glucose transport proteins, and expression of proteins that regulate mitochondrial networks (e.g., mitochondrial fission, fusion, and the unfolded protein response) differed between the right and left hemisphere of TAC animals and compared to SHAM controls. This study specifically targeted the hippocampus given the extensive literature showing it is a subcortical structure that is particularly susceptible to neurodegenerative diseases<sup>5, 84</sup>. A series of independently run 2x2

ANOVA models were used to address whether hippocampal mitochondrial respiration, mitochondrial content, GLUT protein expression, and expression of fission and fusion proteins, as well as HSP-60 differed between condition (TAC v. SHAM) and hemisphere (right v. left). Additionally, as an exploratory analysis, separately run independent samples t-tests or Mann-Whitney U tests were performed to address whether there were sex differences in hippocampal mitochondrial respiration, mitochondrial content, GLUT protein expression, and expression of fission and fusion proteins as well as HSP-60, in each condition (TAC & SHAM), within each hemisphere (right v. left). It was hypothesized that a) Within TAC, respiration rates in the right hippocampus would be lower than the left, b) When compared to SHAM controls right and left hippocampal respiration rates in TAC would be lower, c) Protein expression of hippocampal neuronal and endothelial glucose transport machinery would be downregulated in TAC but not SHAM animals, and d) Hippocampal protein expression of mitochondrial dynamics would favor a fission phenotype and dysregulated unfolded protein response in TAC but not SHAM animals. Lastly, because we previously characterized the time course of alterations in left and right carotid artery hemodynamics and diameter in TAC and SHAM at 20-, 30-, and 40 weeks, we also employed an exploratory correlation analysis to determine whether carotid blood flow velocities and pulsatility at 40 weeks post-surgery were related to hippocampal mitochondrial respiration.

## **Methods**

### Study Design

The current study was approved by the Institutional Animal Care and Use Committee (IACUC) at the University of Maryland College Park. Using a cross-sectional study design, male and female Sprague-Dawley rats underwent the minimally invasive procedure of transverse aortic constriction (TAC) to mimic chronic hypertension and induced heart failure with preserved ejection fraction. Control animals (SHAM) underwent a sham surgical procedure that was identical to that received by TAC animals up to the constriction of the transverse aorta. Following surgical procedures, animals were paired-housed, held on 12/12-hour light/dark cycle, fed water and food ad libitum, and left to age for 40 weeks. Carotid blood flow and artery diameter were measured 20-, 30-, and 40 weeks post-TAC surgery.

### Transverse Aortic Constriction Surgery

Male and female Sprague-Dawley rats (4 weeks old) underwent either the TAC or SHAM surgical procedures as described previously<sup>114</sup>. Briefly, each animal was weighed and anesthetized via inhalation of isoflurane [~2% isoflurane supplemented with 100% oxygen (400-500 mL/min)]. Animals were then placed in the supine position on a heated pad, and body temperature was monitored via anal temperature probe. Once unresponsive, a single dose of buprenorphine (0.05-0.1 mg/kg) was injected via subcutaneous injection. A surgical area was clipped clean and sterilized. A horizontal skin incision was then made at the suprasternal notch region and a longitudinal ~1 cm cut was made in the sternum. In both procedures, a 4-

0 silk suture attached to a blunted needle was passed around the aortic arch between the origin of the right innominate and left common carotid arteries. A bent, blunted 20-gauge needle was then placed next to the aortic arch, the suture was tightened around the needle, and the needle was then promptly removed (**Fig. 1A**). The sternum was closed with a single silk suture and the skin was sutured shut with 5-0 monofilament suture and treated with betadine. SHAM animals received the same procedure as TAC animals but did not have the suture tied around the aortic arch. Doppler ultrasound (**Fig. 1B & 1C**) and cardiac tissue specific measurements (left ventricular wall thickness and diameter) were used to confirm TAC and SHAM status of all animals used in this experiment.

#### Euthanasia and Tissue Isolation

Rats were first anesthetized via isoflurane and clinical signs of anesthesia depth were monitored with tail and toe pinches in accordance with guidelines from the American Veterinary Medical Association. When animals became unresponsive, euthanasia was verified via exsanguination and heart excision. Upon cardiac excision, cervical dislocation and decapitation was used to allow for quick brain isolation. Brain samples were placed in ice-cold 1xPBS, and the bilateral hippocampi were then isolated and weighed. ~11mg of each hippocampal sample was then homogenized in 4.4 mL of ice-cold respiration media (50mM MOPS, 20mM glucose, 1mM EGTA, 100mM KCl, 10mM MgCl<sub>2</sub>, 0.2% BSA) using separate ice-cold Dounce homogenizers. The remaining hippocampal samples were placed in separate conical tubes with ice-cold 1xRIPA lysing buffer containing protease and phosphatase inhibitors (ThermoFisher Scientific, Waltham, MA) and homogenized using a hand-

held motorized microtube homogenizer (VWR, Radnor, PA). Samples were spun at 15xG for 15 minutes to obtain purified protein from each sample, which were then stored at -80°C for further analysis.

### Hippocampal Respiration

Hippocampal mitochondrial oxygen consumption was obtained via liquid-phase respiration in a temperature-controlled respiration chamber fitted with a Clark-type electrode (Oxytherm<sup>+</sup>, Hansatech Instruments, Norfolk, UK). 1 mL of hippocampal homogenate was placed into the respiration chamber with the temperature preset at 37°C with constant stirring at 60 rpm, and a previously published substrate-uncoupler-inhibitor-titration (SUIT) respiration protocol was used to assess mitochondrially-fueled metabolism<sup>129</sup>. First, while continually monitoring oxygen consumption, non-phosphorylating leak respiration was induced by adding the CI-linked substrates pyruvate (5 mM), malate (0.5 mM) and glutamate (10 mM). Then ADP (2.5 mM) was added to measure maximal CI-linked phosphorylating oxygen consumption, and then succinate (10 mM) was added, to assess the combined CI + CII phosphorylating oxygen consumption rate. Maximal uncoupled respiration was obtained with the stepwise titration of protonophore FCCP (0.5 μM additions separated by 60 seconds). Rotenone (0.5 μM) was then used to inhibit CI and obtain CII-linked uncoupled respiration. Lastly, CII and CIII were inhibited with malonate (2mM) and antimycin A (2.5mM) to assess non-mitochondrial oxygen consumption.

### Hippocampal Mitochondrial Content

Citrate synthase activity was assessed as an estimate of mitochondrial content and was performed following previously published protocols<sup>130</sup>. Briefly, homogenates were added to a cuvette containing, 100 mM Tris HCl, 0.11–1 5,5-dithiobis-(2-nitrobenzoic acid) (DTNB), 0.25mM acetyl-CoA, and 0.1% Triton. Substrate dependent activity was initiated by addition of 0.5mM oxaloacetate into a final volume of 1.0 ml and absorbance was followed at 412nm for 180 seconds. Activity was calculated using a millimolar extinction coefficient of 13.6 for the mercaptide ion.

### Protein Quantification and Western Blot

Hippocampal protein concentrations were first determined via Pierce BCA protein assay (ThermoFisher Scientific, Waltham, MA). Expression of glucose transporters (GLUT-1, -3), fission proteins (DRP1, FIS1), fusion proteins (MFN1, OPA1) and UPR<sup>MT</sup> (HSP-60) were then obtained via western blotting. Briefly, equal amounts of protein (30 µg/lane) were loaded and separated by SDS-PAGE using Mini-PROTEAN stain-free TGX precast gels (2% SDS, 25% glycerol, 0.01% bromophenol blue) (Bio-Rad, Hercules, CA), and transferred to PVDF membranes (Bio-Rad, Hercules, CA). Membranes were then blocked in 5-6% milk buffer for one hour and then incubated at 4°C overnight with primary antibodies for target proteins. An HRP-conjugated secondary antibody was used (Cell Signaling Technology, Danvers, MA), and target proteins were visualized using the SuperSignal West Pico Chemiluminescent Substrate detection kit (ThermoFisher Scientific, Waltham, MA)

and the Bio-Rad ChemiDoc system and software (Bio-Rad, Hercules, CA). ImageJ software was used to quantify bands using densitometry. For all western blot experiments, total protein was used as the normalizing control and was obtained using stain-free imaging.

### Statistical Analysis

The primary purpose of this study was to address whether hypoperfusion stemming from pulsatile blood flow and hypoperfusion stemming from low blood flow led to hemispheric differences in hippocampal glucose transport, metabolism, mitochondrial content and quality control, and test whether these differed when compared to the SHAM controls. A series of 2x2 ANOVA models were used to test whether there were any main effects of Condition (TAC v. SHAM), Hemisphere (right v. left), or Condition by Hemisphere interactions on hippocampal respiration, mitochondrial content, and protein expression of markers associated with mitochondrial quality control mechanisms. Because the literature shows hemispheric differences in brain perfusion within TAC, and because we hypothesized these hemispheric differences would be evident in the outcomes of interest, all 2x2 ANOVA models were followed up with planned comparisons to determine whether there were hemispheric differences within TAC. Pearson product-moment correlations were used to determine if carotid artery blood flow velocities and pulsatility 40 weeks post-surgery were related to mitochondrial respiration. Lastly, although not a primary aim in this study, separately run, independent samples t-test were used as an exploratory analysis to test for possible sex differences on hippocampal respiration, mitochondrial content, and protein expression of markers

associated with mitochondrial quality control mechanisms within either the TAC or SHAM conditions. All analyses were conducted using the statistical software JASP (version 0.17.3), and model assumptions for all ANOVA models were checked. Statistical significance was set at  $p < 0.05$ .

## **Results**

### *Animal Characteristics*

Thirty-one animals were utilized (7 TAC male, 6 TAC female, 8 SHAM male, and 10 SHAM female) and included in the analysis for this study. Animal characteristics can be found in **Table 6**. Overall, no significant differences between TAC and SHAM were observed in any of the characteristics, including those used to determine heart failure such as absolute and relative left ventricular width, heart mass, septal width, as well as cardiac parameters obtained from ultrasound imaging including cardiac output, ejection, fraction, and stroke volume (**Table 6**).

**Table 6: Animal Characteristics**

	TAC (n=13) M (SD)	SHAM (n=18) M (SD)
Sex		
Male	7	8
Female	6	10
Age (weeks)	45.5 (1.27)	45.7 (1.46)
Body Mass (g)	470.4 (118.6)	464.7 (160.9)
Heart Mass (g)	1.44 (0.38)	1.34 (0.40)
Heart Mass to Body Mass (mg/g)	3.11 (0.51)	3.00 (0.67)
Heart Rate (BPM)	318.7 (32.0)	327.2 (34.1)
Left Ventricular Width (mm)	3.64 (0.50)	3.58 (0.45)
Left Ventricular Width to Body Mass (mm/mg)	8.09 (1.69)	8.46 (2.58)
Septal Width (mm)	3.21 (0.41)	3.00 (0.34)
Septal Width to Body Mass (mm/mg)	7.19 (1.78)	7.03 (1.83)
Cardiac Output (ml/min)	76.5 (13.4)	82.4 (17.2)
Stroke Volume (ul)	240.3 (36.1)	253.7 (53.8)
Ejection Fraction (%)	72.3 (13.2)	77.3 (8.8)
Tibialis Anterior Mass (g)	1.68 (0.39)	1.56 (0.47)
Hippocampus wet weight (g)		
Right	0.115 (0.01)	0.113 (0.008)
Left	0.057 (0.005)	0.056 (0.005)
	0.058 (0.005)	0.057 (0.004)

**Note:** TAC- transverse aortic constriction, SHAM- sham control, M- mean, SD- standard deviation, wks- weeks, g- grams, mg- milligrams, mg/g- milligrams per gram, BPM- beats per minute, mm- millimeter, mm/mg- millimeter per milligrams, ml/min- milliliter per minute, ul- microliter, %- percent. Data presented as means (M) and standard deviation (SD).

Hippocampal Respiration and Mitochondrial Content in TAC and SHAM Animals.

A primary aim of this study was to expand on previous literature showing hemispheric differences in brain perfusion and determine whether glucose oxidation in TAC differed between hemispheres and compared to SHAM controls. Because the SUIT protocol employed in this study addressed multiple components of the oxidative phosphorylation cascade, each component addressed was analyzed with separate 2x2 ANOVA models. Overall, significant main effects or interactions were only found in CI linked respiration and CII linked uncoupled respiration (**Fig. 11**). Specifically, we first observed a significant main effect of Hemisphere ( $F(1,56)=5.08$ ,  $p<0.05$ ,  $\eta_p^2=0.08$ ) in CI-linked coupled respiration but no significant main effects of Condition ( $F(1,56)=0.134$ ,  $p=0.71$ ,  $\eta_p^2=0.002$ ) nor a significant Condition by Hemisphere interaction ( $F(1,56)=0.568$ ,  $p=0.45$ ,  $\eta_p^2=0.01$ ). Follow up contrast analysis revealed that within condition hemispheric differences were greatest in TAC ( $t(56)=1.94$ ,  $p=0.057$ ) than SHAM ( $t(56)=1.18$ ,  $p=0.24$ ) animals, although it is important to highlight hemispheric differences within TAC did not reach significance (**Fig. 11**). As it pertains to CII-linked uncoupled respiration, there were no significant main effects of Condition ( $F(1,56)=0.045$ ,  $p=0.83$ ,  $\eta_p^2=0.0008$ ) or Hemisphere ( $F(1,56)=3.49$ ,  $p=0.06$ ,  $\eta_p^2=0.05$ ), but a significant Condition by Hemisphere interaction ( $F(1,56)=4.69$ ,  $p<0.05$ ,  $\eta_p^2=0.077$ ) was observed. Follow up contrasts within TAC revealed that the right hippocampus had significantly lower CII-linked uncoupled respiration when compared to the left hippocampus ( $t(56)=-2.60$ ,  $p=0.012$ ) (**Fig. 11**). No other significant hemispheric differences were identified between TAC and SHAM, nor within SHAM controls. Of note, a 2x2 ANOVA model of CI&II-

linked coupled respiration revealed no significant main effects of Condition ( $F(1,56)=1.24, p=0.61, \eta_p^2=0.005$ ), Condition by Hemisphere interaction ( $F(1,56)=2.61, p=0.11, \eta_p^2=0.045$ ), but a main effect of Hemisphere the approached significance ( $F(1,56)=3.75, p=0.058, \eta_p^2=0.063$ ). Follow up contrasts showed hemispheric differences in TAC ( $t(56)=-2.29, p=0.025$ ) but not SHAM ( $t(56)=-0.25, p=0.80$ ), with lower CI&II-linked respiration in the right compared to left hippocampus of TAC animals (**Fig. 11**). No main effects of Condition ( $F(1,56)=0.136, p=0.71, \eta_p^2=0.002$ ), Hemisphere ( $F(1,56)=0.46, p=0.49, \eta_p^2=0.008$ ), nor Condition by Hemisphere interaction ( $F(1,56)=1.71, p=0.19, \eta_p^2=0.03$ ) were observed for leak respiration. Similarly, no main effects of Condition ( $F(1,56)=0.137, p=0.71, \eta_p^2=0.002$ ), Hemisphere ( $F(1,56)=0.42, p=0.51, \eta_p^2=0.008$ ), nor Condition by Hemisphere interaction ( $F(1,56)=0.18, p=0.66, \eta_p^2=0.003$ ) were observed for CI&II-linked uncoupled respiration. Lastly, when addressing citrate synthase activity as a measure of mitochondrial content, no main effects of Condition ( $F(1,56)=1.06, p=0.30, \eta_p^2=0.01$ ), Hemisphere ( $F(1,56)=0.055, p=0.81, \eta_p^2=0.0009$ ), nor condition by hemisphere interaction ( $F(1,56)=0.88, p=0.35, \eta_p^2=0.01$ ) were observed (**Fig. 12**).

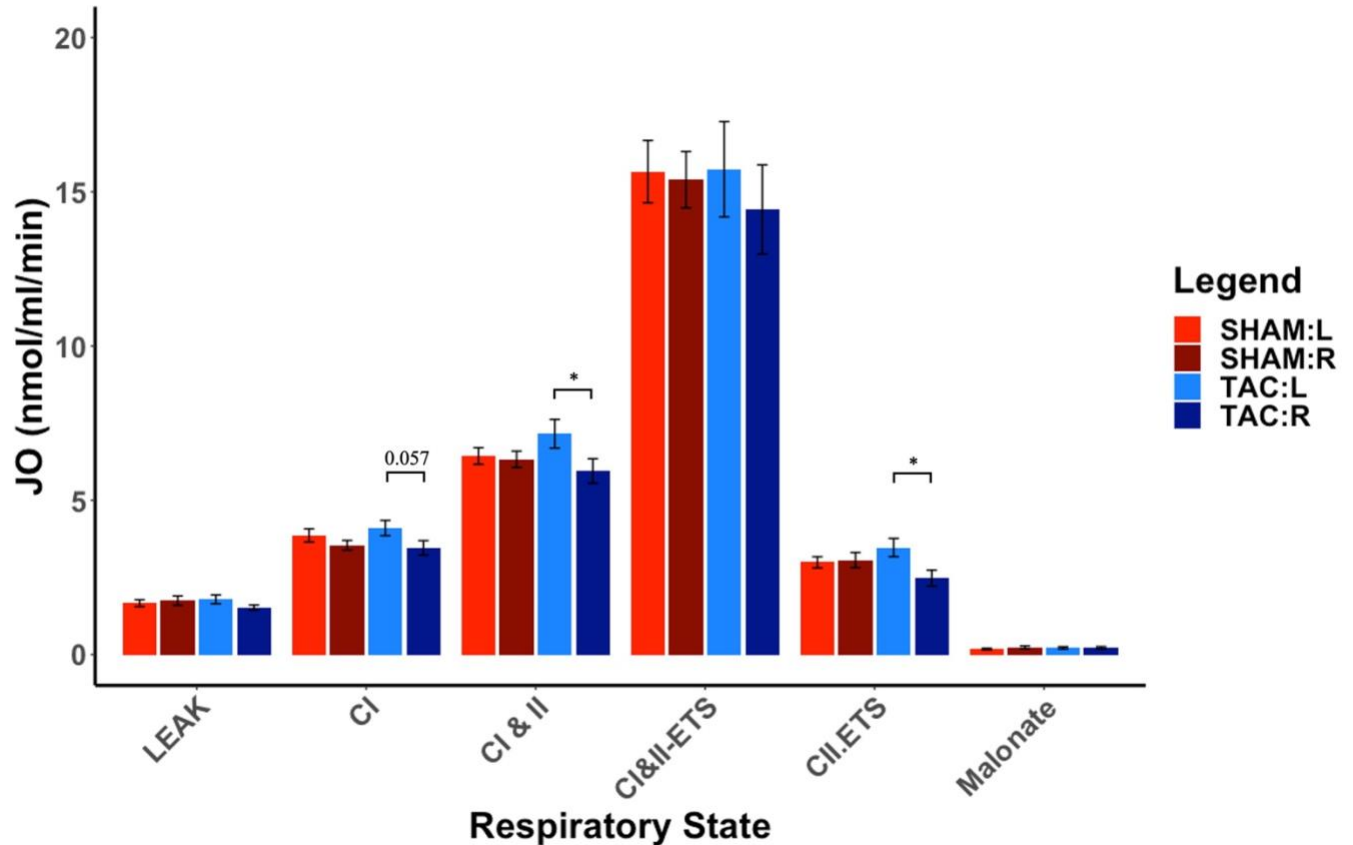


**Figure 11: Impaired Mitochondrial Respiration in the Right, but not Left Hippocampus of TAC.**

JO = oxygen consumption, nmol/ml/min = nanomoles per milliliter per minute, LEAK- leak respiration, CI = complex I, CII = complex II, ETS = electron transfer system, TAC- transverse aortic constriction, SHAM- sham controls, R = right, L = left. Data presented as means + SEM, \* =  $p < 0.05$ .

As an exploratory analysis, Pearson product-moment correlations were used to determine if carotid artery blood flow velocities and pulsatility 40 weeks post-surgery were related to mitochondrial respiration. First, we found that at 40 weeks, carotid artery mean velocity ( $r = -0.448, p = 0.004, [-0.66, -0.15]$ ) (**Fig. 13A**), carotid artery peak velocity ( $r = -0.453, p = 0.004, [-0.67, -0.16]$ ) (**Fig. 13A**), and carotid artery blood pulsatility ( $r = -0.429, p = 0.006, [-0.65, -0.13]$ ) (**Fig. 13A**), were all negatively associated to CI&II-linked coupled respiration, and higher velocities and pulsatility

were associated with impaired respiration. Similarly, carotid artery mean velocity ( $r = -0.45, p = 0.003, [-0.67, -0.16]$ ) (**Fig. 13B**), carotid artery peak velocity ( $r = -0.473, p = 0.002, [-0.68, -0.18]$ ) (**Fig. 13B**), and carotid artery blood pulsatility ( $r = -0.481, p = 0.002, [-0.69, -0.19]$ ) (**Fig. 13B**), were also negatively associated to CII-linked uncoupled respiration, and higher velocities and pulsatility were associated with lower uncoupled respiration.

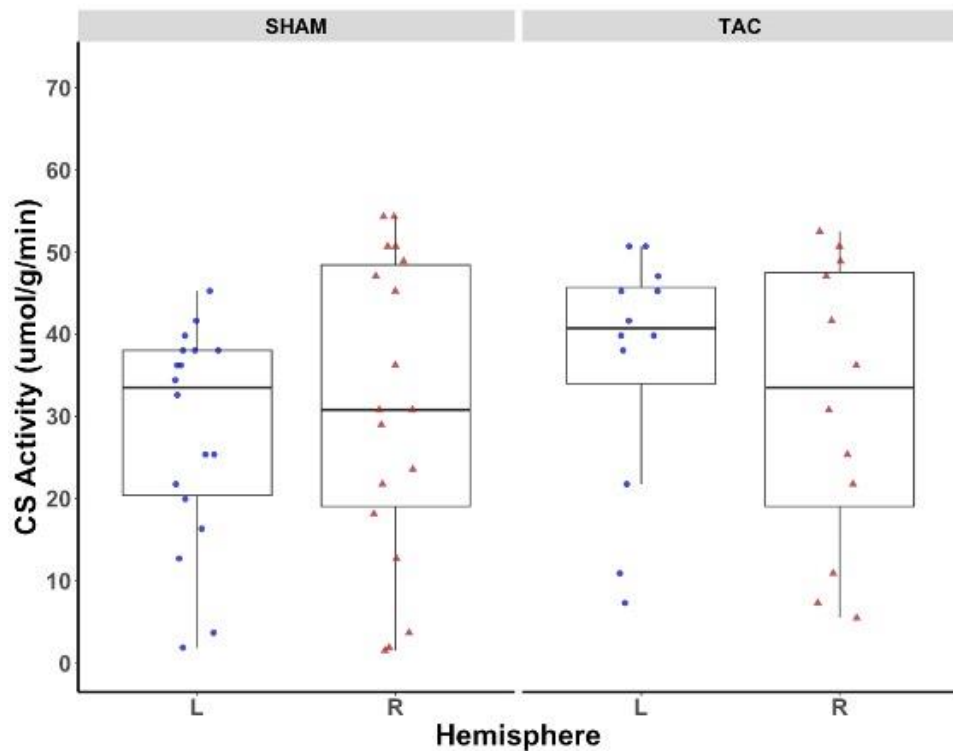


**Figure 12: Transverse Aortic Constriction Does Not Lower Mitochondrial Content.**

CS = citrate synthase,  $\text{umol/g/min}$  = micromoles per gram per minute, TAC- transverse aortic constriction, SHAM- sham controls, R = right, L = left. Data presented as means with distribution of individual data points.

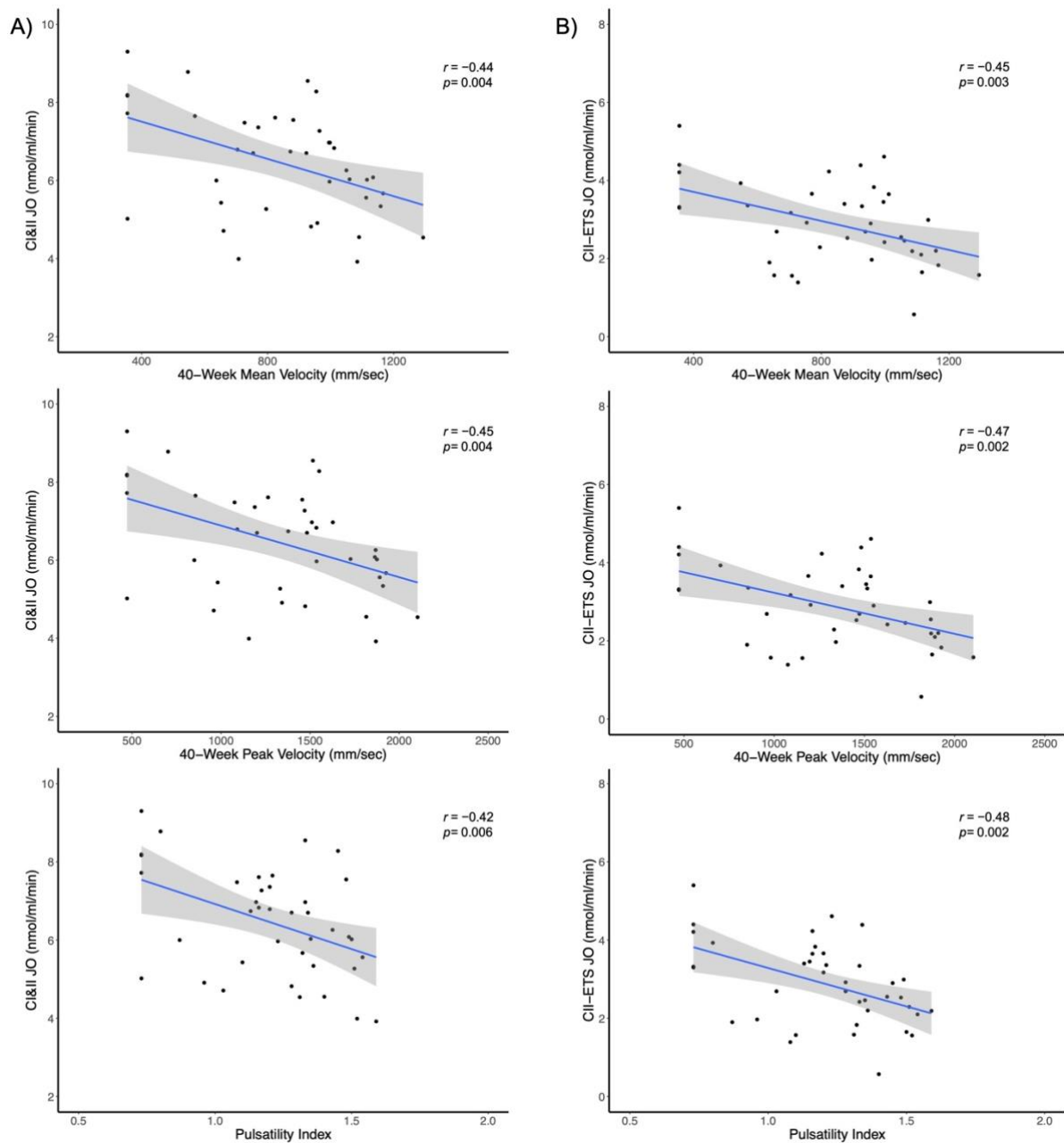


**Figure 13: High Carotid Artery Velocity and Pulsatility is Negatively Associated with Hippocampal Mitochondrial Respiration.**

**A)** Scatterplot depicting the negative association between carotid artery velocity and pulsatility to CI&II coupled hippocampal respiration. **B)** Scatterplot depicting the negative association between carotid artery velocity and pulsatility to CII uncoupled hippocampal respiration. JO = oxygen consumption, nmol/ml/min = nanomoles per milliliter per minute, CI = complex I, CII = complex II, ETS = electron transfer system.

### Expression of Glucose Transporter Proteins in TAC and SHAM Animals

Because brain hypoperfusion is often coupled to glucose hypometabolism, we also determined if TAC led to hemispheric differences in glucose transporter protein expression, and if TAC differed to SHAM controls. Overall, we found no significant main effects of Condition ( $F(1,56)=0.424, p=0.51, \eta_p^2=0.008$ ), Hemisphere ( $F(1,56)=0.33, p=0.56, \eta_p^2=0.006$ ), nor Condition by Hemisphere interaction ( $F(1,56)=0.11, p=0.73, \eta_p^2=0.002$ ) in hippocampal protein expression of GLUT-1 (**Fig. 14**). Similarly, no significant no main effects of Condition ( $F(1,56)=0.38, p=0.53, \eta_p^2=0.007$ ), Hemisphere ( $F(1,56)=0.22, p=0.63, \eta_p^2=0.004$ ), nor a Condition by Hemisphere interaction ( $F(1,56)=0.09, p=0.75, \eta_p^2=0.002$ ) for hippocampal protein expression of GLUT-3 (**Fig. 14**).

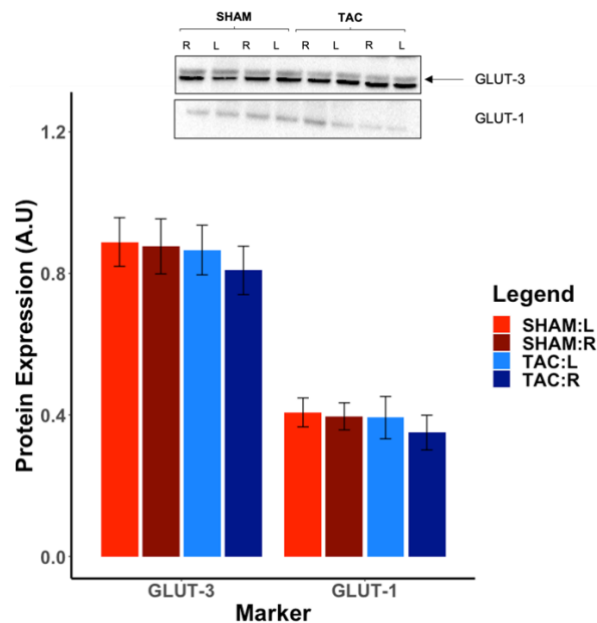


**Figure 14: Protein Expression of Glucose Transporters is not Altered by Traverse Aortic Constriction.**

A.U- arbitrary units, GLUT-3- glucose transporter-3, GLUT-1- glucose transporter-1, , R- right, L- left, TAC- Transverse aortic constriction, SHAM- sham controls. Data presented as means + SEM.

Expression of Mitochondrial Quality Control Proteins in TAC and SHAM Animals.

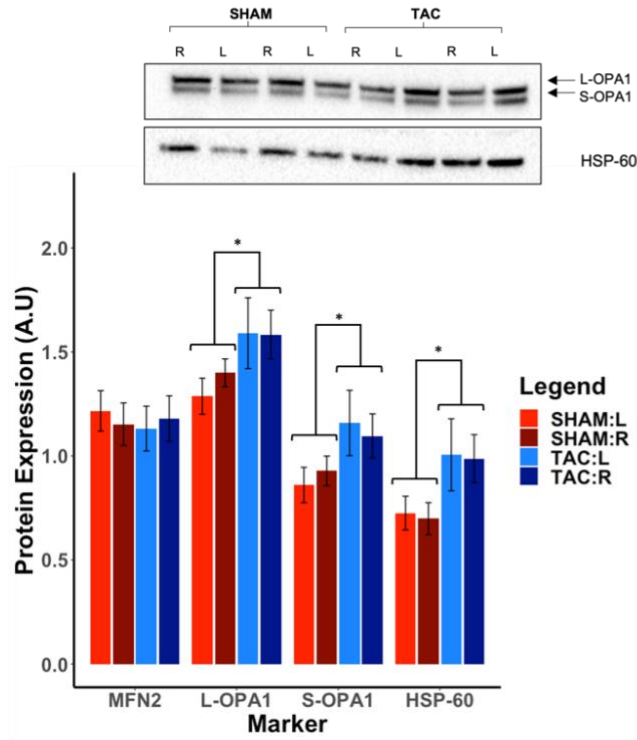
Mitochondrial metabolism is closely associated with mitochondrial quality control mechanisms such as fission, fusion, and the mitochondrial uncoupled protein response (UPR<sup>MT</sup>). As such, this study also aimed to address whether TAC was associated with hemispheric differences in the protein expression of quality control markers, and how the expression of these markers in TAC animals compared to SHAM controls. For this study, OPA1 and MFN2 were used as markers of mitochondrial fusion, DRP1 and FIS1 were used as markers of mitochondrial fission, while HSP-60 was used as a marker of the mitochondrial uncoupled protein response.

First, 2x2 ANOVA models addressing mitochondrial fusion revealed a significant main effect of Condition for both the long- ( $F(1,56)=4.92, p<0.05, \eta_p^2=0.081$ ) and short- ( $F(1,56)=5.01, p<0.05, \eta_p^2=0.082$ ) OPA1 isoforms, with TAC animals displaying higher protein expression than SHAM (**Fig. 15A**). However, no significant main effects of Hemisphere for either long- ( $F(1,56)=0.23, p=0.63, \eta_p^2=0.004$ ) or short- ( $F(1,56)=0.0008, p=0.97, \eta_p^2=0.00001$ ) OPA1, nor a significant Condition by Hemisphere interaction in either the long- ( $F(1,56)=0.29, p=0.59, \eta_p^2=0.005$ ) or short- ( $F(1,56)=0.39, p=0.53, \eta_p^2=0.007$ ) OPA1 isoforms were found. A main effect of Condition was also observed for total OPA1 ( $F(1,56)=5.09, p<0.05, \eta_p^2=0.083$ ), calculated as the sum of the density signal of the short- and long- isoforms, and TAC animals had higher protein expression of total OPA1 than SHAM controls. No significant main effects of Hemisphere ( $F(1,56)=0.07, p=0.79, \eta_p^2=0.001$ ), nor a Condition by Hemisphere interaction ( $F(1,56)=0.34, p=0.55, \eta_p^2=0.006$ ) in total OPA1 were observed. No significant main effects of Condition

( $F(1,56)=0.07$ ,  $p=0.78$ ,  $\eta_p^2=0.001$ ), Hemisphere ( $F(1,56)=0.006$ ,  $p=0.94$ ,  $\eta_p^2=0.00009$ ), nor Condition by Hemisphere interaction ( $F(1,56)=0.28$ ,  $p=0.59$ ,  $\eta_p^2=0.005$ ) were detected in MFN2 protein expression (**Fig. 15A**).

Regarding mitochondrial fission, no significant main effects of Condition ( $F(1,56)=0.18$ ,  $p=0.66$ ,  $\eta_p^2=0.003$ ), Hemisphere ( $F(1,56)=0.40$ ,  $p=0.52$ ,  $\eta_p^2=0.007$ ), nor Condition by Hemisphere interaction ( $F(1,56)=0.66$ ,  $p=0.41$ ,  $\eta_p^2=0.012$ ) were found in the protein expression of FIS1 (**Fig. 15B**). Similarly, no significant main effects of Condition ( $F(1,56)=1.02$ ,  $p=0.31$ ,  $\eta_p^2=0.01$ ), Hemisphere ( $F(1,56)=0.019$ ,  $p=0.88$ ,  $\eta_p^2=0.0003$ ), nor Condition by Hemisphere interaction ( $F(1,56)=0.03$ ,  $p=0.85$ ,  $\eta_p^2=0.0006$ ) were detected for DRP1 (**Fig. 15B**). Meanwhile, a significant main effect of Condition ( $F(1,56)=6.53$ ,  $p<0.05$ ,  $\eta_p^2=0.10$ ), where TAC animals showcased higher protein expression than SHAM, but no main effect of Hemisphere ( $F(1,56)=0.04$ ,  $p=0.83$ ,  $\eta_p^2=0.0007$ ), nor a Condition by Hemisphere interaction ( $F(1,56)=0.001$ ,  $p=0.96$ ,  $\eta_p^2=0.00002$ ) were observed for HSP-60 (**Fig. 15A**).

A)



B)

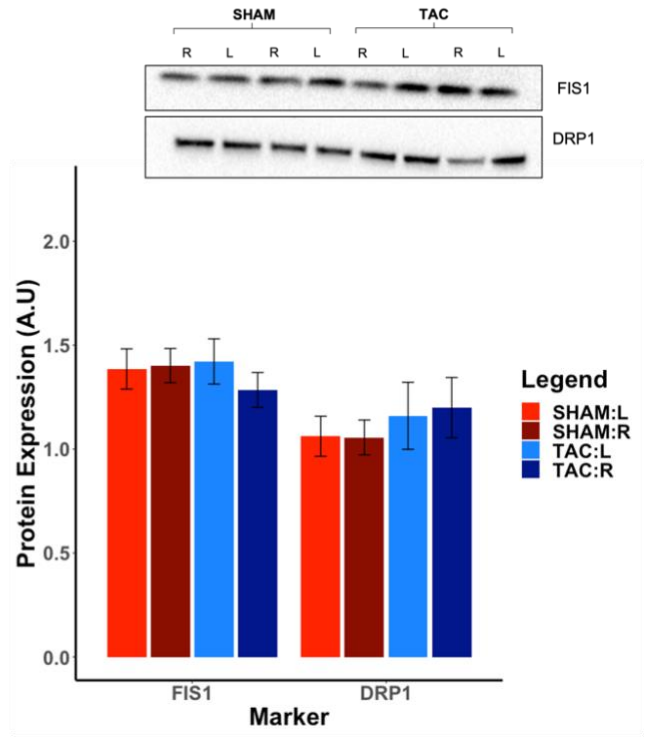


**Figure 15: Greater Protein Expression of Mitochondrial Fusion Markers in Right and Left Hippocampus of TAC.**

**A)** Protein expression of markers associated with mitochondrial fusion and unfolded protein response. **B)** Protein expression of markers associated with mitochondrial fission. A.U- arbitrary units, MFN- mitofusin 2, L-OPA1- OPA1 long isoform, S-OPA1- OPA1 short isoform, HSP-60- heat shock protein-60, FIS1- fission 1, DRP1- dynamin-related protein 1, TAC- transverse aortic constriction, SHAM- sham controls, R- right, L- left, \* =  $p < 0.05$ . Data presented as means + SEM.

### Sex Differences in TAC and SHAM Animals

An exploratory analysis was conducted to assess whether, within each hemisphere for each condition, hippocampal mitochondrial respiration and protein expression of mitochondrial quality control markers differed between males and females. Sex differences were addressed with separately run independent samples t-tests, or with the non-parametric Mann-Whitney U test when t-test assumptions were violated. Overall, we found no significant sex differences in hippocampal mitochondrial respiration in either the right or left hemisphere (**Fig. 16A**) of TAC animals but significant sex differences in mitochondrial content were found on the left hemisphere of TAC animals. Specifically, mitochondrial content was found to be significantly higher in the left hippocampus of TAC females when compared to the left hippocampus of TAC males ( $M=46.6\pm 2.0$  v.  $M=29.2\pm 5.9$ ,  $U=32.0$ ,  $p<0.05$ ,  $r=0.82$ ) (**Fig. 16B**). Meanwhile, sex differences in protein expression of mitochondrial quality control proteins were only found within the right hippocampus of TAC animals, where females were found to have significantly higher protein expression of the short ( $M=1.33\pm 0.12$  v.  $M=0.89\pm 0.12$ ,  $t(11)=2.47$ ,  $p<0.05$ ,  $d=1.36$ ) and long ( $M=1.88\pm 0.13$  v.  $M=1.32\pm 0.11$ ,  $t(11)=2.86$ ,  $p<0.05$ ,  $d=1.76$ ) OPA1 isoforms compared to males (**Fig. 16C**). No significant sex differences in hippocampal protein expression were found in the left hemisphere of TAC.

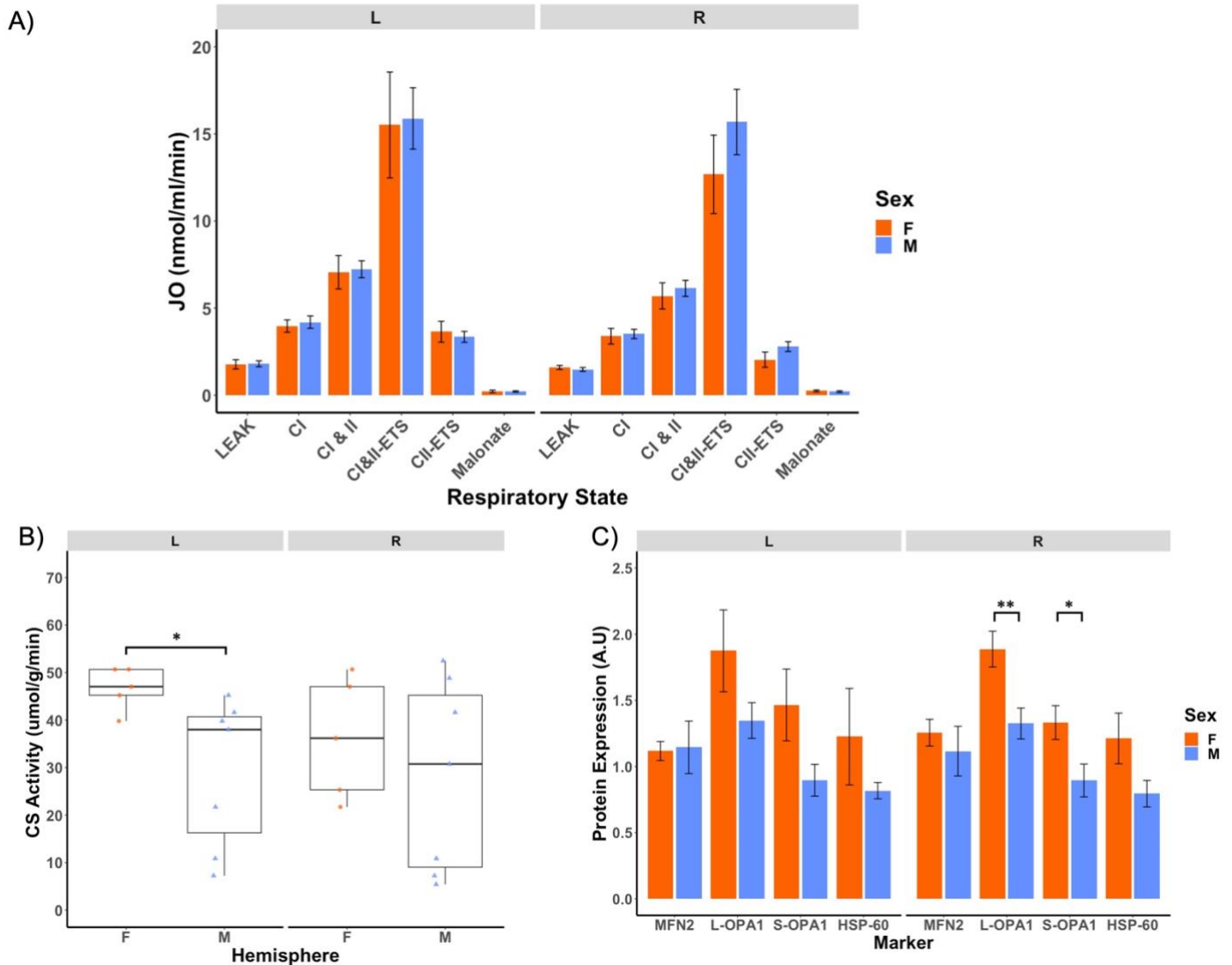


**Figure 16: Lower Mitochondrial Content in Female TAC is Coupled to the Upregulation of Mitochondrial Fusion.**

**A)** Hemispheric differences in hippocampal respiration in male and female TAC animals. **B)** Hemispheric differences in mitochondrial content in male and female TAC animals. **C)** Upregulation of mitochondrial fusion markers in the right hemisphere of female TAC animals when compared to male TAC. JO- oxygen consumption nmol/ml/min- nanomoles per milliliter per minute, CI- complex I, CII- complex II, ETS- electron transfer system, CSA- citrate synthase activity, umol/g/min- micromoles per gram per minute, M- male, F- female, R- right, L- left, \* =  $p < 0.05$ , \*\*\* =  $p < 0.001$ . Data presented as means and S.E.M, as well as distribution of individual data points for mitochondrial content.

In SHAM animals, sex differences in mitochondrial respiration were evident for CI-linked coupled, and CI&II-linked coupled respiration. Specifically, CI-linked coupled respiration in female SHAM was found to be significantly lower than male counterparts in both the right ( $M=3.10\pm0.16$  v.  $M=4.09\pm0.12$ ,  $t(16)=-4.69$ ,  $p<0.05$ ,  $d=-2.22$ ) and left ( $M=3.57\pm0.31$  v.  $M=4.22\pm0.23$ ,  $U=12.5$ ,  $p<0.05$ ,  $r=-0.68$ ) hippocampus (**Fig. 17A**). Similarly, female SHAM also displayed lower CI&II-linked coupled respiration when compared to male counterparts in both the right ( $M=5.76\pm0.33$  v.  $M=7.04\pm0.26$ ,  $U=11.5$ ,  $p<0.05$ ,  $r=-0.71$ ) and the left ( $M=5.88\pm0.37$  v.  $M=7.12\pm0.22$ ,  $t(16)=-2.68$ ,  $p<0.05$ ,  $d=-1.27$ ) hippocampus (**Fig. 17A**). No sex differences in mitochondrial content were observed in either the right or left hippocampus of SHAM controls (**Fig. 17B**). Intriguingly, we only found sex differences in expression of quality control proteins in the left hippocampus of SHAM animals, and on average, females had higher protein expression than males of DRP1 ( $M=1.23\pm0.11$  v.  $M=0.81\pm0.12$ ,  $t(15)=2.48$ ,  $p<0.05$ ,  $d=1.22$ ) and MFN2 ( $M=1.40\pm0.22$  v.  $M=0.95\pm0.40$ ,  $t(15)=2.63$ ,  $p<0.05$ ,  $d=1.30$ ) (**Fig. 17C**). No other sex differences were evident in SHAM controls.

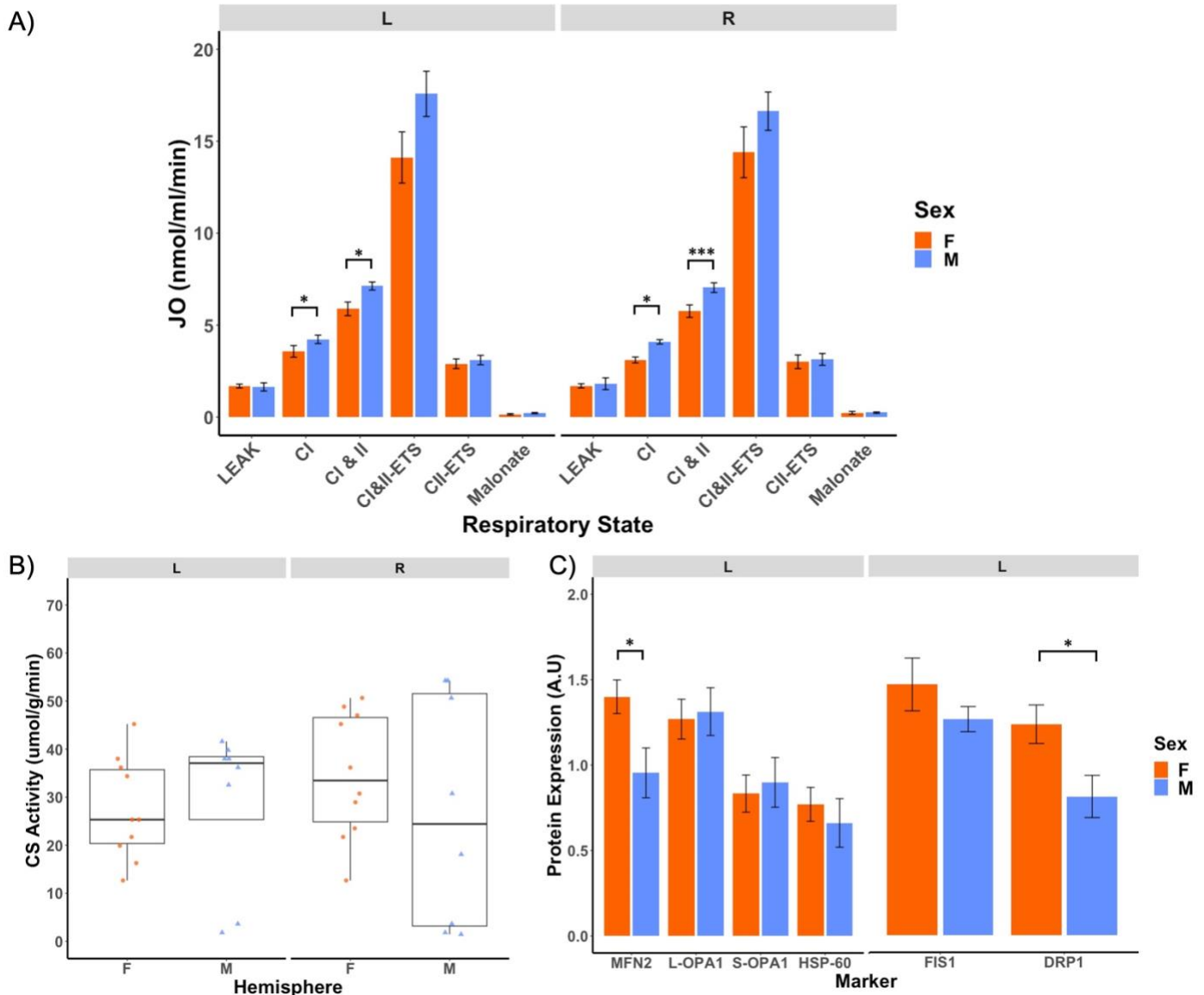


**Figure 17: Right and Left Hippocampal Respiration is Impaired in Female SHAM.**

**A)** Hemispheric differences in hippocampal respiration in male and female SHAM animals. **B)** Hemispheric differences in mitochondrial content in male and female SHAM animals. **C)** Sex differences in protein expression of fusion and fission markers in the left hemisphere of SHAM animals. JO- oxygen consumption nmol/ml/min = nanomoles per milliliter per minute, CI- complex I, CII- complex II, ETS = electron transfer system, CSA- citrate synthase activity, umol/g/min- micromoles per gram per minute, M- male, F- female, R- right, L- left, \* =  $p < 0.05$ , \*\*\* =  $p < 0.001$ . Data presented as means and S.E.M, as well as distribution of individual data points for mitochondrial content.

## Discussion

Chronic brain hypoperfusion is a central component of the intersection between cardiovascular disease and neurodegenerative conditions such as dementia<sup>16, 44, 58</sup>. Human studies employing clinical neuroimaging such as fluorodeoxyglucose positron emission tomography (FDG-PET) have found brain hypoperfusion is often coupled to glucose hypometabolism<sup>65</sup>. Because glucose is the main energetic substrate used by neurons, impaired glucose metabolism may hint at energetic deficits that compromise basic neurophysiological processes and facilitate neurodegeneration<sup>26</sup>. Mitochondria are key organelles that form extensive functional networks, and in neurons, they supply the vast majority of ATP needed to meet the energetic needs of neuronal communication and maintenance<sup>26, 29-31</sup>. Therefore, chronic hypoperfusion may be disrupting mitochondrial substrate metabolism and network dynamics. Chronic hypoperfusion may stem from either limited blood flow volumes reaching the brain (as seen with low cardiac output)<sup>131</sup>, or from chronic tissue damage from sustained blood flow pulsatility (as seen in chronic hypertension)<sup>24</sup>. However, most animal models of brain hypoperfusion rely on lowering overall blood flow supply through arterial constriction, and largely ignore the role of blood flow pulsatility in brain hypoperfusion<sup>25</sup>. Therefore, the literature distinguishing these two distinct mechanisms of brain hypoperfusion and its downstream consequences remain heavily understudied. The primary purpose of this study was to take advantage of the TAC model where divergent (low left, high pulsatile right) carotid blood flows<sup>25</sup> have been shown to lead to hemispheric differences in cerebral hypoperfusion<sup>46</sup>, to address whether divergent hypoperfusive

mechanisms affect glucose transport, and hippocampal mitochondrial function and health. Additionally, because human epidemiological data has found sex disparities in cardiovascular and brain health throughout the lifespan, we also explored whether sex differences in glucose transport and mitochondrial health were present in animals with TAC, as well as control animals.

### Animal Characteristics

The rodent model of TAC is widely accepted as a reliable model of pressure overload to study heart failure and hypertension<sup>113</sup>. However, we were initially surprised to find that although our TAC animals tended to display a phenotype suggestive of impaired cardiac function and cardiac hypertrophy, these were not significantly different than our SHAM controls. At first glance, the lack of significant differences between TAC and SHAM may suggest a lack of cardiovascular disease. However, it is worth noting that the gauge of the needle dictates the severity of constriction and therefore, TAC phenotype<sup>132</sup>. Compared to needles with higher diameter (e.g., low gauge number) such as the 20G needle used in this study, needles with smaller diameters (e.g., high gauge number) lead to more severe TAC due to a tighter constriction of the transverse aorta<sup>132</sup>. In fact, a recent study in mice found that even seemingly close gauges can overtly affect TAC phenotype, and using a 27G needle leads to significantly more pronounced manifestations of heart failure than 26G and 25G needles<sup>132</sup>. Specifically, left ventricular mass, atrial weight, septal width, and cardiac function are all significantly worse in mice whose TAC was performed using 27G than in those whose TAC was done using 25G<sup>132</sup>. Moreover, while most animals whose TAC procedure involved 25G and 26G showed full

survivability, 15% of the animals whose TAC procedure involved 27G died within 4 days post-operation<sup>132</sup>. As such, it is clear not all TAC procedures are equal and the severity of TAC is closely tied to both, the heart failure phenotype and animal longevity. Although there is no consensus as to what needle gauge should be used for TAC, in mice the vast majority of the TAC literature involves the use of a 27G needle and timeframes 15 weeks or lower<sup>113</sup>. In this context, to our knowledge, we are the first to extend the TAC model to 40 weeks post-surgery, and the use of a 20G needle facilitated the survivability of our animals to the intended end point. Moreover, we note that while we do not have a robust heart failure phenotype, our TAC animals displayed the very same carotid hemodynamic phenotype reported in previous work with more aggressive ligation<sup>25, 39, 46, 111</sup>. Therefore, the blunted cardiac function and cardiac hypertrophy phenotypes did not translate to a loss in the brain hemodynamics that were central to this study, and our use of TAC was suitable to address the gaps in the literature. With that in mind, given that to study chronic disease animal survivability is key, future studies should build on existing literature and better characterize the cardiac adaptations to TAC when low gauge needles are used, and the time-course of these adaptations. Addressing these gaps in the literature will help better understand how TAC can be leveraged to study the intersection between chronic cardiovascular disease, hypoperfusion, and brain health.

### *Mitochondrial Respiration and Content*

Although the literature on how mitochondrial function is affected in neurodegenerative conditions such as Alzheimer's Disease<sup>29, 133</sup> and Parkinson's

Disease<sup>100</sup> is extensive, the literature on how chronic brain hypoperfusion in the context of chronic cardiovascular disease influences neuronal mitochondria is more limited and has often relied on complete obstruction models<sup>134, 135</sup>, or acute time scales<sup>40</sup>. Therefore, because there are hemispheric differences in brain hypoperfusion within TAC animals, we first explored whether mitochondrial substrate oxidation and content were differentially affected in the cerebral hemispheres within TAC, and how these compared with SHAM controls. Overall, we found that hemispheric differences in mitochondrial respiration were present in TAC but not SHAM. Specifically, contrast analysis within TAC animals revealed that when compared to the left hippocampus, the right hippocampus displayed significantly lower CI&II-linked coupled respiration, as well as CII-linked uncoupled respiration. Because coupled respiration represents the maximal respiratory capacity of the electron transfer pathways in the presence of saturating substrates and ADP<sup>136</sup>, CI&II-linked coupled respiration represents the upper limits in coupling the transfer of electrons via NADH and FADH<sub>2</sub> to the phosphorylation of ADP to ATP<sup>137</sup>. Moreover, because uncoupled respiration employs protonophores to disrupt the inner mitochondrial membrane and dissipate the protonmotive force, CII-uncoupled represents the maximal electron transfer through complex II, III, & IV without the phosphorylation of ADP to ATP<sup>136, 138</sup>. As such, severe hypoperfusion in the right hippocampus of TAC animals and ensuing low CI-II-linked coupled respiration may be partially explained by a limitation in the electron transferring capacity along CII that lowers the protonmotive force generated by the flux of electrons via CII during oxidative phosphorylation. Further, although not considered statistically significant ( $p=0.057$ ), we note that the

right hippocampus in TAC also displayed lower CI-linked coupled respiration when compared to the left hippocampus ( $M=3.46\pm 0.23$  v  $M=4.10\pm 0.24$ ) within TAC animals. Therefore, it may be possible that on top of limitations in the electron transferring capacity, there may also be limitations in the electron carrier pool that feed CI and CII, which may place further limitations in the protonmotive force during coupled respiration. This possibility is partially supported by work from Du and colleagues that reported bilateral carotid occlusion can progressively lower state 3 hippocampal mitochondrial respiration 9-, 13-, and 17 weeks post-surgery<sup>135</sup>. Since state 3 respiration in this study involved the use of saturating glutamate, malate, and ADP, the reported state 3 respiratory state reflects CI-linked coupled respiration<sup>136</sup>. Therefore, the findings by Du et. al. suggest severe hypoperfusion can inhibit the maximal respiratory capacity through CI. However, this work by Du et. al. did not address whether respiratory deficits in state 3 differed between hemispheres, despite the fact that the right carotid was occluded first, and the left carotid was occluded one-week later<sup>136</sup>. Given that previous studies have found TAC induces a more robust hypoperfusive response in the right hemisphere than the left<sup>46</sup>, our results suggest that the pulsatility associated with the right cerebral hemisphere in TAC can also translate into metabolic deficits within the right hemisphere. Importantly, while we did not measure brain perfusion, our results also suggests that in TAC, moderate left cerebral hypoperfusion does not lead to deficits in mitochondrial function. These findings provide novel insight into the metabolic consequences of brain hypoperfusion in TAC, and additionally clarify that chronic hypoperfusion due to pulsatile blood flow and hypoperfusion due to limited blood supply do not necessarily lead to the same

metabolic changes. However, since there is a large degree of heterogeneity in the models used to study brain hypoperfusion<sup>25</sup>, and because the consequences of occlusion in TAC<sup>113, 132</sup> and bilateral carotid occlusion<sup>139</sup> are highly dependent on methods that are yet to be standardized, there remains much work to be done to understand the downstream consequences of brain hypoperfusion. Indeed, there is a dire need to establish whether the methods used to induce hypoperfusion lead to similar outcomes, and how these reflect human disease. Taken together, our results expand on the existing TAC literature, and suggest that beyond divergent bilateral carotid hemodynamics, and hemispheric brain perfusion, TAC also leads to divergent responses in mitochondrial respiration.

#### *Glucose Transport and Mitochondrial Quality Control*

Because glucose serves as the primary energetic substrate for neurons<sup>26, 90</sup>, glucose transporters (GLUTs) serve an integral role in facilitating the delivery of circulating blood glucose to active neurons<sup>91</sup>. As such, this study also aimed to determine whether the protein expression of prominent GLUTs such as GLUT-1 and GLUT-3 were differentially affected in the cerebral hemispheres of TAC animals and how these compared to SHAM controls. We did not find any hemispheric differences in the protein expression of either GLUT-1 or GLUT-3 within TAC, nor any differences between TAC and SHAM. Within the context of the TAC literature, our findings are somewhat at odds with work from Poulet and colleagues, whose study found hippocampal GLUT-1 (but not GLUT-3) mRNA to be downregulated in TAC animals when compared to SHAM controls 3 weeks and 4 weeks post-surgery<sup>39</sup>.

Intriguingly, when looking at the cortex, GLUT-1 was only downregulated 4 weeks post-surgery<sup>39</sup>. Although these results suggest GLUT-1 levels in the brain may be downregulated in TAC, it is important to note that changes in mRNA expression are difficult to interpret in the absence of protein expression, given that mRNA expression does not reflect protein abundance nor functional changes in these proteins<sup>140</sup>. Moreover, because ischemia reperfusion studies have shown acute increases in blood flow are accompanied by an initial upregulation in GLUT mRNA levels<sup>141</sup>, it is possible that downregulation of GLUT mRNA in acute models of TAC is the equilibrating response<sup>140, 142</sup> to an initial upregulation in mRNA, and possible subsequent protein overexpression of GLUTs. Therefore, although difficult to directly compare, it is possible that the acute changes in GLUT mRNA do not reflect the long-term adaptations to GLUT protein expression in TAC we observed. However, because we focused on a chronic time scale of 40 weeks, the present study does not provide sufficient evidence to endorse or to refute this notion. Therefore, the way TAC affects expression of GLUTs both acutely and chronically, remains a gap in the literature to be further studied.

Meanwhile, we also report that although there were no hemispheric differences in the protein expression of markers of mitochondrial fusion, fission, or unfolded protein response, we did find that when compared to SHAM controls, markers associated with mitochondrial fusion and the unfolded protein response were upregulated in both hemispheres of TAC animals. Indeed, both, the long- and short-OPA1 isoforms, as well as HSP-60 were significantly higher in both hemispheres of TAC animals. While little is known regarding either mitochondrial dynamics or the

unfolded protein response in TAC, models of acute cardiovascular events such as ischemia-reperfusion injury and stroke suggest abrupt changes in brain blood flow can promote the upregulation of mitochondrial fission markers concomitant to the downregulation of fusion markers<sup>41, 143</sup>. Despite the fact there is ample evidence showing mitochondrial dynamics are dysregulated during neurodegeneration<sup>31, 144</sup> within the context of chronic hypoperfusion, it is a heavily understudied topic<sup>145</sup>. To our knowledge, only one published study that has addressed mitochondrial dynamics in the context of brain hypoperfusion<sup>145</sup>. Feng and colleagues found that in a transgenic line of Alzheimer's disease, bilateral carotid obstruction was associated with higher levels (assessed via immunohistochemistry) of DRP1 and FIS1 concomitant with lower levels of OPA1 and MFN<sup>146</sup>. While this is contrary to the current findings, we note that although immunohistochemical assays provide excellent spatial resolution that allow for protein localization, measurement of protein expression via western blotting can be more sensitive in detecting quantifiable measures of the target protein<sup>36</sup>. Therefore, this discrepancy may be partially explained by the different methodologies used. Moreover, while it is widely accepted that mitochondrial fragmentation (and upregulation of fission proteins) is common in the late stages of neurodegenerative diseases<sup>101</sup>, upregulation of fusion proteins such as MFN2 has been reported to not only attenuate mitochondrial fragmentation, but also neuronal loss<sup>147</sup>. Thus, because we also observed an upregulation of HSP-60 in both hemispheres of TAC animals, it may be possible that, collectively, the upregulation of OPA1 and HSP-60 represent a protective mechanism against hypoperfusion and neuronal stress. To contextualize this, it must be underscored that

in order to sustain mitochondrial energetic networks during fission and fusion events, mitochondria have to constantly regulate ETC stoichiometries, clear stress-denatured proteins, and ensure that the segregation or adjoining of mitochondria does not cause imbalances in the mitochondrial proteome<sup>101</sup>. This task is largely regulated by a delicate interaction between the UPR<sup>MT</sup> and molecular protein chaperones of the heat shock protein family<sup>30, 34</sup> that, stabilize protein imports, and facilitate the assembly of protein complexes to prevent the aggregation of stress-denatured proteins<sup>106, 107</sup>. There is ample yet controversial evidence that prominent HSPs such as mortalin, TRAP-1, and HSP60 are dysregulated in neurodegenerative diseases<sup>36, 109</sup>, and dysregulation of these HSPs is associated with proteotoxic burden in Alzheimer's disease<sup>109</sup>. Thus, the upregulation of OPA1 in TAC may be an adaptive response to improve mitochondrial substrate metabolism in the presence of low tissue perfusion, while the dual upregulation of HSP-60 may serve to ensure mitochondrial stoichiometries are sustained while proteotoxic stress is blunted. However, this possibility should be better characterized in future studies, and the roles of other prominent HSPs such as mortalin and TRAP-1 should also be considered.

### Sex Differences

We also performed an exploratory analysis to determine whether sex differences in mitochondrial respiration, content, and protein expression of quality control markers were present in each hemisphere of each condition. In TAC animals, there were significant sex differences in mitochondrial content in the left hippocampus, with females displaying higher levels of mitochondrial content than

males. Moreover, within the right hippocampus, protein expression of mitochondrial fusion markers was found to be significantly higher in females when compared to males. Although not significant, within the left hippocampus, females also tended to, on average, have higher protein expression of S-OPA1 ( $M=1.46\pm 0.27$  v.  $M=0.89\pm 0.12$ ,  $p=0.068$ ,  $d=1.18$ ) and total OPA1 ( $M=3.33\pm 0.57$  v.  $M=2.24\pm 0.25$ ,  $p=0.09$ ,  $d=1.01$ ). Together, these suggest that sex differences in mitochondrial quality control are possible within TAC. Taking into account that previous work has found, in rodents, extensive sex differences in the hippocampal transcriptome<sup>148</sup>, including transcripts that regulate mitochondrial health<sup>149</sup>, it is not surprising to find sex differences in the protein expression of mitochondrial quality control in TAC animals. Because OPA1 is associated with mitochondrial fusion<sup>102</sup>, concomitant upregulation this marker in females along with higher mitochondrial content on the left hippocampus may suggest TAC females have better regulation of mitochondrial health than males. However, because the vast majority of studies that use TAC as a model do not include sex comparisons<sup>113</sup>, nor fully address brain mitochondrial health<sup>25</sup>, whether this is the case remains poorly understood. Nevertheless, the inclusion of sex and hemispheric comparisons in the context of brain mitochondrial function is a novel contribution of this study towards the wider literature employing the TAC surgery as a model of cardiovascular disease.

We also report sex differences in mitochondrial health in SHAM controls. We observed that SHAM females had significantly lower CI-linked and CI&II-linked coupled respiration, concomitant with higher protein expression of fusion (MFN2) and fission (DRP1) markers compared to SHAM males. These observations

contribute to existing animal data where sex-based differences in mitochondrial function and quality control have been reported. For example it has been previously shown that CI-linked respiration is higher in 13-month old female mice compared to males<sup>150</sup>. These sex differences are no longer present at 85 weeks, suggesting that, these dimorphisms may wane in older age<sup>150</sup>. This same initial pattern was also found in an independent study where sex dimorphisms were present in 10-week old mice, and female mice were seen to have higher CI-linked, CI&II-linked coupled respiration when compared to male counterparts<sup>151</sup>. Although, these findings were not consistent with previous reports, those observations were all been made in mice at younger life stages compared to the current study in rats at relatively older ages. Because hormones such as estradiol may also influence brain mitochondria<sup>152</sup>, it is possible that our results differ from those seen in young mice due to changes in circulating estrogen. In this context, complete removal of estrogens in ovariectomized macaque monkeys is reported to alter brain mitochondrial shape from elongated tubules to a more donut-shaped phenotype<sup>153</sup>. Because donut-shaped mitochondria are associated with mitochondrial stress<sup>152</sup>, the presence of sex dimorphisms in respiration and markers of mitochondrial dynamics in our SHAM animals could suggest that circulating hormone levels may be partially involved. However, given that we did not measure estrogen, or completely ablated it from the circulation of our animals, this is an interpretation that is not directly supported by the collected data. Future studies should aim to address this gap in the literature. Despite this, because we studied sex differences at an intermediate point between the existing data in young an extremely aged mice, this study makes contributions that may aid in better

understanding how sex dimorphisms in brain mitochondrial function and dynamics change throughout the lifespan.

### Limitations

Despite the compelling evidence showing hemispheric differences in brain hypoperfusion within TAC, we did not in fact, measure brain hypoperfusion in our animals. This limits our ability to directly compare the outcomes of this study to the hypoperfusive phenotype previously reported. Nevertheless, because our carotid hemodynamics outcomes paralleled those observed in the literature, it can be inferred that the hypoperfusive phenotype was manifested in our TAC rats. Future work should aim to obtain both, perfusion, and mitochondrial function parameters to corroborate the observations of this study. Additionally, because we only targeted mitochondrial dynamics and a heat shock protein associated with the UPR<sup>MT</sup>, the results from the present study cannot address how TAC influences other quality control mechanisms such as mitophagy. Despite this, the observed differences in protein expression of fusion proteins and HSP-60 suggest the inclusion of mitophagy markers would be an exciting avenue to explore in future studies and may provide meaningful insights into the upregulation of these markers within the context of TAC. Nevertheless, the present study makes meaningful contributions not only to the TAC literature, but also to the literature aiming to understand how brain hypoperfusion can influence brain mitochondrial health.

## Conclusion

To conclude, we report that despite leading to whole brain hypoperfusion, hemispheric differences in hypoperfusion within TAC are coupled to hemispheric differences in mitochondrial respiration. Further, although both TAC hemispheres upregulated markers associated with mitochondrial quality control, high carotid artery hemodynamics and pulsatility were negatively associated with mitochondrial respiration. These results suggest that although tissue hypoperfusion may promote neuroprotective adaptations, these responses are not sufficient when hypoperfusion stems from chronic high blood flow velocity and pulsatility. Whether high blood flow pulsatility to the brain differentially affect other aspects of brain metabolism (such as the accumulation of ROS), when compared to low brain blood flow remains unknown and can offer exciting avenues for future research that complement the findings of this study. Moreover, because we also report sex dimorphisms in TAC and SHAM mitochondrial metabolism and quality control, this supports the growing discourse calling for the incorporation of sex comparisons when animal models of human disease are employed. Indeed, sex differences in cardiovascular and brain health are found throughout the human lifespan, and the exclusion of sex comparisons in animal studies of human disease leaves important biological and physiological processes disregarded. Altogether, this study makes a novel contribution to the literature by highlighting that the metabolic consequences to tissue hypoperfusion may differ based on the mechanism (high blood flow pulsatility v. lower blood flow) of action. This is particularly relevant because most animal models used to address a central link between cardiovascular disease and neurodegeneration (e.g., brain

hypoperfusion) rely on arterial occlusion models that leave blood flow pulsatility largely overlooked. Thus, these results can help inform the literature addressing the intersection between cardiovascular disease and neurodegeneration.

## Chapter 4: Summary of Findings

The primary objective of this dissertation was to investigate hippocampal glucose transport and mitochondrial function in response to two mechanisms of brain hypoperfusion (e.g., high blood flow velocity and pulsatile blood flow v. physical limitation in blood flow). To this end, we used the rodent model of transverse aortic constriction (TAC), because the binding of the transverse aorta results in opposing carotid hemodynamics. That is, in this model, the right common carotid is exposed to sustained, but pulsatile, blood flow while the left common carotid is exposed to low blood flow. Much of the TAC literature has focused on time scales (<15 weeks) that fail to characterize the long-term carotid hemodynamics of this procedure. Therefore, the first study of this dissertation focused on characterizing the bilateral carotid artery hemodynamic changes in TAC 20-, 30-, and 40 weeks post-surgery. Carotid artery diameter, blood flow velocity, and blood flow pulsatility were quantified and compared to SHAM controls. Moreover, we also addressed whether the time post-surgery magnified the TAC-related changes in carotid artery hemodynamics and explored sex-differences in TAC and SHAM animals.

As found in previous studies, we report that all time points within TAC, right carotid blood flow velocities and pulsatility were greater than the left. Because the present study used a low needle gauge (20G) to ensure animal longevity, we do not report differences between TAC and SHAM in the cardiac parameters (e.g., left ventricular width, septal width, cardiac output, ejection fraction, etc.) traditionally used to assess heart failure. Despite similar blood flow velocities in TAC compared to the right and left carotids of SHAM controls, blood flow pulsatility was consistently

higher in the right carotid of TAC animals, while velocities and pulsatility were consistently lowest in the left carotid of TAC. Therefore, this study successfully induced the high right carotid pulsatility and low right carotid blood flow response found in more aggressive TAC models. Unlike what was hypothesized, we found that the TAC-related changes in right and left carotid hemodynamics did not worsen with time. Acute studies have found the opposing bilateral carotid blood flow in TAC can be detected as soon as 24-hours post-surgery and remain stable over 7 days. Thus, changes in carotid blood flows in TAC may be characterized by a rapid onset that is stable over time. Lastly, we also found that sex differences in carotid artery velocity found in SHAM animals occurred 10 weeks earlier in TAC animals, and female animals recorded higher velocities than males. Wild-type rats have been noted to display sex differences in vascular structure and function, whereby the structural components of vasculature in females tend to translate in functional impairments when compared to male rats. Thus, female animals may have a reduced ability to cope with sustained higher and possibly pulsatile blood flow velocities, and this may explain why sex differences presented earlier in TAC.

Recent work in TAC mice shows both, right carotid pulsatile blood flow, and low left carotid blood flow induce brain hypoperfusion. However, this brain hypoperfusion differs between hemispheres, and the right cerebral hemisphere of TAC animals is more severely under-perfused than the left hemisphere. After having achieved the carotid hemodynamic phenotype associated with TAC, we then set out to study right and left hippocampal respiration, mitochondrial content, and protein expression of glucose transporters and markers of mitochondrial quality control. The

overall purpose of this component was to determine if the reported hemispheric differences in hypoperfusion led to hemispheric differences in glucose transport and mitochondrial function.

There were hemispheric differences in coupled and uncoupled mitochondrial respiration within TAC animals, with the right hippocampus showing deficits in mitochondrial respiration when compared to the left. That said, we did not find any hemispheric differences in mitochondrial content within TAC animals, nor between TAC and SHAM animals. Therefore, impairments in mitochondrial respiration are not driven by lower mitochondrial content within the right hippocampus of TAC animals. Moreover, although we did not find hemispheric differences in the protein expression of mitochondrial quality control markers, there were differences between TAC and SHAM. Specifically, we found that when compared to SHAM animals, TAC animals showcased an upregulation of mitochondrial fusion and UPR<sup>MT</sup> markers in both hemispheres. This upregulation may be a compensatory response to chronic hypoperfusion in both hemispheres of TAC animals. However, because we find impaired mitochondrial respiration in the right hippocampus of TAC animals, it may be possible that this adaptive response is insufficient when blood flow pulsatility is the source of hypoperfusion. Last, we did not find any hemispheric differences within TAC, nor between TAC and SHAM on protein expression of glucose transporters. While counterintuitive, this may indicate that deficits in glucose metabolism during hypoperfusion are not entirely the result of the acute downregulation in glucose transporter mRNA levels reported prior. In fact, because we saw that TAC animals had similar levels of GLUT protein expression, it may be possible any acute

downregulation in GLUT mRNA does not translate into chronic dysregulation of GLUT protein synthesis. Together, these results provide novel insight into the degree of resilience neuronal tissue can have in response to divergent mechanisms of hypoperfusion. That is, while it may be possible to sustain metabolic function to low blood flow and ensuing hypoperfusion, this is not the case when hypoperfusion stems from high blood flow velocity and pulsatility.

### **Future Directions**

Although this dissertation contributes novel insights into the use of TAC to study prospective mechanisms of VaD, there is much work needed to establish TAC as a representative model of human VaD. First, future work could build on the findings of the first study and chronically characterize the TAC-related changes in brain perfusion, and whether these get altered by time. This, in turn, would provide much needed information on whether the hemispheric differences in brain hypoperfusion from blood flow pulsatility and limited brain blood flow seen acutely are sustained past 8 weeks post-surgery. Additionally, this study did not include the use of behavioral testing assays (such as the Morris Water Maze or Y-Maze) that are normally used to link adverse physiological changes to cognitive health. Because molecular data and cognitive batteries are key in the establishment of animal models of neurodegenerative disease, future work should aim to include cognitive assays to help determine the behavioral consequences of TAC. More importantly, because human studies suggest chronic blood flow pulsatility and brain hypoperfusion are etiological hallmarks of VaD, the dual incorporation of brain perfusion metrics and

behavioral assays in this model can further inform whether this animal model can in fact be used as a representative model of human VaD.

From a mechanistic point of view, while we quantified the protein expression of GLUT in TAC, quantifying glucose transporter expression in the brain is challenging since GLUT isoforms are widely expressed by cell populations throughout the brain. That is, because we addressed protein expression in homogenates, any possible changes happening in specific cell populations such as endothelial cells or neurons could be masked by the presence of other cell populations that co-express the targeted GLUT isoforms (e.g., co-expression of GLUT-1 in endothelial cells and astrocytes). Despite being a widely used and sensitive technique, a methodological limitation of quantifying protein expression via immunoblotting is that it does not provide information as to what cells within the homogenate are driving the signal being detected<sup>36</sup>. Immunohistochemistry is another widely used biochemical technique with excellent spatial resolution that allows for the localization of target proteins to specific cell types, but is not as sensitive and quantifiable as immunoblotting<sup>36</sup>. Therefore, future studies should strive for the dual use of immunoblot and immunohistochemistry to comprehensively characterize the changes in glucose transport machinery that may be happening in the brain during hypoperfusion. This approach may help draw more straightforward conclusions as to whether glucose transport is in fact a rate limiting step in glucose metabolism in neurodegenerative diseases such as VaD, as suggested by the literature.

Neural tissue has an inherently low antioxidant defense system and prior work shows brains from animals with TAC and aortic binding have higher indices of

oxidative stress. Since the majority of ROS can be traced to mitochondrial oxidative phosphorylation, determining ROS production and oxidative stress in TAC brains should be a goal of future work. Determining whether hemispheric differences in mitochondrial respiration translate into hemispheric differences in either ROS production or oxidative stress can help further delineate how the consequences of blood flow pulsatility differ from those from limited brain blood flow. In the long run, because hypoperfusion, brain hemodynamics, and arterial compliance are all heavily implicated in VaD and other neurodegenerative conditions, addressing all these gaps in the literature would contribute to our understanding of the intersection between cardiovascular health and brain health.

Overall, this dissertation provides meaningful insight into the link between cardiovascular disease and neuronal health. Specifically, despite similar changes to mitochondrial quality control, mitochondrial respiration was unaffected by low blood flow velocities in the left side, while higher blood flow velocities and pulsatility associated with the right side led to impaired mitochondrial respiration. Thus, while both high blood flow and pulsatility as well as low cerebral blood flow may lead to brain hypoperfusion the neurophysiological consequences of the two may not be the same. Since most animal models of VaD rely on limiting brain blood flow to induce hypoperfusion, these results suggest there may be a clear disconnect between the inferences made from animal models of VaD and human VaD etiology. From a wider perspective, a paradigm shift is needed whereby animal models of VaD should be refined and include the use of blood flow pulsatility to induce brain hypoperfusion. Doing so would help clarify how changes in blood flow hemodynamics seen across

cardiovascular disease may influence the neurophysiological processes that contribute to the development of VaD.

## Bibliography

1. Le Couteur DG, Thillainadesan J. What is an aging-related disease? An epidemiological perspective. *The Journals of Gerontology: Series A*. 2022.
2. Niccoli T, Partridge L. Ageing as a risk factor for disease. *Current biology*. 2012; 22:R741-R52.
3. Ahmad FB, Anderson RN. The leading causes of death in the US for 2020. *Jama*. 2021; 325:1829-30.
4. Fulop T, Witkowski JM, Olivieri F, Larbi A. The integration of inflammaging in age-related diseases. *Seminars in immunology*; 2018: Elsevier.
5. Association As. 2019 Alzheimer's disease facts and figures. *Alzheimer's & Dementia*. 2019; 15:321-87.
6. Dall TM, Gallo PD, Chakrabarti R, West T, Semilla AP, Storm MV. An aging population and growing disease burden will require a large and specialized health care workforce by 2025. *Health affairs*. 2013; 32:2013-20.
7. Garrett N, Martini EM. The boomers are coming: a total cost of care model of the impact of population aging on the cost of chronic conditions in the United States. *Disease Management*. 2007; 10:51-60.
8. ODPHP. Healthy People 2020. U.S Department of Health and Human Services; [cited 2022 1/10/2022]; Available from: <https://www.healthypeople.gov/2020/topics-objectives/topic/older-adults>.
9. ODPHP. Healthy People 2030. Department of Health and Human Services; [cited 2022 1/10/2022]; Available from: <https://health.gov/healthypeople/objectives-and-data/browse-objectives/older-adults>.
10. Kennedy BK, Berger SL, Brunet A, Campisi J, Cuervo AM, Epel ES, et al. Geroscience: linking aging to chronic disease. *Cell*. 2014; 159:709-13.
11. Behr LC, Simm A, Kluttig A, Grosskopf A. 60 years of healthy aging: On definitions, biomarkers, scores and challenges. *Ageing Research Reviews*. 2023:101934.
12. Dugger BN, Dickson DW. Pathology of neurodegenerative diseases. *Cold Spring Harbor perspectives in biology*. 2017; 9:a028035.
13. Gonçalves RA, De Felice FG. The crosstalk between brain and periphery: Implications for brain health and disease. *Neuropharmacology*. 2021; 197:108728.
14. Matejuk A, Vandenbark AA, Offner H. Cross-talk of the CNS with immune cells and functions in health and disease. *Frontiers in neurology*. 2021; 12:672455.
15. Le Page A, Dupuis G, Frost EH, Larbi A, Pawelec G, Witkowski JM, et al. Role of the peripheral innate immune system in the development of Alzheimer's disease. *Experimental gerontology*. 2018; 107:59-66.
16. T O'Brien J, Thomas A. Vascular dementia. *The Lancet*. 2015; 386:1698-706.
17. Corriveau RA, Bosetti F, Emr M, Gladman JT, Koenig JI, Moy CS, et al. The science of vascular contributions to cognitive impairment and dementia (VCID): a framework for advancing research priorities in the cerebrovascular biology of cognitive decline. *Cellular and molecular neurobiology*. 2016; 36:281-8.
18. de La Torre JC. Cardiovascular risk factors promote brain hypoperfusion leading to cognitive decline and dementia. *Cardiovascular psychiatry and neurology*. 2012; 2012.

19. von Cederwald BF, Josefsson M, Wåhlin A, Nyberg L, Karalija N. Association of Cardiovascular Risk Trajectory With Cognitive Decline and Incident Dementia. *Neurology*. 2022; 98:e2013-e22.
20. Du S-Q, Wang X-R, Xiao L-Y, Tu J-F, Zhu W, He T, et al. Molecular mechanisms of vascular dementia: what can be learned from animal models of chronic cerebral hypoperfusion? *Molecular neurobiology*. 2017; 54:3670-82.
21. Kalaria RN. The pathology and pathophysiology of vascular dementia. *Neuropharmacology*. 2018; 134:226-39.
22. Kalaria RN. Comparison between Alzheimer's disease and vascular dementia: implications for treatment. *Neurological Research*. 2003; 25:661-4.
23. Mitchell GF, van Buchem MA, Sigurdsson S, Gotlib JD, Jonsdottir MK, Kjartansson Ó, et al. Arterial stiffness, pressure and flow pulsatility and brain structure and function: the Age, Gene/Environment Susceptibility–Reykjavik study. *Brain*. 2011; 134:3398-407.
24. Thorin-Trescases N, de Montgolfier O, Pinçon A, Raignault A, Caland L, Labbé P, et al. Impact of pulse pressure on cerebrovascular events leading to age-related cognitive decline. *American Journal of Physiology-Heart and Circulatory Physiology*. 2018; 314:H1214-H24.
25. Bink DI, Ritz K, Aronica E, Van Der Weerd L, Daemen MJ. Mouse models to study the effect of cardiovascular risk factors on brain structure and cognition. *Journal of Cerebral Blood Flow & Metabolism*. 2013; 33:1666-84.
26. Cunnane SC, Trushina E, Morland C, Prigione A, Casadesus G, Andrews ZB, et al. Brain energy rescue: an emerging therapeutic concept for neurodegenerative disorders of ageing. *Nature Reviews Drug Discovery*. 2020; 19:609-33.
27. Sebastián D, Palacín M, Zorzano A. Mitochondrial dynamics: coupling mitochondrial fitness with healthy aging. *Trends in molecular medicine*. 2017; 23:201-15.
28. McBride HM, Neuspiel M, Wasiak S. Mitochondria: more than just a powerhouse. *Current biology*. 2006; 16:R551-R60.
29. Raefsky SM, Mattson MP. Adaptive responses of neuronal mitochondria to bioenergetic challenges: Roles in neuroplasticity and disease resistance. *Free Radical Biology and Medicine*. 2017; 102:203-16.
30. Castro JP, Wardelmann K, Grune T, Kleinridders A. Mitochondrial chaperones in the brain: safeguarding brain health and metabolism? *Frontiers in endocrinology*. 2018; 9:196.
31. Ingram T, Chakrabarti L. Proteomic profiling of mitochondria: what does it tell us about the ageing brain? *Aging (Albany NY)*. 2016; 8:3161.
32. Tilokani L, Nagashima S, Paupe V, Prudent J. Mitochondrial dynamics: overview of molecular mechanisms. *Essays in biochemistry*. 2018; 62:341-60.
33. Forte M, Schirone L, Ameri P, Basso C, Catalucci D, Modica J, et al. The role of mitochondrial dynamics in cardiovascular diseases. *British Journal of Pharmacology*. 2021; 178:2060-76.
34. Muñoz-Carvajal F, Sanhueza M. The mitochondrial unfolded protein response: a hinge between healthy and pathological aging. *Frontiers in Aging Neuroscience*. 2020; 12:581849.

35. Joshi AU, Saw NL, Shamloo M, Mochly-Rosen D. Drp1/Fis1 interaction mediates mitochondrial dysfunction, bioenergetic failure and cognitive decline in Alzheimer's disease. *Oncotarget*. 2018; 9:6128.
36. Leak RK. Heat shock proteins in neurodegenerative disorders and aging. *Journal of cell communication and signaling*. 2014; 8:293-310.
37. Martín-Maestro P, Gargini R, García E, Perry G, Avila J, García-Escudero V. Slower dynamics and aged mitochondria in sporadic Alzheimer's disease. *Oxidative Medicine and Cellular Longevity*. 2017; 2017.
38. Monzio Compagnoni G, Di Fonzo A, Corti S, Comi GP, Bresolin N, Masliah E. The role of mitochondria in neurodegenerative diseases: the lesson from Alzheimer's disease and Parkinson's disease. *Molecular neurobiology*. 2020; 57:2959-80.
39. Carnevale D, Mascio G, Ajmone-Cat MA, D'Andrea I, Cifelli G, Madonna M, et al. Role of neuroinflammation in hypertension-induced brain amyloid pathology. *Neurobiology of Aging*. 2012; 33:205. e19-. e29.
40. Lopez-Campistrous A, Hao L, Xiang W, Ton D, Semchuk P, Sander J, et al. Mitochondrial dysfunction in the hypertensive rat brain: respiratory complexes exhibit assembly defects in hypertension. *Hypertension*. 2008; 51:412-9.
41. Peng C, Rao W, Zhang L, Wang K, Hui H, Wang L, et al. Mitofusin 2 ameliorates hypoxia-induced apoptosis via mitochondrial function and signaling pathways. *The international journal of biochemistry & cell biology*. 2015; 69:29-40.
42. Gooch J, Wilcock DM. Animal models of vascular cognitive impairment and dementia (VCID). *Cellular and molecular neurobiology*. 2016; 36:233-9.
43. Raz L, Knoefel J, Bhaskar K. The neuropathology and cerebrovascular mechanisms of dementia. *Journal of Cerebral Blood Flow & Metabolism*. 2016; 36:172-86.
44. Sinha K, Sun C, Kamari R, Bettermann K. Current status and future prospects of pathophysiology-based neuroprotective drugs for the treatment of vascular dementia. *Drug Discovery Today*. 2020; 25:793-9.
45. Li Y-H, Hsieh C-Y, Wang DL, Chung H-C, Liu S-L, Chao T-H, et al. Remodeling of carotid arteries is associated with increased expression of thrombomodulin in a mouse transverse aortic constriction model. *Thrombosis and haemostasis*. 2007; 97:658-64.
46. de Montgolfier O, Pinçon A, Pouliot P, Gillis M-A, Bishop J, Sled JG, et al. High systolic blood pressure induces cerebral microvascular endothelial dysfunction, neurovascular unit damage, and cognitive decline in mice. *Hypertension*. 2019; 73:217-28.
47. Prince MJ, Wu F, Guo Y, Robledo LMG, O'Donnell M, Sullivan R, et al. The burden of disease in older people and implications for health policy and practice. *The Lancet*. 2015; 385:549-62.
48. Barquera S, Pedroza-Tobías A, Medina C, Hernández-Barrera L, Bibbins-Domingo K, Lozano R, et al. Global overview of the epidemiology of atherosclerotic cardiovascular disease. *Archives of medical research*. 2015; 46:328-38.
49. Waldstein SR, Rice SC, Thayer JF, Najjar SS, Scuteri A, Zonderman AB. Pulse pressure and pulse wave velocity are related to cognitive decline in the Baltimore Longitudinal Study of Aging. *Hypertension*. 2008; 51:99-104.

50. Song R, Pan KY, Xu H, Qi X, Buchman AS, Bennett DA, et al. Association of cardiovascular risk burden with risk of dementia and brain pathologies: A population-based cohort study. *Alzheimer's & Dementia*. 2021; 17:1914-22.
51. Murphy MP, Corriveau RA, Wilcock DM. Vascular contributions to cognitive impairment and dementia (VCID). 2016. p. 857-9.
52. Behl T, Makkar R, Sehgal A, Singh S, Sharma N, Zengin G, et al. Current trends in neurodegeneration: Cross talks between oxidative stress, cell death, and inflammation. *International Journal of Molecular Sciences*. 2021; 22:7432.
53. Zlokovic BV, Gottesman RF, Bernstein KE, Seshadri S, McKee A, Snyder H, et al. Vascular contributions to cognitive impairment and dementia (VCID): a report from the 2018 National Heart, Lung, and Blood Institute and National Institute of Neurological Disorders and Stroke Workshop. *Alzheimer's & Dementia*. 2020; 16:1714-33.
54. Goodman RA, Lochner KA, Thambisetty M, Wingo TS, Posner SF, Ling SM. Prevalence of dementia subtypes in United States Medicare fee-for-service beneficiaries, 2011–2013. *Alzheimer's & dementia*. 2017; 13:28-37.
55. Gorelick PB, Scuteri A, Black SE, DeCarli C, Greenberg SM, Iadecola C, et al. Vascular contributions to cognitive impairment and dementia: a statement for healthcare professionals from the American Heart Association/American Stroke Association. *stroke*. 2011; 42:2672-713.
56. Ahmad A, Patel V, Xiao J, Khan MM. The role of neurovascular system in neurodegenerative diseases. *Molecular Neurobiology*. 2020; 57:4373-93.
57. Rajeev V, Fann DY, Dinh QN, Kim HA, De Silva TM, Lai MK, et al. Pathophysiology of blood brain barrier dysfunction during chronic cerebral hypoperfusion in vascular cognitive impairment. *Theranostics*. 2022; 12:1639.
58. Bir SC, Khan MW, Javalkar V, Toledo EG, Kelley RE. Emerging concepts in vascular dementia: a review. *Journal of Stroke and Cerebrovascular Diseases*. 2021; 30:105864.
59. Safar ME, Nilsson PM, Blacher J, Mimran A. Pulse pressure, arterial stiffness, and end-organ damage. *Current hypertension reports*. 2012; 14:339-44.
60. Iadecola C. The pathobiology of vascular dementia. *Neuron*. 2013; 80:844-66.
61. Claassen JA, Thijssen DH, Panerai RB, Faraci FM. Regulation of cerebral blood flow in humans: physiology and clinical implications of autoregulation. *Physiological reviews*. 2021; 101:1487-559.
62. Sabayan B, Jansen S, Oleksik AM, van Osch MJ, van Buchem MA, van Vliet P, et al. Cerebrovascular hemodynamics in Alzheimer's disease and vascular dementia: a meta-analysis of transcranial Doppler studies. *Ageing research reviews*. 2012; 11:271-7.
63. Haller S, Zaharchuk G, Thomas DL, Lovblad K-O, Barkhof F, Golay X. Arterial spin labeling perfusion of the brain: emerging clinical applications. *Radiology*. 2016; 281:337-56.
64. Watts JM, Whitlow CT, Maldjian JA. Clinical applications of arterial spin labeling. *NMR in Biomedicine*. 2013; 26:892-900.
65. Heiss W-D. PET imaging in ischemic cerebrovascular disease: current status and future directions. *Neuroscience bulletin*. 2014; 30:713-32.

66. Morovic S, Budincevic H, Govori V, Demarin V. Possibilities of dementia prevention-it is never too early to start. *Journal of medicine and life*. 2019; 12:332.
67. Diniz BS, Butters MA, Albert SM, Dew MA, Reynolds CF. Late-life depression and risk of vascular dementia and Alzheimer's disease: systematic review and meta-analysis of community-based cohort studies. *The British Journal of Psychiatry*. 2013; 202:329-35.
68. Swanson KA, Carnahan RM. Dementia and comorbidities: an overview of diagnosis and management. *Journal of Pharmacy Practice*. 2007; 20:296-317.
69. Venkat P, Chopp M, Chen J. Models and mechanisms of vascular dementia. *Experimental neurology*. 2015; 272:97-108.
70. Mohammadi MT, Dehghani GA. Acute hypertension induces brain injury and blood-brain barrier disruption through reduction of claudins mRNA expression in rat. *Pathology-Research and Practice*. 2014; 210:985-90.
71. Schreiber S, Bueche CZ, Garz C, Braun H. Blood brain barrier breakdown as the starting point of cerebral small vessel disease?-New insights from a rat model. *Experimental & Translational Stroke Medicine*. 2013; 5:1-8.
72. Krueger M, Bechmann I, Immig K, Reichenbach A, Härtig W, Michalski D. Blood-brain barrier breakdown involves four distinct stages of vascular damage in various models of experimental focal cerebral ischemia. *Journal of Cerebral Blood Flow & Metabolism*. 2015; 35:292-303.
73. Shabir O, Berwick J, Francis SE. Neurovascular dysfunction in vascular dementia, Alzheimer's and atherosclerosis. *BMC neuroscience*. 2018; 19:1-16.
74. Heiss W-D, Zimmermann-Meinzingen S. PET imaging in the differential diagnosis of vascular dementia. *Journal of the neurological sciences*. 2012; 322:268-73.
75. Nishio K, Ihara M, Yamasaki N, Kalaria RN, Maki T, Fujita Y, et al. A mouse model characterizing features of vascular dementia with hippocampal atrophy. *Stroke*. 2010; 41:1278-84.
76. Johnson AC, Miller JE, Cipolla MJ. Memory impairment in spontaneously hypertensive rats is associated with hippocampal hypoperfusion and hippocampal vascular dysfunction. *Journal of Cerebral Blood Flow & Metabolism*. 2020; 40:845-59.
77. Calderón-Cortés E, Cortés-Rojo C, Clemente-Guerrero M, Manzo-Avalos S, Villalobos-Molina R, Boldogh I, et al. Changes in mitochondrial functionality and calcium uptake in hypertensive rats as a function of age. *Mitochondrion*. 2008; 8:262-72.
78. Washida K, Hattori Y, Ihara M. Animal models of chronic cerebral hypoperfusion: from mouse to primate. *International Journal of Molecular Sciences*. 2019; 20:6176.
79. Mansour A, Rashad S, Niizuma K, Fujimura M, Tominaga T. A novel model of cerebral hyperperfusion with blood-brain barrier breakdown, white matter injury, and cognitive dysfunction. *Journal of neurosurgery*. 2019; 133:1460-72.
80. Drake C, Boutin H, Jones MS, Denes A, McColl BW, Selvarajah JR, et al. Brain inflammation is induced by co-morbidities and risk factors for stroke. *Brain, behavior, and immunity*. 2011; 25:1113-22.

81. Grootendorst J, Oitzl MS, Dalm S, Enthoven L, Schachner M, De Kloet E, et al. Stress alleviates reduced expression of cell adhesion molecules (NCAM, L1), and deficits in learning and corticosterone regulation of apolipoprotein E knockout mice. *European Journal of Neuroscience*. 2001; 14:1505-14.
82. Yang C-P, Gilley JA, Zhang G, Kernie SG. ApoE is required for maintenance of the dentate gyrus neural progenitor pool. *Development*. 2011; 138:4351-62.
83. Deardorff WJ, Grossberg GT. Behavioral and psychological symptoms in Alzheimer's dementia and vascular dementia. *Handbook of clinical neurology*. 2019; 165:5-32.
84. Henneman W, Sluimer J, Barnes J, Van Der Flier W, Sluimer I, Fox N, et al. Hippocampal atrophy rates in Alzheimer disease: added value over whole brain volume measures. *Neurology*. 2009; 72:999-1007.
85. Scott JG, Schoenberg MR. Frontal lobe/executive functioning. *The little black book of neuropsychology*: Springer; 2011. p. 219-48.
86. Anor CJ, O'Connor S, Saund A, Tang-Wai DF, Keren R, Tartaglia MC. Neuropsychiatric symptoms in Alzheimer disease, vascular dementia, and mixed dementia. *Neurodegenerative Diseases*. 2017; 17:127-34.
87. Perlman SB, Pelphrey KA. Regulatory brain development: balancing emotion and cognition. *Social Neuroscience*. 2010; 5:533-42.
88. Frackowiak R, Pozzilli C, Legg Nd, Du Boulay G, Marshall J, Lenzi G, et al. Regional cerebral oxygen supply and utilization in dementia. A clinical and physiological study with oxygen-15 and positron tomography. *Brain: a journal of neurology*. 1981; 104:753-78.
89. Libon DJ, Lamar M, Price CC, Jefferson AL, Swenson R, Au R. Neuropsychological evaluation for vascular dementia. 2018.
90. Bordone MP, Salman MM, Titus HE, Amini E, Andersen JV, Chakraborti B, et al. The energetic brain—A review from students to students. *Journal of neurochemistry*. 2019; 151:139-65.
91. Shah K, DeSilva S, Abbruscato T. The role of glucose transporters in brain disease: diabetes and Alzheimer's disease. *International journal of molecular sciences*. 2012; 13:12629-55.
92. Albert B, Johnson A, Lewis J, Raff M, Roberts K, Walter P. *Molecular Biology of the Cell* 5th edition. Garland Science. Taylor & Francis Group, LLC; 2008.
93. Shi L, Tu BP. Acetyl-CoA and the regulation of metabolism: mechanisms and consequences. *Current opinion in cell biology*. 2015; 33:125-31.
94. Benard G, Bellance N, Jose C, Rossignol R. Relationships between mitochondrial dynamics and bioenergetics. *Mitochondrial Dynamics and Neurodegeneration*: Springer; 2011. p. 47-68.
95. Willis WT, Jackman MR, Messer JI, Kuzmiak-Glancy S, Glancy B. A simple hydraulic analog model of oxidative phosphorylation. *Medicine and science in sports and exercise*. 2016; 48:990.
96. Brand M. Mitochondrial proton and electron leaks essays in biochemistry. *Essays Biochem*. 2010; 47:53-67.

97. Bolisetty S, Jaimes EA. Mitochondria and reactive oxygen species: physiology and pathophysiology. *International journal of molecular sciences*. 2013; 14:6306-44.
98. Müller WE, Eckert A, Kurz C, Eckert GP, Leuner K. Mitochondrial dysfunction: common final pathway in brain aging and Alzheimer's disease—therapeutic aspects. *Molecular neurobiology*. 2010; 41:159-71.
99. Hernansanz-Agustín P, Enríquez JA. Generation of reactive oxygen species by mitochondria. *Antioxidants*. 2021; 10:415.
100. Yan X, Wang B, Hu Y, Wang S, Zhang X. Abnormal mitochondrial quality control in neurodegenerative diseases. *Frontiers in Cellular Neuroscience*. 2020; 14:138.
101. Liu YJ, McIntyre RL, Janssens GE, Houtkooper RH. Mitochondrial fission and fusion: A dynamic role in aging and potential target for age-related disease. *Mechanisms of ageing and development*. 2020; 186:111212.
102. Sebastián D, Zorzano A. Mitochondrial dynamics and metabolic homeostasis. *Current Opinion in Physiology*. 2018; 3:34-40.
103. Forte M, Stanzione R, Cotugno M, Bianchi F, Marchitti S, Rubattu S. Vascular ageing in hypertension: Focus on mitochondria. *Mechanisms of ageing and development*. 2020; 189:111267.
104. Legros F, Lombes A, Frachon P, Rojo M. Mitochondrial fusion in human cells is efficient, requires the inner membrane potential, and is mediated by mitofusins. *Molecular biology of the cell*. 2002; 13:4343-54.
105. Van Laar VS, Berman SB. The interplay of neuronal mitochondrial dynamics and bioenergetics: implications for Parkinson's disease. *Neurobiology of disease*. 2013; 51:43-55.
106. Mottis A, Jovaisaite V, Auwerx J. The mitochondrial unfolded protein response in mammalian physiology. *Mammalian genome*. 2014; 25:424-33.
107. Haynes CM, Ron D. The mitochondrial UPR—protecting organelle protein homeostasis. *Journal of cell science*. 2010; 123:3849-55.
108. Young JC, Hoogenraad NJ, Hartl FU. Molecular chaperones Hsp90 and Hsp70 deliver preproteins to the mitochondrial import receptor Tom70. *Cell*. 2003; 112:41-50.
109. Daneri-Becerra C, Ciucci SM, Mazaira G, Galigniana MD. Role of Mitochondrial Heat-shock Proteins and Immunophilins in Neuro Degenerative Diseases. *Current Drug Targets*. 2021; 22:1596-617.
110. Bacmeister L, Schwarzl M, Warnke S, Stoffers B, Blankenberg S, Westermann D, et al. Inflammation and fibrosis in murine models of heart failure. *Basic Research in Cardiology*. 2019; 114:1-35.
111. Poulet R, Gentile MT, Vecchione C, Distaso M, Aretini A, Fratta L, et al. Acute hypertension induces oxidative stress in brain tissues. *Journal of Cerebral Blood Flow & Metabolism*. 2006; 26:253-62.
112. Conceicao G, Heinonen I, Lourenco A, Duncker D, Falcao-Pires I. Animal models of heart failure with preserved ejection fraction. *Netherlands Heart Journal*. 2016; 24:275-86.

113. Bosch L, de Haan JJ, Bastemeijer M, van der Burg J, van der Worp E, Wesseling M, et al. The transverse aortic constriction heart failure animal model: a systematic review and meta-analysis. *Heart failure reviews*. 2021; 26:1515-24.
114. Cauley E, Wang X, Dyavanapalli J, Sun K, Garrott K, Kuzmiak-Glancy S, et al. Neurotransmission to parasympathetic cardiac vagal neurons in the brain stem is altered with left ventricular hypertrophy-induced heart failure. *American Journal of Physiology-Heart and Circulatory Physiology*. 2015; 309:H1281-H7.
115. Wielicka M, Neubauer-Geryk J, Kozera G, Bieniaszewski L. Clinical application of pulsatility index. *Medical Research Journal*. 2020; 5:201-10.
116. Li H, Guo Q, Inoue T, Polito VA, Tabuchi K, Hammer RE, et al. Vascular and parenchymal amyloid pathology in an Alzheimer disease knock-in mouse model: interplay with cerebral blood flow. *Molecular neurodegeneration*. 2014; 9:1-15.
117. Lu D, Kassab GS. Role of shear stress and stretch in vascular mechanobiology. *Journal of the royal society interface*. 2011; 8:1379-85.
118. Boesen ME, Singh D, Menon BK, Frayne R. A systematic literature review of the effect of carotid atherosclerosis on local vessel stiffness and elasticity. *Atherosclerosis*. 2015; 243:211-22.
119. Sengupta P. The laboratory rat: relating its age with human's. *International journal of preventive medicine*. 2013; 4:624.
120. Appelman Y, van Rijn BB, Monique E, Boersma E, Peters SA. Sex differences in cardiovascular risk factors and disease prevention. *Atherosclerosis*. 2015; 241:211-8.
121. Stanhewicz AE, Wenner MM, Stachenfeld NS. Sex differences in endothelial function important to vascular health and overall cardiovascular disease risk across the lifespan. *American Journal of Physiology-Heart and Circulatory Physiology*. 2018; 315:H1569-H88.
122. Volgman AS, Bairey Merz CN, Aggarwal NT, Bittner V, Bunch TJ, Gorelick PB, et al. Sex differences in cardiovascular disease and cognitive impairment: another health disparity for women? *Journal of the American Heart Association*. 2019; 8:e013154.
123. Humphries KH, Izadnegahdar M, Sedlak T, Saw J, Johnston N, Schenck-Gustafsson K, et al. Sex differences in cardiovascular disease—impact on care and outcomes. *Frontiers in neuroendocrinology*. 2017; 46:46-70.
124. Matrai M, Mericli M, Nadasy GL, Szekeres M, Varbiro S, Banhidy F, et al. Gender differences in biomechanical properties of intramural coronary resistance arteries of rats, an in vitro microarteriographic study. *Journal of biomechanics*. 2007; 40:1024-30.
125. Ibrahim J, McGee A, Graham D, McGrath JC, Dominiczak AF, Ibrahim J. GENDER DIFFERENCES IN CEREBRAL ARTERIAL MYOGENIC TONE IN HYPERTENSIVE AND NORMOTENSIVE RATS. 2005.
126. Wang S, Zhang H, Liu Y, Li L, Guo Y, Jiao F, et al. Sex differences in the structure and function of rat middle cerebral arteries. *American Journal of Physiology-Heart and Circulatory Physiology*. 2020; 318:H1219-H32.
127. Hayden KM, Zandi PP, Lyketsos CG, Khachaturian AS, Bastian LA, Charoonruk G, et al. Vascular risk factors for incident Alzheimer disease and vascular

dementia: the Cache County study. *Alzheimer Disease & Associated Disorders*. 2006; 20:93-100.

128. Blanken AE, Nation DA. Does gender influence the relationship between high blood pressure and dementia? Highlighting areas for further investigation. *Journal of Alzheimer's Disease*. 2020; 78:23-48.

129. Burtscher J, Zangrandi L, Schwarzer C, Gnaiger E. Differences in mitochondrial function in homogenated samples from healthy and epileptic specific brain tissues revealed by high-resolution respirometry. *Mitochondrion*. 2015; 25:104-12.

130. Kuzmiak S, Glancy B, Sweazea KL, Willis WT. Mitochondrial function in sparrow pectoralis muscle. *Journal of Experimental Biology*. 2012; 215:2039-50.

131. Meng L, Hou W, Chui J, Han R, Gelb AW. Cardiac output and cerebral blood flow: the integrated regulation of brain perfusion in adult humans. *Anesthesiology*. 2015; 123:1198-208.

132. Richards DA, Aronovitz MJ, Calamaras TD, Tam K, Martin GL, Liu P, et al. Distinct phenotypes induced by three degrees of transverse aortic constriction in mice. *Scientific reports*. 2019; 9:5844.

133. Armand-Ugon M, Ansoleaga B, Berjaoui S, Ferrer I. Reduced mitochondrial activity is early and steady in the entorhinal cortex but it is mainly unmodified in the frontal cortex in Alzheimer's disease. *Current Alzheimer Research*. 2017; 14:1327-34.

134. Aliev G, Horecký J, Vančová O, Ashraf GM, Hassan I, Bragin V, et al. The three-vessel occlusion as a model of vascular dementia—oxidative stress and mitochondrial failure as an indicator of brain hypoperfusion. *Systems Biology of Free Radicals and Antioxidants* (Laher, I ed), Springer Berlin Heidelberg. 2014:2023-32.

135. Du J, Ma M, Zhao Q, Fang L, Chang J, Wang Y, et al. Mitochondrial bioenergetic deficits in the hippocampi of rats with chronic ischemia-induced vascular dementia. *Neuroscience*. 2013; 231:345-52.

136. Gnaiger E, Arnould T, Detraux D, STORDER J. Mitochondrial respiratory states and rates. *MitoFit Preprint Arch* (2019). 2019:1-40.

137. Alberts B, Johnson A, Lewis J, Raff M, Roberts K, Wlatter P. *Molecular Biology of the Cell*: Garland Science; 2007.

138. Gnaiger E. Mitochondrial pathways and respiratory control: an introduction to OXPHOS analysis. *Bioenergetics communications*. 2020; 2020:2-.

139. Cechetti F, Worm PV, Pereira L, Siqueira IR, A Netto C. The modified 2VO ischemia protocol causes cognitive impairment similar to that induced by the standard method, but with a better survival rate. *Brazilian Journal of Medical and Biological Research*. 2010; 43:1178-83.

140. Buccitelli C, Selbach M. mRNAs, proteins and the emerging principles of gene expression control. *Nature Reviews Genetics*. 2020; 21:630-44.

141. Zhang W-w, Zhang L, Hou W-k, Xu Y-x, Xu H, Lou F-c, et al. Dynamic expression of glucose transporters 1 and 3 in the brain of diabetic rats with cerebral ischemia reperfusion. *Chinese medical journal*. 2009; 122:1996-2001.

142. Liu Y, Beyer A, Aebersold R. On the dependency of cellular protein levels on mRNA abundance. *Cell*. 2016; 165:535-50.

143. Kaur MM, Sharma S. Mitochondrial repair as potential pharmacological target in cerebral ischemia. *Mitochondrion*. 2022.

144. Itoh K, Nakamura K, Iijima M, Sesaki H. Mitochondrial dynamics in neurodegeneration. *Trends in cell biology*. 2013; 23:64-71.
145. Scheffer S, Hermkens DM, Van Der Weerd L, De Vries HE, Daemen MJ. Vascular hypothesis of Alzheimer disease: topical review of mouse models. *Arteriosclerosis, Thrombosis, and Vascular Biology*. 2021; 41:1265-83.
146. Feng T, Yamashita T, Zhai Y, Shang J, Nakano Y, Morihara R, et al. Chronic cerebral hypoperfusion accelerates Alzheimer's disease pathology with the change of mitochondrial fission and fusion proteins expression in a novel mouse model. *Brain Research*. 2018; 1696:63-70.
147. Wang L, Liu M, Gao J, Smith AM, Fujioka H, Liang J, et al. Mitochondrial fusion suppresses tau pathology-induced neurodegeneration and cognitive decline. *Journal of Alzheimer's Disease*. 2021; 84:1057-69.
148. Haghani A, Johnson RG, Woodward NC, Feinberg JI, Lewis K, Ladd-Acosta C, et al. Adult mouse hippocampal transcriptome changes associated with long-term behavioral and metabolic effects of gestational air pollution toxicity. *Translational psychiatry*. 2020; 10:218.
149. Bundy JL, Vied C, Nowakowski RS. Sex differences in the molecular signature of the developing mouse hippocampus. *BMC genomics*. 2017; 18:1-17.
150. Gaignard P, Saviouroux S, Liere P, Pianos A, Thérond P, Schumacher M, et al. Effect of sex differences on brain mitochondrial function and its suppression by ovariectomy and in aged mice. *Endocrinology*. 2015; 156:2893-904.
151. Khalifa ARM, Abdel-Rahman EA, Mahmoud AM, Ali MH, Noureldin M, Saber SH, et al. Sex-specific differences in mitochondria biogenesis, morphology, respiratory function, and ROS homeostasis in young mouse heart and brain. *Physiological reports*. 2017; 5:e13125.
152. Picard M, McEwen BS. Mitochondria impact brain function and cognition. *Proceedings of the National Academy of Sciences*. 2014; 111:7-8.
153. Hara Y, Yuk F, Puri R, Janssen WG, Rapp PR, Morrison JH. Presynaptic mitochondrial morphology in monkey prefrontal cortex correlates with working memory and is improved with estrogen treatment. *Proceedings of the National Academy of Sciences*. 2014; 111:486-91.